Spring 1-1-2013

A First-Order Reliability Approach to Building Portfolio Loss Estimation and Mitigation Prioritization

Holly Lynn Bonstrom
University of Colorado at Boulder, HBonstrom@gmail.com

A FIRST-ORDER RELIABILITY APPROACH TO BUILDING PORTFOLIO LOSS ESTIMATION AND MITIGATION PRIORITIZATION

by

Holly Bonstrom
BSCE, University of Central Florida, 2008
MSCE., University of Colorado, 2011

A thesis submitted to the
Faculty of the Graduate School of the
University of Colorado in partial fulfillment
of the requirement for the degree of
Doctor of Philosophy
Department of Civil, Environmental and Architectural Engineering

2013

A FIRST-ORDER RELIABILITY APPROACH TO
BUILDING PORTFOLIO LOSS ESTIMATION AND
MITIGATION PRIORITIZATION

By Holly Bonstrom

The final copy of this thesis has been examined by signatories, and we find that both the content and form meet acceptable presentation standards of scholarly work for the Department of Civil, Environmental and Architectural Engineering.

_____
(Ross B. Corotis) Committee Chair

_____
(Shideh Dashti)

_____
(Jim Harris)

_____
(Abbie Liel)

_____
(Keith Porter)

Date _____

Abstract

Bonstrom, Holly (Ph.D., Department of Civil, Environmental and Architectural Engineering)

A First-Order Reliability Approach to Building Portfolio Loss Estimation and Mitigation Prioritization

Thesis directed by Professor Ross. B. Corotis

The prediction of future losses from earthquake events and other natural hazards is of importance to community developers, insurance entities, political organizations and many others in hazard-prone regions. Often, this risk assessment is preferred at a regional level as many private and public entities are concerned with the impact of an earthquake on a suite of buildings, as opposed to that for a single site. Assessing risk at a regional level is more complicated than doing so for individual sites due to the correlation that exists between the performances of spatially distributed buildings within a single hazard. This spatial correlation has been shown to be vital for characterizing potential loss at a regional level; however, it is often neglected in existing loss estimation methodologies.

This dissertation proposes the use of the First-Order Reliability Method (FORM) to quantify probabilistic losses to a portfolio while incorporating the spatial correlation that exists between building performances. FORM is an approximate, analytical structural reliability

technique that computes failure probability based on a linearization of a performance limit state. Unlike existing loss estimation tools that evaluate loss based on expected values or with the use of simulation, the proposed method evaluates the distribution of potential losses analytically and is also computationally efficient. In addition, sensitivity measures are computed using FORM to prioritize cost-effective retrofit strategies within a building portfolio.

This proposed method is applied to a selected San Francisco building inventory to estimate total structural and nonstructural repair cost in the form of loss exceedance curves. Sensitivity measures are used to prioritize building types that yield the most reduction in regional risk per dollar of retrofit.

In additional to quantifying losses, the proposed framework is extended to assess the seismic resilience for the San Francisco building portfolio. Sensitivity measures are computed relative to changes in system resilience for each dollar allocated to pre-disaster retrofit and to increasing post-disaster restoration efficiency.

Finally, the study also investigates the extension of the proposed FORM-based approach to assess the cumulative hazard-induced risk for regions subjected to multiple hazards. In this extended study, FORM is used to compute the distribution of loss for Charleston County, South Carolina, specific to potential earthquake and hurricane wind hazards.

The proposed approach provides an analytical and efficient tool for quantifying hazard risk at a regional level. By more effectively quantifying hazard-induced loss, resilience and sensitivities within a portfolio system, information is provided to improve hazard risk assessments and support more efficient risk management decision making.

Acknowledgments

I would like to express my sincere gratitude to my advisor, Professor Ross Corotis, for his constant support, generosity with his time and his vast knowledge, and encouragement throughout my doctoral studies. I am grateful to him for believing in my abilities and for giving me the freedom to explore my way through this dissertation. I feel honored to have had the opportunity to work with him and share in his research.

I gratefully appreciate the guidance and support from the other members of my doctoral advisory committee. Thanks to Keith Porter for the multiple research discussions, useful suggestions and for generously sharing building inventory data used in this dissertation. I am thankful to Abbie Liel for the meaningful discussions, inspiration and encouragement over the years. I also wish to thank Shideh Dashti and Jim Harris for their keen insight and valuable feedback throughout the evolution of my dissertation studies.

Additionally, thanks to Kevin Mackey for useful conversations and guidance in the early phases of my dissertation and Charlie Kircher for sharing his work on building height distributions within a portfolio.

I would also like to recognize my friends and fellow students within my research office for their valuable feedback, fruitful discussions and words of encouragement they shared with me

during my Ph.D. experience. Special thanks to Meera Raghunandan, Siamak Sattar, Emily Elwood, Jared DeBock, Sarah Welsh-Huggins, Lan Nguyen, Yolanda Lin and Cody Harrington. Additional thanks to Jared DeBock for our many meaningful research discussions and to Sarah Welsh-Huggins for the valuable review of my dissertation.

Lastly, I would like to express sincere appreciation to my family for their incredible support throughout my doctoral studies. Words cannot express how thankful I am to my husband, Jay, for his uplifting encouragement and creative inspiration over the past few years. Whether it is through surprise study snacks or his unsuccessful, yet continuous attempts to use structural engineering jargon, he has truly been by my side, cheering me on every step of the way. Thanks to my loving grandparents and mother- and father-in-law for all of their support and encouragement. Special thanks to my chubby pug, Bill, for never failing to make me smile. Finally, I wish to thank my mom and dad, Jeanette and Bob, for their unconditional reassurance and support over the years. I wouldn't be where I am today without the dedication and values they stressed while raising me, and the inspirational example they set each day.

This research is supported by the National Science Foundation, grant number CMMI 1063790. This support is acknowledged and greatly appreciated. Any opinions, findings or recommendations expressed in this dissertation are those of the author and do not necessarily reflect the views or policies of NSF.

Contents

List of Tables

List of Figures

Chapter 1. Introduction

1.1 Problem Definition

The devastating effects of earthquakes over the past few decades, including those that took place in Loma Prieta, Northridge, New Zealand, Chili and Japan, demonstrated that risk management is a paramount issue for seismically active areas. Not only did these events prompt the awareness of seismic risk, but they also exposed difficulties in mitigating this risk.

An informed decision-making process with optimal resource allocation is needed to reduce seismic risk efficiently, and this requires the aid of reliable and quantitative risk assessment tools. These tools are often desired at a regional level as many private and public entities are concerned with the impact of an earthquake to a portfolio of buildings as opposed to that for a single site. For example, a regional assessment may be of interest to political or community organizations deciding how to mitigate the collective risk to their infrastructure. Insurance or other private firms may also be interested in the collective risk present among a suite of buildings within a specified region and time period of interest. Given the large uncertainties involved in assessing the demands and capacities of a portfolio, probabilistic estimates are often desired to adequately capture the predicted seismic risk.

Assessing potential losses for a portfolio of buildings is more complex than for a single site because of the correlations that exist between building performances (i.e., characterized by building damage or loss) in a seismic event. A building portfolio can be thought of as a system of interconnected, as opposed to individual, building components. The influence of correlation between building parameters is apparent when estimating large infrequent losses for a portfolio. Such losses are of particular interest since they tend to dominate earthquake repair costs over time. These large consequences occur when many of the buildings within a region perform poorly in the same earthquake. The probability of such a phenomenon can only be estimated accurately if the correlations between the building performances are included in the loss assessment process.

This correlation between the performances of spatially distributed buildings is a function of shared effects from the seismic source, and similarities in site effects, structural components and analytical models used to assess loss (Schubert and Faber 2012). For example, sites in close proximity to each other will experience similar ground motion time histories due to shared seismic source conditions, commonality of wave paths, site conditions and distance between sites (Baker and Cornell 2006; Thompson et al. 2010). Disregarding this correlation in ground motion intensity (referred to as spatial correlation) has been shown to underestimate large rare losses for a building portfolio and overestimate small frequent losses (Jayaram and Baker 2010a; Park et al. 2007). Neglecting such correlation also influences the prioritization of cost-effective retrofit schemes, leading to the selection of less than optimum risk-mitigation spending for a region (Lee and Kiremidjian 2007).

The primary focus of this dissertation is to develop a method for assessing seismic risk and cost-effective retrofit schemes for a suite of buildings, while incorporating this spatial

correlation. Significant efforts have been made previously to predict the seismic risk to infrastructure portfolios subject to seismic hazards. The HAZUS-MH software developed for the Federal Emergency Management Agency (FEMA) offers one of the most widely used contributions to this field, given its general capabilities and available inventory data (NIBS 2012). Using seismic hazard curves paired with building fragility information, HAZUS-MH computes monetary losses and fatalities given a hazard. Regional loss is computed, however, as the summation of the expected costs for each building type, rather than the distribution of potential losses. By not including the variance in loss, the correlations that exist between building performances are also not included, therefore omitting valuable information that may assist in risk management decision making (Schubert and Faber 2012).

Many recent research studies use Monte Carlo Simulation (MCS) to quantify the distribution of system loss and do include spatial correlation in the assessment (Crowley and Bommer 2006; Goda and Hong 2008; Jayaram and Baker 2010a). In such studies, a multivariate probabilistic distribution for the seismic demand is paired with fragility information to simulate predicted losses for a region. However, MCS is often criticized as being computationally expensive, particularly when computing large, rare losses. MCS is also not a convenient tool for computing the sensitivities of each component relative to the reliability of the system (Melchers 1999).

As a result of these drawbacks, this research proposes the use of the First-Order Reliability Method (FORM) to quantify the potential loss to a portfolio of buildings given either a known or probabilistic earthquake scenario. The basic theory behind FORM is to approximate the limit state failure surface by a linearized surface to compute the failure probability. The approximate failure surface is fit to the original limit state at a "design point," which is

characterized by the most likely combination of variables that cause failure. FORM provides accurate results for limit state surfaces without significant nonlinearities, and unlike traditional MCS, is very computationally efficient (Karamchandani and Cornell 1992; Melchers 1999). Sensitivity measures, which provide the relative importance of each variable to the overall loss, are computed directly in the FORM evaluation. These measures are paired with retrofit costs, and used to prioritize the most cost-effective retrofit scheme with respect to reducing portfolio loss.

By evaluating a building portfolio as a system of spatially correlated building components, and using FORM as the basis for evaluating risk to such a system, the distribution of potential losses and system sensitivities can be evaluated. This additional information may be used to further support hazard management and risk-mitigation efforts.

1.2 Objectives

This research aims to develop a consistent, quantitative and realistic earthquake risk assessment framework for building portfolios. The proposed FORM method is intended for public and private entities interested in risk management and mitigation, whether through retrofitting, new construction practices, emergency response planning or public policy initiatives. The framework is intended to be generic, such that it can be adapted to the characteristics of any building portfolio of a selected neighborhood, city or county size.

This new approach offers a probabilistic method for quantifying seismic risk efficiently and analytically. Its development followed from a review of existing earthquake loss estimation methodologies. The use of FORM in the proposed framework offers several advantages when compared to traditional schemes for regional seismic risk assessment. Probabilistically

evaluating loss as a distribution preserves influential system effects (e.g., correlations and scale effects) that influence the variance and confidence thresholds associated with loss to a portfolio. In contrast to existing methods, sensitivities are also easily computed using FORM relative to the change in regional seismic risk for each dollar of retrofit. These sensitivity measures can provide efficient retrofit prioritization methods and therefore decision support on how to optimize investments into risk reducing measures.

The application of the proposed framework is illustrated by assessing the seismic risk of a selected San Francisco building portfolio. FORM is used to evaluate the seismic loss due to structural and nonstructural damage, and resilience faced by the portfolio given a scenario earthquake. It is shown that the inclusion of spatial correlation in seismic intensity has a significant impact on the predicted loss and resilience distribution for the portfolio. The results are compared to the distributions computed using MCS to validate the accuracy and efficiency of the proposed method. Sensitivity measures directly computed in the FORM analysis are used to prioritize mitigation options based on building types within the case study portfolio. In doing so, this dissertation attempts to establish a framework that assists in effective risk-mitigation decision making given regional budgetary constraints.

Throughout this dissertation, it should be noted that the terms “loss” and “risk” may be used interchangeably. For this research, “risk” is defined mathematically as the probability of an event occurring multiplied by the consequence (loss) of that event. While loss does not imply probability, the proposed assessment in this dissertation quantifies loss probabilistically. `

1.3 Outline

The premise of the proposed framework is based on the characterization of a building portfolio as a system of correlated building components. Chapter 2 discusses the parameters involved in characterizing a region as such a complex system. This chapter presents the influences site-to-site correlation of seismic intensities as well as correlation between building properties have on the predicted seismic loss. The influence of critical facilities with respect to their role in the community is also discussed. The chapter closes with the importance and characteristics involved in prioritizing retrofit at the regional level.

Existing methodologies used to predict regional seismic risk and prioritize regional retrofit schemes are presented in Chapter 3. A brief overview of FORM and how it is utilized in the proposed framework is then given, addressing limitations in existing methodologies.

Chapter 4 discusses the identification and development of the variables considered in the proposed reliability framework, along with the formulation and evaluation of portfolio limit state thresholds used to evaluate system loss. The computations required to perform a sensitivity analysis, which is used to prioritize risk-mitigation schemes, are also presented.

The application of the proposed framework to a San Francisco building portfolio is provided in Chapter 5, highlighting the advantages and disadvantages of using the FORM approach. In addition, the influence spatial correlation between building sites has on the estimated regional loss and retrofit prioritization is investigated further.

Finally, Chapter 6 and Chapter 7 include additional applications of the proposed FORM-based framework. The FORM method is extended for quantitatively assessing and enhancing the seismic resilience of a building portfolio. A review of community resilience quantification methods is presented, as well as a proposed extension of the FORM-based method to evaluate

portfolio seismic resilience. The extended method is used to predict the resilience for the San Francisco case study region and prioritize measures to increase seismic resilience through retrofit and decreased restoration time. In Chapter 7, the proposed FORM-based loss estimation tool is extended to assess multi-hazard regional risk due to earthquake and hurricane winds. This chapter includes an overview of multi-hazard risk assessments and presents an introductory example application used to predict multi-hazard risk for Charleston County, South Carolina.

Chapter 2. Characterizing a Portfolio as a System

Given the critical role risk management and mitigation decisions play in the economic and social prosperity of seismically-active regions, it is important that the estimates of potential loss on which these decisions are based are as accurate and comprehensive as possible. Loss estimates are often characterized by two quantities: the expected value and the variance of losses. Many commercial loss assessment tools, such as HAZUS-MH, use the expected value of economic losses, casualties, etc. as the measure of risk. Although in a risk neutral context, minimizing expected losses is consistent with maximizing utility for a region (von Nuemann and Morgenstern 1944), the uncertainty around this loss is not quantified. According to Schubert and Faber (2012), decision makers often prefer decisions that yield a low probability of experiencing large losses. This is captured only by including the uncertainty in loss, and can be represented by a probabilistic distribution. This distribution, which is typically presented in the form of a loss exceedance curve, includes the effects of uncertainties as well as the correlations that exist between the components of a system.

Similarly, the performance of a building portfolio is determined by the performance of the individual buildings and the spatial correlations that exist between the building performances.

These correlations, paired with uncertainties in the loss assessment process, characterize the variance in the collective loss probability distribution for a suite of buildings. Such correlations may be a result of effects from an earthquake affecting more than one building in a portfolio simultaneously. This is a function of the spatial distribution of the group of buildings, where each building site may share common hazard source or site effects.

To understand the influence these spatial correlations have on a loss distribution, consider a large group of buildings with uncorrelated distributions of loss (e.g., repair costs) for any future earthquake event. The distribution of potential portfolio loss is based on the summation of losses for each building. In this case, the expected total loss $E(TL)$ is equal to the summation of expected losses at each building site, i. When the building losses at each site are independent, it is expected that some buildings within the portfolio will experience higher than average losses in a given event, while others will experience lower than average losses. Therefore, when there is a large number of buildings, the expected total loss is approximately equal to the summation of losses at each site (l_i) for a given event. This is written as:

$$E(TL) = \sum_i E(l_i) \approx \sum_i l_i \tag{2.1}$$

On the other hand, if the performances of individual buildings are strongly positively correlated, the portfolio may experience losses that are skewed primarily either higher or lower than average for a given event. Therefore, the variance of the predicted losses is much greater than if there was no correlation considered between buildings. The variance of the total loss can be expressed as:

$$V(TL) = \sum_i V(l_i) + 2 * \sum_{i<j} \sum_j COV(l_i, l_j) \tag{2.2}$$

where $COV(l_i, l_j)$ is the covariance matrix, and is a function of the correlation between at sites i and j. Figure 2.1 provides an illustration of a representative loss distribution and loss exceedance curve for a portfolio with and without spatial correlation considered.

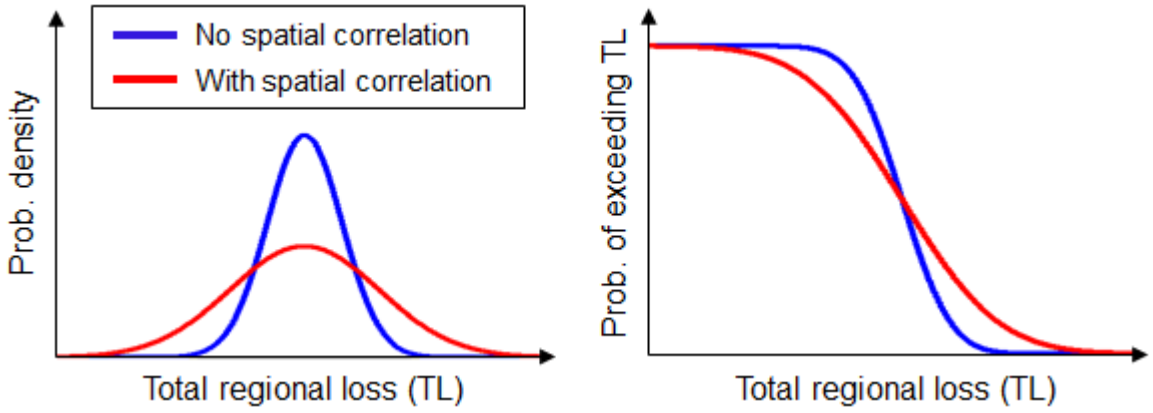

Figure 2.1: Representative loss distribution and loss exceedance curves for a portfolio with and without spatial correlation considered.

Equation (2.2) and Figure 2.1 demonstrate the importance of considering correlations between building performances for understanding the real performance of a portfolio and determining accurate probabilistic loss results. The following sections provide a detailed review of the sources of correlations that exist within a building portfolio, as well as their effects on the portfolio loss assessment.

2.1 Correlation in Ground Motion Intensities

Recent studies have demonstrated that consideration of spatial correlation in seismic intensities across a region is essential for the estimation of seismic loss for a portfolio given a scenario or probabilistic earthquake event (Baker and Cornell 2006; Bazzurro and Luco 2005; Goda and Hong 2008; Park et al. 2007; Schubert and Faber 2012; Sokolov and Wenzel 2011).

Three main sources contribute to the correlation between seismic demand at two sites: 1) ground shaking generated by the same earthquake; 2) commonality in the seismic wave paths from source to site (attributed to similar site locations and fundamental building periods); and 3) similarities in site soil properties.

Ground motion models used to predict the joint occurrence of ground motion intensities at several sites take the following form (Jayaram and Baker 2008):

$$\ln\left(S_{a_{ij}}\right) = \ln\left(\bar{S}_{a_{ij}}\right) + \sigma_{ij}\varepsilon_{ij} + \tau_j\eta_j \tag{2.3}$$

where $S_{a_{ij}}$denotes the spectral acceleration at the period of interest at site *i* during earthquake *j*, $\bar{S}_{a_{ij}}$ is the predicted median spectral acceleration determined by ground motion prediction equations (GMPEs; e.g., Abrahamson and Silva 2008; Boore and Atkinson 2008; Campbell and Bozorgnia 2008; Chiou and Youngs 2008; Idriss 2008), ε_{ij} and $\eta_j$are the normalized intra- and inter-event residuals (also referred to as "error" terms), and σ_{ij} and τ_j are the corresponding standard deviations of the residual terms, also determined by GMPEs. Inter-event residual terms measure the variability in seismic intensity values specific to each earthquake event and building period, whereas intra-event residual terms measure the variability in seismic intensity at each building site.

Modern GMPEs implicitly recognize the first source of ground motion correlation by assuming that the inter-event residual term (η_j) computed at any particular period is constant across all sites for each earthquake event. The shared characteristics from a common earthquake event are likely, however, to have similar effects on resulting seismic intensities at sites with different building periods (Baker and Cornell 2006; Jayaram and Baker 2008; Park et al. 2007). To predict this correlation in seismic intensity within an earthquake event, Baker and Cornell

(2006) developed an empirical model to estimate inter-event correlation as a function of the similarity in two building periods.

Intra-event variability, represented by the normalized residual term ε and standard deviation σ, is attributed to a commonality in seismic wave paths and similarities in distance from fault asperities. In the past decade, many studies have proposed mathematical models to compute correlation between intra-event residual terms as a function of inter-site distance (Goda and Hong 2008; Jayaram and Baker 2009; Wang and Takada 2005) and dissimilarities in building period (Baker and Cornell 2006; Loth and Baker 2012). The many past studies have shown that two closely spaced sites often have highly correlated intensities, tending to be higher or lower than the expected intensity for a given event. Correlation decreases with increasing distances, but may still be present in distances up to 100km (Park et al. 2007). Inter- and intra-event correlation also generally decrease with an increasing dissimilarity in site period, although Baker and Cornell (2006) have demonstrated a few instances when this is not the case.

Many researchers have examined the influence of spatial correlation between seismic intensity residual terms on regional loss estimation studies (Jayaram and Baker 2010a; Miller et al. 2011; Park et al. 2007; Schubert and Faber 2012). Park et al. (2007) predicted seismic-induced losses for a suite of buildings and showed that neglecting spatial correlations in ground motion intensity leads to underestimation of rare, large losses and overestimation of frequent, small losses. As such, the total potential loss for a building stock given an earthquake has a larger variance than the total loss predicted when spatial correlations are ignored. Other loss estimation studies listed above came to a similar conclusion, which is consistent with the mathematical relationship provided in Equation (2.2).

Soil properties also tend to exhibit a strong spatial correlation structure, which may influence the spatial correlation between building performances in an earthquake event (Baise et al. 2006; DeGroot and Baecher 1993; Thompson et al. 2006, 2010). Studies suggest that, similar to correlation in seismic intensity, the spatial correlation between soil properties is high at small separation distances and decreases with increasing distance between sites. Specifically, time-averaged shear-wave velocity averaged over a depth of 30m (V_{S30}), used for site amplification in computing expected seismic intensities in GMPEs, is shown to be spatially correlated for inter-site distances exceeding 4km (Thompson et al. 2006). This correlation is due to similar soil properties in a given location as well as shared uncertainties in V_{S30} predictions as a result of the inherent variability in soil deposits, and in sampling and testing errors.

To compute this spatial correlation, Thompson et al. (2006) fit a semivariogram model (used to measure dissimilarities between values) to V_{S10} values (averaged shear-wave velocity to 10m), but their study lacked sufficient data to conclusively model spatial correlation in V_{S30} values. Testing results in the San Francisco Bay area show, however, that the spatial correlation in V_{S30} measurements is greater than that of V_{S10} at all inter-site separation distances (Thompson et al. 2006). In a later study by Thompson et al. (2010), spatial correlation in V_{S30} is extrapolated from a semivariogram model for S_{S30} spatially distributed values, which measure the average S-wave slowness (i.e., inverse of velocity for transverse or shear waves) to 30m depth. The influence that V_{S30} spatial correlation has on portfolio loss assessments is examined in Chapter 5.

2.2 Correlation between Building Types

In addition to correlations in hazard intensity between sites, correlations between building performances also arise from similarities in building properties. These may be properties of

shared basic characteristics of two structures, such as similarities in the lateral force resisting system, building material, number of stories or construction period. Estimated building performance in seismic design codes is based on the observation that different types of buildings categorized into a particular building class have experienced similar performance in earthquakes. This leads to the assumption that similar structures built within the same time frame will share comparable performance behaviors (Bazzurro and Luco 2005).

This type of building-to-building correlation and its influence on regional loss assessments was further investigated by Debock et al. (2013). In this study, the authors quantified the spatial correlations between building responses in historical and simulated earthquake scenarios and related the nature of these correlations to similarities in seismic intensity and building response characteristics. Their analysis demonstrated that correlations between the natural logarithm of the spectral acceleration at the first-mode period ($\ln S_a$), and the natural logarithm of a variety of engineering demand parameters used to capture the building response ($\ln EDP$), are very similar. This suggests that the observed or predicted ground motion intensity paired with a single building property, e.g., the fundamental building period, provide critical insight into the spatial correlation in structural response for a suite of structures. These results also show that the nonlinearities present in the relationship between spectral ordinates and structural response parameters do not significantly affect the spatial correlation in building response behavior. Therefore, the spatial correlation between seismic intensity variables used in this study is considered sufficient to capture the spatial variation in building response.

Other characteristics that may influence the building-to-building correlation include whether structures are built by the same construction or design firm, which may assume a similar application of design or construction techniques. This is often the case in bridge networks as

similar contractors are often used in each state and/or federal transportation departments. As a result, different types of structures may all perform weaker or stronger than predicted for structures of that class. This was the case in the 1988 Spitak earthquake where at least 25,000 people were killed, 19,000 injured and 500,000 left homeless, primarily as a result of poor construction practices (Brand 1988). It is assumed that this type of duplicate construction or prevalence of poor construction does not exist in most community centers, cities or counties. This type of correlation is therefore not considered in the proposed loss estimation framework; however, it could be added to the assessment if such information is available.

Other building-to-building correlations may exist as a result of physical interaction between building performances. In particular, structure-soil-structure behavior may provide a significant source of dependency between building performance, and warrants future investigation to quantitatively model this phenomenon in the proposed approach (Lou et al. 2011).

An additional level of correlation, or better referred to as a 'bias' in the loss estimation process, results from systematic differences or classifications in models used to assess loss. For example, this may be a function of consistent differences between the hazard model used in the loss assessment and the actual state of nature. In addition, this bias may be introduced by classifying different buildings into representative building categories. For example, the proposed method adapts a similar classification scheme that is used in HAZUS-MH, such that buildings are classified by building type (i.e. structural framing type), occupancy category, number of stories and construction period. Therefore, the same epistemic uncertainties involved in modeling the performance of a specific structure type may simultaneously influence the loss prediction of a large number of different buildings in that class. This bias may introduce an

additional correlation between building performances that consequently increases the variance in total portfolio loss. The modeling and classification assumptions that address this bias are discussed in Chapter 5.

2.3 Community-Related Dependencies

In addition to immediate portfolio losses, there are secondary impacts that greatly influence the total loss and seismic resilience of a portfolio. These may be quantified as economic or social losses accrued over time based on the time period of building downtime and recovery. Such losses are influenced significantly by the interdependence between the physical, economic and social infrastructure units within a system. In this study, infrastructure units refer to the physical, social and economic assets of each building, though, they can also be representative of any type of infrastructure system. The concept of seismic resilience and how it is quantified using the proposed framework will be further discussed in Chapter 6. This section focuses instead on the sources of these community-related dependencies and their influence on portfolio loss and resilience.

The interdependence between infrastructure components is related to the reliance one infrastructure unit has on a service provided by another. Failure in a system can significantly affect the function of many other dependent systems. This produces the risk of cascade failure, which may have serious consequences for a region. According to Robert et al. (2013), in order to anticipate and limit the consequences of this 'domino effect' phenomenon, it is necessary to understand fully how infrastructure systems are related and dependent on one another.

One of the most notable infrastructure interdependencies is prevalent in utility and transportation lifelines. In post-disaster situations, relief operations require well-functioning

systems for transport, electricity, water supply, communications, etc. If any of these systems fails, the performance of other systems, as well as regional response and recovery actions, may be affected greatly.

Infrastructure interdependence plays a large role in the assessment of time dependent losses and resilience specific to a suite of buildings. Residents of a community depend on regional businesses based on employee pay, and the supply of goods and services. By comparison, businesses depend on residents based on their employment and demand for goods and services (Lindell and Prater 2003). If there is an excessive amount of loss to residential, commercial or industrial buildings within a portfolio, those dependent on the functioning of these buildings will also be affected. In addition to business-related losses, the loss of certain building types may also jeopardize dependent industries such as tourism, healthcare, education and recreation.

The level of interdependence between building assets is specific to the spatial, economic and social configurations of a region (Cimellaro et al. 2010; Rinaldi et al. 2001). For example, critical facilities (e.g., hospitals) located in different communities may have different interdependence relations, which influence the magnitude of post-disaster losses and recovery periods. For example, large interdependence may exist between hospitals in a region with only two medical facilities, because the failure of one unit may significantly impact the operation of the other. In contrast, in a region with many hospitals, the interdependence between units may not be as significant.

A review of studies that examine these community-related dependencies and their influence on regional loss and resilience is provided in Oh et al. (2010). Since the primary focus of the proposed framework is estimating repair costs due to structural and nonstructural damage

following a hazard, the predicted losses are not influenced by these community-related interdependencies. Future research on the resilience assessment presented in Chapter 6, however, will require further investigation into incorporating this type of dependency.

2.4 Prioritization of Retrofit

In a building-by-building analysis, structural and cost-benefit analyses can be performed to gauge the effectiveness of retrofit for each individual structure. Community and public policy decision makers are often interested, however, in managing and mitigating these vulnerabilities at a regional level (Porter 2013). While retrofitting every vulnerable building would reduce regional seismic risk, it is likely prohibitive based on available resources, constituency budget constraints and general community opposition (as a result of mandates on owners, ripple effects on tenants, etc.). Therefore, when budgetary constraints restrict the number of buildings that can be retrofitted, the existing resources must be allocated to the most effective retrofit schemes in terms of reducing regional risk.

Prioritizing the effectiveness of retrofit strategies at a regional level often involves a cost-benefit analysis to gauge the reduction in seismic risk (benefit) for each dollar spent on retrofit (cost). A sensitivity analysis can be performed to capture changes in regional loss with respect to specific retrofit regimes for an individual building or class of buildings, and then further utilized to rank cost-benefit ratios of each retrofit task (see Section 4.4). In a probabilistic context, such sensitivity measures capture the change in the probability of exceeding a regional loss threshold per dollar of retrofit. Since correlations are shown to influence the distribution of loss, this would also affect the magnitude and ordering of sensitivities computed relative to exceeding loss thresholds not equal to the expected loss. Consequently, this may skew retrofit prioritization for

regions interested in reducing the probability of exceeding higher or lower than expected loss levels. The influence this correlation has on the ranking retrofit schemes is further explored in the case study presented in Chapter 5.

Chapter 3. Methodologies

3.1 Existing Earthquake Loss Estimation Methods

The prediction of seismic risk for a building portfolio is vital for effective risk mitigation, emergency response, public policy and insurance management. Loss estimation tools used to predict such risk can be either based on regional or site-specific loss assessments. Site-specific studies evaluate hazard-induced losses for a single site, while regional loss evaluation tools estimate losses for a particular quantity of components. These components may include a building portfolio, transportation network or utility system located within a specific region, such as a city, county or state.

As discussed in the previous chapter, estimating regional loss as a probability distribution is not only a function of individual component losses, but also of the additional uncertainties and correlations that exist between components. In earthquake loss estimation, these uncertainties exist in the seismic hazard, structural behavior, damage and loss functions, and must therefore be included for accurate modeling of the potential regional loss induced by a hazard.

This section offers a review of existing earthquake loss estimation methodologies, along with a discussion of their respective advantages and disadvantages. While this overview is by no means exhaustive, it is intended to highlight areas in existing methodologies that may benefit

from additional work. These are then investigated further in the development of the FORM-based approach proposed in this dissertation. It is recognized that there are existing propriety loss estimation models developed by consulting and reinsurance firms such as EQECAT, Risk Management Solutions (RMS) and AIR Worldwide. Since limited information is available on these methods, this section will focus on publicly available commercial models and academic studies.

The earliest hazard loss estimation tools based empirical modeling of future damage and loss on information garnered from past hazard events. One of the first empirical methods was developed by Freeman (1932), who used previous recorded earthquake damage to develop rough estimates of future earthquake loss for insurance planning. Most regional hazard loss assessments were performed within the insurance industry until the early 1970's, when a series of regional loss studies were conducted for the United States federal government to study the hazard impact on essential facilities. Using an interdisciplinary group of experts in seismology, geology and structural engineering, Algermissen et al. (1972) estimated the damage and losses given a major earthquake occurring in the San Francisco Bay Area, Los Angeles, Salt Lake City and Puget Sound. The estimated losses, although deterministic, were based on several empirical relations between collected loss data and casualties.

The first probabilistic earthquake loss assessment was performed by Steinbrugge et al. (1969), who developed percentage losses using fuzzy-based matrices to relate construction classes and seismic intensities with damage ratios. Whitman et al. (1973) introduced the concept of damage probability matrices, where damage was quantified as a damage ratio and the intensity of ground motion was in terms of the Modified Mercalli Intensity (MMI). Similarly, the Applied Technology Council published the study ATC-13 (ATC 1985), which characterized ground

motions based on MMI, and used probabilistic damage matrices to estimate future losses. ATC-13 was also one of the first systematic tools to incorporate expert opinion in the earthquake loss estimation process.

By the mid 1980's, numerous other loss estimation tools were developed, primarily for disaster preparedness. Reitherman (1985) provided a summary of over 30 existing earthquake loss estimation tools, which included a description of the input data, analysis type and output of each method. Most methods require the ground motion intensity input in terms of MMI. Employing either probabilistic or empirical relations, the output of such methods is expressed as regional dollar loss estimates, casualty estimates or qualitative vulnerability ratings.

With the advancement of methods used to predict hazard losses and the expanding user base, there was increasing need for consistency between each method. As a result, FEMA-177 (1989) and FEMA-249 (1994a) were developed to provide guidelines for a consistent and standardized loss estimation framework based on an extensive review of existing methodologies. Both reports brought attention to the fact that previously available loss estimation studies did not properly incorporate uncertainty associated with the seismic hazard. From these findings, a standardized regional loss estimation methodology was developed that measured ground motion shaking quantitatively though elastic spectral intensities, as opposed to qualitative ground motion measures such as the MMI (NIBS 1997). This tool, introduced under the name HAZUS-MH, is one of the most widely used public regional loss assessment methodologies today.

HAZUS-MH is a GIS-based software tool developed for the U.S. Federal Emergency Management Agency (FEMA) to assess the consequences due to earthquake, hurricane, or flooding scenarios (NIBS 2012). The software is divided into several interdependent modules for assessing the physical, direct and indirect economic, and social consequences given a hazard

occurrence at a specified region of interest. Pre-established capacity and fragility functions are provided for 36 building types based on lateral force resisting system and building material (e.g., concrete moment frame) and 33 occupancy categories (e.g., multi-family dwelling). These are further subdivided by number of stories and construction period.

In the HAZUS-MH framework, the economic losses associated with structural and nonstructural consequences are computed as the summation of expected repair costs for each building type and occupancy category combination. This output represents the mean loss that is expected to occur given an earthquake event. While the expected consequence for regional building and infrastructure systems is often used in loss estimation methodologies, it does not include information about the distribution of loss. By only considering the expected loss, the assessment also excludes the correlations that exist between building performances. As discussed in the previous chapter, this can lead to suppressing important system effects when estimating loss distributions and prioritizing retrofit for infrastructure and building systems.

INLET (Internet-based Loss Estimation Tool) is the first online real-time loss estimation system developed by ImageCat as a part of the NSF-sponsored RESCUE project (Huyck et al. 2006). Using simplified HAZUS-MH damage functions and building inventory information, INLET can be used to estimate regional building damage, transportation impacts and causalities in the Southern California region minutes after an earthquake event. The primary advantage is that it is geared to be a more simplistic and flexible tool than HAZUS-MH, and can be constantly updated for "real-time" loss assessments. Similar to HAZUS-MH, INLET estimates loss based on its expected value.

The assessment of seismic risk is also a subject well-covered in many academic studies that utilize probability- and reliability-based methods to estimate regional loss. Bayraktarli and

Faber (2007) developed a risk assessment framework using Bayesian Probabilistic Networks (BPNs) categorized by modules for the seismic hazard, soil failure, damage and consequences given an earthquake. Use of BPNs enables explicit modeling of dependencies between variables, and in this study, the authors include correlation between peak ground acceleration values (used in liquefaction analysis) and spectral displacement intensities (used in structural damage analysis). Site-to-site correlation in ground motion intensity parameters, however, is not included. Similarly, Bensi et al. (2009) employ BPNs to quantify seismic loss for a transportation. In this study, the spatial correlation between seismic intensities at each network component is included.

Mahsuli and Haukaas (2011) developed a loss assessment software tool that utilizes first- and second-order reliability transformation methods to compute loss distributions for large portfolios of buildings given a probabilistic earthquake or multi-hazard scenario. This study computes loss based on regional and building-specific models. The regional model uses an empirical relation to compute the total regional repair cost as a function of seismic demand and other regional model parameters. The building-specific models estimate loss by evaluating building response, damage, and finally repair cost based on finite element analyses and damage estimates. Some correlation between the seismic intensity among sites is included inherently in modeling the magnitude and location of the hazard relative to the sites. There is no further inclusion, however, of site-to-site correlation in residual terms based on site separation distance or commonality in seismic wave paths to spatially distributed building sites within a region.

Another widely used method for estimating regional loss is through Monte Carlo Simulation (MCS). Jayaram and Baker (2010a) developed a simulation-based framework to evaluate the seismic risk posed to a lifeline network. A catalog of spatially correlated seismic

intensity maps are generated using importance sampling, and paired with fragility functions to assess the total disruption in lifelines given a seismic event. The simulation-based ground motion generation developed by Jayaram and Baker (2010a) was also used in a lifeline risk assessment study that utilized first-order reliability techniques as a means of overcoming the drawbacks of simulation (Miller et al. 2011). In this method, two random variables are assigned to each component of the lifeline network to model the corresponding seismic demand and structural capacity. The limit state for the network is defined as the total reduction in function flow for the network. The theory behind such seismic demand and capacity random variable assignments for each site is a key attribute of the method used in this dissertation.

In each of the existing loss estimation methods listed, it is noted that expanding loss computations from the expected value to a probability distribution of loss is a noteworthy advancement for recent and future studies. In addition, an analysis providing sensitivities in system loss relative to each input component is another valuable attribute to add to most assessment methods. It is recognized that ease of use and availability of building input data are also desirable characteristics. In the coming discussion, each of these characteristics will be addressed relative to the capabilities of the proposed FORM-based loss estimation method presented in Section 3.3.2.

3.2 Existing Mitigation Prioritization Methods

The loss estimation methodologies presented in the previous section demonstrate how the ability to forecast the potential hazard-induced loss to a region is improving continuously. This provides an opportunity for policy initiatives to focus on pre-disaster risk mitigation, particularly through structural retrofit. Budget and other resource constraints, however, limit which

vulnerable buildings within a region are to be retrofitted to desirable levels of seismic resistance. For optimal regional risk mitigation given limited resources, it is essential to prioritize vulnerable buildings that will yield the most effective, risk-reducing retrofit strategy. In fact, regional jurisdictions are now requiring retrofit prioritization to receive mitigation funding. For example, the Federal Emergency Management Agency (FEMA) Disaster Mitigation Act of 2000 now mandates state and local governments to prioritize cost-effective mitigation actions in order to receive Hazard Mitigation Grant Program funds (FEMA 2002).

Prioritization of risk-mitigation measures must evaluate the benefits of mitigation, such as reduced damage costs, limited housing displacement, or fewer deaths and injuries, against the costs. In many cases, this is simply a comparison of dollars to dollars. Benefit-cost analysis (BCA) methodologies have been performed to assess the future savings resulting from FEMA mitigation grants from 1993 to 2003 (Rose et al. 2007). In addition, several past studies have employed BCA assessments to identify and rank potential retrofit schemes for reducing the seismic vulnerability to individual structures (e.g., FEMA 2009a; Liel and Deierlein 2013; Padgett et al. 2010; Porter et al. 2006; Smyth et al. 2004; Takahashi et al. 2004).

A number of studies have also focused on mitigation prioritization at the regional level for building and other infrastructure components. Visual screening methodologies such as FEMA-154 (1988) have been used to identify, inventory and rank buildings vulnerable to seismic hazards. Grant et al. (2007) integrated an analytical structural vulnerability assessment with visual inspection to prioritize seismic retrofit for school buildings in Italy. Tesfamariam and Saatcioglu (2008) developed a ranking scheme for older reinforced concrete buildings using a fuzzy-based modeling assessment for building vulnerability. In a series of papers by Dodo et al.

(2005, 2007) building retrofit schemes are evaluated for optimal retrofit spending using linear programming techniques.

Most of the studies used to prioritize retrofit and reduce uncertainty use a "one-factor-at-a-time" (OAT) method (Saltelli et al. 2006). In such an approach, a variable (representing a mitigation alternative) is modified as desired while others are fixed to assess its relative sensitivity with respect to the overall loss of the system. While this approach is straightforward, drawbacks that may result from using this approach include: 1) most simulation models used to run this type of analyses for a large set of mitigation alternatives are complex, computationally expensive and often unmanageable; 2) there may be a large uncertainty associated with performing a such an analysis with and without a variable change in a probabilistic assessment; and 3) these approaches may not account for simultaneous variations in inputs that may result from correlations between variables. In addition, many retrofit prioritization methods only focus on the expected value of losses and benefits, without consideration of the variance or spatial correlation of losses and benefits within a region. This may influence the prioritization of retrofit when it is desired to minimize loss other than the expected value.

Many of these limitations can be addressed using a local sensitivity analysis to identify and rank effective retrofit schemes (Morio 2011). These involve taking the partial derivative of the output, Y, with respect to each input variable distribution, X, in each dimension. This is written mathematically as:

$$\delta_i = \frac{\partial Y}{\partial X_i} \tag{3.1}$$

where δ is the sensitivity measure with respect to variable X at a single point. As will be discussed in Section 3.3.1, these partial derivatives can be computed simultaneously for each

input variable within reliability evaluation techniques such as FORM.

Many studies focused on the retrofit prioritization of bridge and lifeline networks have employed such a sensitivity analysis based on seismic vulnerability and strategic importance of each network component, but often without consideration of retrofit cost (Lee et al. 2009; Lee and Kiremidjian 2006; Miller et al. 2011). In addition, Riederer and Haukaas (2007) utilize this type of analysis to identify the most cost efficient improvements to structural parameters within a building system to reduce roof drift.

To the author's knowledge, Mahsuli and Haukaas (2013) are the first to employ a local sensitivity analysis to prioritize buildings for retrofit within a portfolio. While the analysis used in Mahsuli and Haukaas (2013) is similar in its general definition to the one proposed in this paper, the random variables used to define the reliability problem for a building portfolio are modeled differently. In addition, the method presented in this study makes two important extensions: 1) it accounts for spatial correlation in building performances across a region and investigates the influence this has on retrofit prioritization; and 2) it examines the implications a chosen level of loss to be mitigated has on optimal mitigation prioritization for other loss thresholds. An overview of the sensitivity analysis method proposed in this dissertation to prioritize mitigation is presented in Chapter 4.

3.3 Proposed Framework

To add to the state-of-the-art in loss estimation and retrofit prioritization methods, this dissertation proposes a new FORM-based framework to probabilistically estimate the total seismic-induced loss to a building portfolio. This section first reviews the applications and theory

behind FORM, then discusses the advantages and disadvantages of using this type of reliability evaluation method for estimating regional loss.

3.3.1 First-Order Reliability Method (FORM)

FORM is one of many structural reliability methods used to probabilistically evaluate the performance of structures. Performance expectations, typically in the form of limit states, must be specified in order to gauge how a structure will perform. In basic structural design, performance criteria include structural safety and serviceability limit state requirements. These limit states are formulated as a function of the loading and structural properties that define the reliability problem.

In structural reliability, the parameters that represent the magnitude and uncertainty in demand and capacity of a problem are modeled with probability density functions. These components are referred to as random variables, as opposed to deterministic values. Each is modeled by the probability distribution that best fits the respective uncertainty in each component. The parameters that define the distribution, such as a mean and standard deviation, are included in the reliability assessment.

Figure 3.1 demonstrates this concept by illustrating a basic structural engineering problem comprised of two variables: 1) the load effect, *S*, used to model the effect an imposed load has on a structure; and 2) the resistance variable, *R*. Each variable is represented by a probability density function, $f_S(s)$ and $f_R(r)$, and the combination of both variables characterize the joint bivariate distribution, $f_{RS}(r, s)$.

As with most safety performance checks in structural engineering, failure of the structure results when the load effect is greater than the structural resistance. Therefore, the limit state associated with failure, $G(R, S)$, can be written as:

$$G(R,S) = R - S = 0 \tag{3.2}$$

The probability of failure, $P(F)$, associated with this limit state can be written as:

$$P(F) = P(G(R,S) \leq 0) = P(R - S \leq 0) \tag{3.3}$$

The probability of failure is represented by the volume under the joint density function on the failure side of the limit state, indicated by the red region in Figure 3.1. This probability can be calculated using a variety of methods, including direct integration, numerical approximate methods, simulation and approximate transformation methods. Using direct integration, the failure space (i.e., failure probability) shown in Figure 3.1 can be evaluated as:

$$P(F) = \int_D \int f_{RS}(r,s)\, dr\, ds \tag{3.4}$$

where *D* represents the failure domain. When *R* and *S* are independent, Equation (3.4) can be written as:

$$P(F) = \int_{s=-\infty}^{s=\infty} \int_{r=-\infty}^{s} f_R(r)\, f_S(s)\, dr\, ds \tag{3.5}$$

and expressed by the single convolution integral:

$$P(F) = \int_{-\infty}^{\infty} F_R(x)\, f_s(x)\, dx \tag{3.6}$$

where F_R is the cumulative distribution function for *R*.

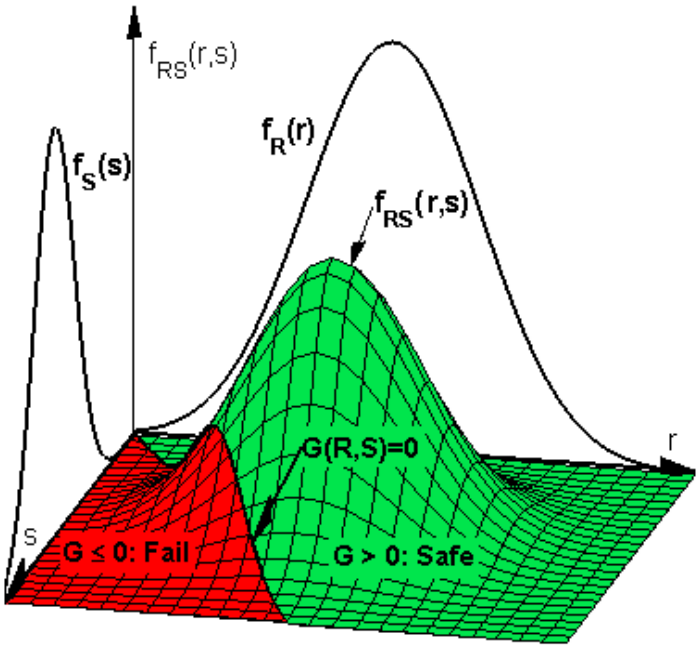

Figure 3.1: Bivariate density function characterized by a load effect random variable, *S*, and resistance variable, *R*.

When *R* and *S* are not independent, or when there are more than two random variables, it is rare that the failure probability can be integrated analytically in closed form. In such cases, approximate numerical methods can be used in place of direct integration, but these methods are only feasible for reliability evaluations with a small number of random variables ($n \leq 5$) (Melchers 1999). Simulation techniques such as Monte Carlo Simulation, in contrast, can provide accurate reliability evaluations, and are often used in loss estimation studies for high-dimension problems. As mentioned previously, however, simulation is often criticized for being computationally expensive, although adaptive simulation methods can improve this efficiency significantly. Moreover, simulation does not capture component sensitivities easily in a reliability assessment (e.g., Melchers 1999).

As a result of these draw-backs, reliability transformation methods, stimulated by the work of Cornell (1969), gained popularity. These methods provide an approximate, yet analytical

and efficient technique to evaluate the reliability of a structure. They have been refined and extended in their applications, and have become among the most widely used reliability evaluations in practical engineering design (Karamchandani and Cornell 1992; Zhang and Du 2010). Reliability transformation methods provide the foundation for the probability-based partial safety factor design codes in use today, building from one of the first risk-based publications by Ellingwood et al. (1980).

An advantageous first step for using transformation methods is converting each random variable to its standardized, normal form, with zero mean and unit standard deviation. In addition, if any correlations exist between random variables, an additional transformation is used to decouple the random variables (e.g., Rosenblatt 1952). The result of this transformation is illustrated by a basic reliability problem characterized by random variables y_1 and y_2, shown in standardized, normal, uncorrelated space in Figure 3.2.

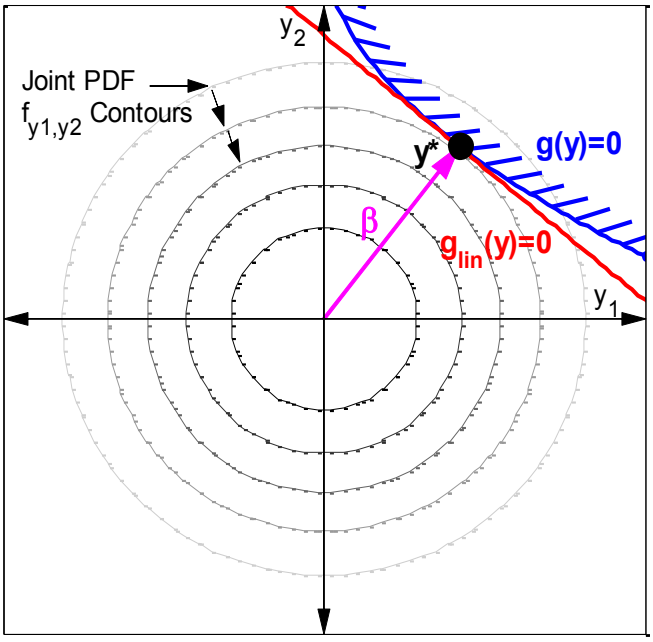

Figure 3.2: Probability density function contours for bivariate distribution f_{y_1,y_2} in standardized space. The design point y^*, β vector, and original nonlinear and linearized limit states are shown relative to an arbitrary limit state threshold.

The reliability index, β, represents the shortest distance from the origin to the original limit state surface, $g(y) = 0$. This index can be computed by minimizing the following equation:

$$\beta = \min \sqrt{\sum_{i=1}^{n} y_i^2} \tag{3.7}$$

where y_i represents the coordinates of any point on the limit state surface in n-dimensional reliability space and *n* refers to the number of random variables in the reliability problem.

The point on the limit state surface with the shortest distance to the origin is called the 'design' or 'checking' point. This point, labeled y^* in Figure 3.2, is associated with the largest probability content under the bivariate density function, f_{y_1,y_2}, on the failure side of the limit state. The failure probability assumed by first-order transformation methods is represented by the probability content on the failure side of a linearized limit state fit tangent to the actual limit state at the design point. This is shown by the red line labeled $g_{lin}(y) = 0$ in Figure 3.2. The failure probability can then be evaluated as:

$$P(F) = \Phi(-\beta) \tag{3.8}$$

where $\Phi(\,)$ is the standard normal cumulative distribution function. Since failure is evaluated based on linearization, first-order methods provide an exact measure of failure probability for problems with linear limit states in standardized space (shown in Figure 3.2), and an approximate method for those with nonlinear limit states. Assuming *R* and *S* in the reliability problem shown in Figure 3.1 are normal, failure probability can be related directly to β with the following equation:

$$P(F) = P(R - S \leq 0) = P(Z \leq 0) = \Phi\left(\frac{0 - \mu_z}{\sigma_Z}\right) = \Phi(-\beta) \tag{3.9}$$

where $Z = R - S$ and $\beta = \mu_z/\sigma_Z$. In this case, "normal" implies preservation of a linear limit state when transformed to standardized space

The simplest reliability transformation method is called the First-Order Second Moment (FOSM) method. FOSM considers only the first two moments of each random variable, the mean and standard deviation. This is the equivalent of representing each random variable by a normal distribution. By comparison, the First-Order Reliability Method (FORM) is capable of incorporating non-normal variables into the reliability analysis with one additional transformation. This involves transforming the random variables to normal reliability space, thus inherently distorting the shape of the limit state surface. The Second-Order Reliability Method (SORM) follows a similar approach, but estimates failure probability based on a fitted second-order approximate limit state surface (Melchers 1999). The increase in accuracy with each of these methods is specific to the reliability problem of interest.

Each transformation method is applicable to higher dimensions. When using FORM in higher dimensions, a hyper-plane limit state, as opposed to the 2-D limit state threshold shown in the figures above, is evaluated at a design point. It is possible, however, that the approximations inherent in linearizing or fitting a second-order surface to a limit state in high-dimension space may induce significant error. This approximation is explored further in Section 4.5.

Since FORM computations often employ a gradient-based algorithm to minimize β in Equation (3.7), additional information is also provided as to the sensitivity of the system with respect to each random variable. A set of simultaneously derived sensitivity measures provide

the order and magnitude of sensitivities of the computed reliability with respect to the random variables that compose the reliability problem. Similar to Equation (3.1), these are computed as:

$$\delta = \frac{\partial \beta}{\partial X} \tag{3.10}$$

where δ is the sensitivity measure with respect to random variable parameter X and β is the output of the reliability assessment.

3.3.2 Proposed Framework Objectives

Using FORM, as described in the previous section, this dissertation establishes a new, robust framework for the comprehensive and efficient assessment of building portfolio earthquake risks. With the characteristic advantages of using FORM for the proposed approach, this research builds on the capabilities of current methodologies presented in Section 3.1 by accomplishing the following:

1. Analytical computation of failure probability
2. Probabilistic evaluation of risk
3. Explicit modeling of spatial correlations between variables
4. Computational efficiency
5. Easy computation of sensitivity measures

These advantages are further discussed below with respect to the added capabilities in using FORM.

Analytical computation of failure probability

FORM provides an approximate, yet analytical means of quantifying the distribution of regional loss. Section 4.1 presents how each random variable used to characterize the hazard

demand and structural response is expressed as a closed-form distribution. The ability to analytically characterize and quantify portfolio loss is considered advantageous to simulation since it provides a mathematical relationship between random variable inputs and the evaluated reliability.

Probabilistic evaluation of risk

Demand and capacity variables are included in the reliability analysis as probability distributions to model the uncertainty among these variables. Using these random variables, FORM computes the probability of loss exceeding a predefined arbitrary threshold. The probability distribution of loss is then computed by evaluating the reliability associated with varying severities of loss thresholds. Unlike many existing loss estimation tools that compute loss based on the expected value, evaluating the distribution provides additional information about the uncertainty in potential loss, which can assist in risk management decision making.

Explicit modeling of spatial correlations between variables

FORM is capable of including the spatial correlations that exist between building performances, which are shown to significantly influence the variability in regional loss estimates. In this study, this spatial correlation is modeled based on the correlation in seismic intensity, as detailed in Section 2.1. This is computed and tabulated in the form of a correlation matrix relative to the seismic intensity random variables for each site of interest. FORM employs one additional transformation to decouple the correlated variables to an uncorrelated space to facilitate the reliability evaluation.

Computational efficiency

This is one of the most notable advantages to using FORM (Karamchandani and Cornell

1992; Zhang and Du 2010). FORM analyses often employ a gradient-based algorithm for computing the design point based on Equation (3.7). Unlike MCS, the required computation time is often independent of the likelihood of failure. It is a function, however, of the number of random variables that make up the reliability problem. Since this reliability approach is proposed for regional portfolios comprised by a large number of buildings, each characterized by a set of random variables, the FORM computation in this study employs a robust tool for large-scale optimization computation (*TOMLAB* 2012).

SORM is more time intensive than FORM because it requires the computation of second-order derivatives of the limit state with respect to each random variable. While SORM often provides an increase in accuracy relative to FORM, Section 4.5 suggests that this is not necessarily the case for the proposed framework.

Easy computation of sensitivity measures

As discussed in the previous section, another useful by-product of FORM is the resulting set of sensitivity measures. These are computed from the gradient-based algorithm used to minimize β in Equation (3.7) and provide information as to the order of sensitivity each variable parameter has on the overall reliability. Section 4.4 discusses how these sensitivity measures are used to prioritize the most effective retrofit schemes based on the reduction in seismic risk for each dollar of retrofit.

While it is expected that FORM will attain the objectives outlined above, the disadvantages to using FORM must also be addressed. As mentioned in the previous section, FORM is only able to provide approximate reliability estimates for problems with nonlinear limit states. This is often the case for most structural problems. Since most of the failure probability

contribution is located within close proximity to the design point (i.e., in the domain just beyond where the original limit state surface matches the linearized limit state assumed by FORM), FORM usually provides accurate results. However, substantial nonlinearities in the limit state, particularly around the design point, can provide a significant source of error in the FORM assessment. The level of resulting inaccuracy in building portfolio loss assessment due to this approximation is examined in Section 4.5 and in the case studies presented in Chapter 5-7.

Another limitation to using FORM is that the demand, capacity and performance objectives must all be expressed analytically by probability density functions. This requires careful characterization of the uncertainties in each variable, as well as addressing the uncertainties involved in modeling each variable by a specific distribution. Section 4.1 presents some discussion on defining the variables analytically within this proposed framework.

Chapter 4. Proposed FORM Method

4.1 Random Variables

Since FORM requires β to be minimized relative to all random variables of interest, an increase in random variables results in an increase in required computation time as well as difficulty in characterizing limit state nonlinearities. Therefore, it is useful to minimize the number of random variables used in reliability assessments. In this study, only two random variables are used to evaluate loss at each site, specific to each combination of building type and occupancy category. Building combination assignments are discussed further in Section 4.1.2 and Chapter 5. The two variables, $\ln S_a$ and γ_{IDR}, are used to model the seismic intensity and variability in building structural response. The variables for each site and building combination are combined to compute loss for a suite of buildings, given the modeling assumptions discussed in the following sections.

4.1.1 Seismic Intensity

The uncertainties and correlation between seismic intensities at each site must be accounted for in order to capture the spatially distributed seismic demand for a portfolio. These parameters relate to uncertain characteristics in the seismic source, site-to-source distance and

orientation, and site effects. To assess loss for a probabilistic earthquake scenario, a simulation procedure motivated by Jayaram and Baker (2010) is used to compute simultaneous ground motion intensities at each site, based on the seismic intensity model presented in Equation (2.3). These simulated ground motions are used to model a distribution of seismic intensity for each site and correlation between sites. This resulting multivariate distribution is then used in the FORM analysis to compute the distribution of portfolio loss. This simulation reduces the computational efficiency in the overall assessment, but FORM still provides a major computational advantage over a full simulation approach (see Section 3.3.2 and 5.3).

In the simulation method, the first step is to simulate earthquakes of varying magnitudes on all faults of interest. Potential magnitudes are simulated using appropriate magnitude-recurrence relationships, such as those provided within USGS (2012). Fault locations are sampled using fault rupture occurrence rates for a region. Site-specific shear-wave velocity to 30m (V_{S30}), can also be simulated based on the availability of information on the spatial distribution and variance in V_{S30} for all sites of interest (e.g., Allen and Wald 2009). The following equation, based on Degroot and Baecher (1993) and Thompson et al. (2010), is used to capture the variation in V_{S30}:

$$\ln(V_{S30_i}) = \ln(\overline{V_{S30_i}}) + \sigma_i r_i \tag{4.1}$$

where $\overline{V_{S30_i}}$ is the expected shear wave velocity to 30m at site *i*, determined from sampling or empirical models, σ_i is the standard deviation in V_{S30_i} and r_i is the normalized residual term associated with variability in V_{S30_i}. The normalized residual terms are sampled from a standardized multivariate normal distribution characterized by a spatial correlation model developed in existing literature (Boore et al. 2011; Thompson et al. 2006, 2010). The case study

presented in Chapter 5 provides insight on the influence that spatial correlation in soil properties may have on regional portfolio loss estimations and accuracy in the proposed FORM method.

For each magnitude, fault location and V_{S30} realization, the median ground motion intensity and standard deviations ($\bar{S}_{\mathrm{a}}, \sigma$ and τ in Equation (2.3)) are computed at each site of interest using one or more GMPEs (e.g., Abrahamson and Silva 2008; Boore and Atkinson 2008; Campbell and Bozorgnia 2008; Chiou and Youngs 2008; Idriss 2008). In most GMPEs, the standard deviation of ground motion intensity, which is a function of building period, can be disaggregated to an inter-event term (τ) and an intra-event term (σ) as follows:

$$\sigma_T = \sqrt{\sigma^2 + \tau^2} \tag{4.2}$$

where σ_T is the total standard deviation for the predicted ground motion intensity at a site. Note that in most GMPEs, near-fault effects such as rupture directivity and directionality are not explicitly accounted for. This is the case for the models used here, but in the future, this effect could be incorporated by taking advantage of GMPE-adjustment models (e.g., Baker et al. 2012).

The inter- and intra- event normalized residual terms, represented as ε and η in Equation (2.3), are simulated from multivariate distributions. The multivariate distributions have a mean of zero and standard deviation of one, and are assumed to be best represented by a normal distribution based on Jayaram and Baker (2008). These distributions are characterized by spatial correlations between site-specific residual terms, modeling similarities in seismic intensity between sites and earthquake events. In this study, the spatial correlation among intra-event residual terms is computed using the mathematical model proposed in Loth and Baker (2012), and inter-event residual correlations are computed based on Baker and Cornell (2006).

Finally, seismic intensity samples are obtained by combining simulated median ground motions with simulated values of normalized inter- and intra- event residual terms per Equation (2.3). This produces a map of ground motion intensities for a given earthquake scenario. Each simulated scenario is intended to capture the uncertainty in earthquake occurrence, magnitude, and resulting ground motion intensity across a region. These simulated spectral intensities are each related to a single event, and as such, cannot be used directly in a FORM analysis. They can, however, be used to model a multivariate distribution representing the joint seismic intensity at all sites of interest.

The $\ln S_a$ variable computed in Equation (2.3) is a function of many variables, including magnitude and site-to-source distance that may be modeled by non-normal distributions. It is therefore not clear whether the computed seismic intensity samples follow a particular distribution. Results in Miller et al. (2011), however, show that the normal distribution fits the simulated $\ln S_a$ values well, specific to a single site. From these results it is assumed that the combination of site-specific normal distributions can be modeled by a multivariate normal distribution. Using a linear regression analysis, the correlation between $\ln S_a$ at each site can be calculated based on the simulated seismic intensity values. Following this approach, the spatial correlation between $\ln S_a$ variables is a function of shared seismic source effects and commonality in seismic wave paths. As discussed in Section 2.1, these are based on similarities in building location, fundamental period and soil conditions.

Figure 4.1 shows fitted distribution contours, representing 1, 2 and 3 standard deviations from the mean. The computed correlation between simulated seismic intensities at two representative building sites is also shown. The buildings have identical building periods and are

located approximately 1km from each other. Therefore, in this scenario, it is expected that the seismic intensities will exhibit a strong correlation.

It is noted that the simulation procedure outlined above decreases the computational efficiency in using the proposed FORM method to compute portfolio loss. This is due to the extensive number of simulations required to accurately model the multivariate distribution of potential seismic intensities for a region. This does not detract from the other primary advantages of FORM, including its capability to perform an efficient sensitivity analysis. It also does not reduce the contribution of providing an analytical tool to compute regional loss.

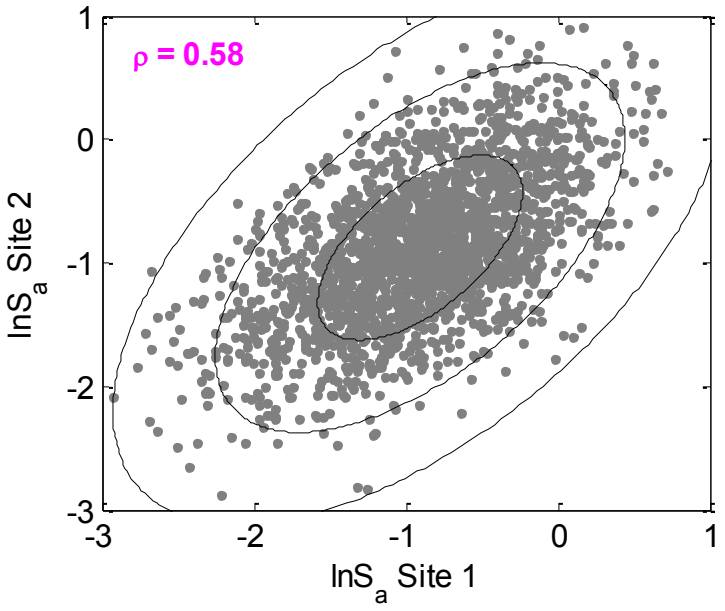

Figure 4.1: Grey dots represent the simulated lnS_a data for Site 1 and Site 2 with the estimated bivariate normal distribution contours and correlation between sites shown.

There are two primary cases where it is possible to circumvent the simulation procedure outlined above, and therefore take full advantage of the computational efficiency in using the FORM approach. First, if the distributions and correlation between seismic intensities for a region are known for a specified event (e.g., taken from historical events), these can be used to

formulate the multivariate distribution for seismic intensity at each site. Second, if the magnitude, fault location and soil properties at each site are considered deterministic, but the uncertainty in residual terms remains random, a simple mathematical computation can be used to compute this distribution. This is the case when it is desired to estimate regional loss given a specific earthquake scenario and deterministic soil properties for a region.

In either case, the multivariate distribution of site-specific seismic intensities can be characterized by expected median spectral accelerations determined by GMPEs and the following covariance matrix:

$$COV(\ln S_a) = COV(\tilde{\varepsilon}) + COV(\tilde{\eta}) \tag{4.3}$$

where $\tilde{\varepsilon}$ is the multivariate distribution of intra-event residuals ($\tilde{\varepsilon}_i = \sigma_i \varepsilon_i$ for site *i*) and $\tilde{\eta}$ is the multivariate distribution of inter-event residuals ($\tilde{\eta}_i = \tau_i \eta_i$ specific to each unique building period at site *i*). Since each residual distribution is assumed to be modeled by a multivariate normal distribution, $\ln S_a$ is also multivariate normal. Using this method, the analytical computation of the spatially correlated seismic intensity random variable properties preserves the inherent efficiency in using FORM.

4.1.2 Building Structural Response: Seismic

The performance of a building depends jointly on the ground motion demand and structural capacity. Structural capacity has been represented by many engineering demand parameters, which are structural response characteristics used to predict damage to structural and nonstructural components. With the exception of some brittle structural systems and acceleration-sensitive building components, building damage is primarily related to building displacement, rather than force (NIBS 2012). Building displacement is often characterized by the

maximum inter-story drift ratio (IDR), defined as the maximum difference in lateral displacements in between two consecutive floors normalized by the story height.

Maximum *IDR* is often used in the formulation of fragility curves used in loss estimation studies (FEMA 2000, 2009; NIBS 2012). These curves help to predict the probability of exceeding various damage levels, given a seismic demand. It was initially thought in the preliminary work of this study that the random variable used to model structural response could be the distribution of seismic intensity associated with the building-specific fragility for each damage state. Given the multiple damage states to be considered for each type of building damage, this formulation would dramatically increase the number of random variables in the reliability assessment. This in turn may significantly reduce the efficiency of using FORM. Moreover, if the limit state is formulated as a function of discrete damage states, it may lose the continuity necessary for convergence of the gradient-based algorithm that FORM employs to find the design point.

To overcome these limitations, this study proposes modeling building-specific structural response by one random variable characterized by the distribution of the maximum *IDR* given a seismic intensity value. To predict building displacement response in the elastic and inelastic range, the HAZUS-MH methodology provides capacity curves, which describe the nonlinear pushover displacement of a building (expressed as spectral displacement) as a function of a laterally-applied earthquake load. As is further discussed below, the information provided by these curves is used to formulate the distribution for the structural response random variables used in this study. This is combined with information from acceleration-sensitive component fragility curves and loss functions, also provided in HAZUS-MH and further discussed below, to compute building repair costs. The functions provided by the HAZUS-MH methodology are

used because of their availability and general application to a wide range to buildings provided in the HAZUS-MH building inventory data set, which is also used in this study. There is no claim being made as to the accuracy or validity of such data. As such, it is noted that there are other damage and loss functions, such as those provided in FEMA P-58 (2012), that could be used within the FORM-based approach proposed in this dissertation. As other fragility curves and data sets become widely available and verified, their use is encouraged.

The capacity curves provided with the HAZUS-MH methodology are formulated for 36 representative building types (e.g., high-rise steel braced frame) and high-, moderate-, low- and pre-code seismic design levels. Approximate height-dependent modal factors listed in NIBS (2012) are used to express the curves in terms of maximum *IDR*. The HAZUS-MH methodology also provides the approximated variability in structural capacity. This is shown in Figure 4.2 as the median, 84th percentile (+1β_c) and 16th percentile (-1β_c) capacity curve relating spectral acceleration to *IDR* for a representative building type.

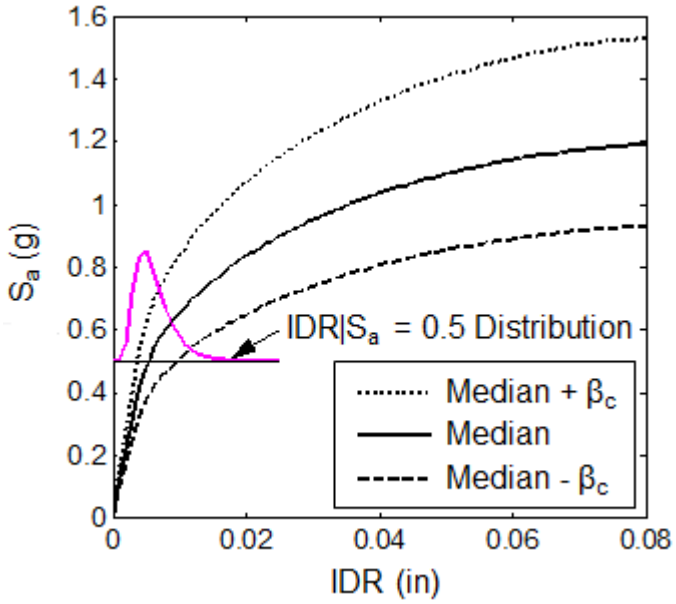

Figure 4.2: Representative median, 84th percentile (+1β_c) and 16th percentile (-1β_c) capacity curves relating S_a to *IDR*.

Using the variability in the capacity curves, the distribution of $IDR|S_a$ can be determined as shown in Figure 4.2 for S_a = 0.5g. The Kolmogorov-Smirnov test (KS-test) suggests that the lognormal distribution provides a reasonable model for the $IDR|S_a$ values obtained from the HAZUS-MH capacity curves (i.e., failed to reject the null hypothesis at a 5% significance level).

As discussed in Section 3.3.1, a useful first step in a FORM analysis is to transform all variables to uncorrelated, standardized, normal space. If the original variables do not follow a normal distribution and are correlated, this transformation is a two-step process (see Rosenblatt 1952). While $IDR|S_a$ can be used as the random variable to model the structural response for each building type, the distribution type and dependency of IDR on S_a would increase the complexity and required transformations in the reliability problem. A first step to reduce this complexity prior to the reliability analysis is to use the natural logarithm of $IDR|S_a$ in the analysis. Since building-specific $IDR|S_a$ values are well modeled by a lognormal distribution, this means $\ln IDR|S_a$ can be modeled by a normal distribution, written as the following:

$$\ln IDR|S_a \sim N(\mu_{\ln IDR|Sa}, \sigma_{\ln IDR|Sa}) \tag{4.4}$$

where $\mu_{\ln IDR|Sa}$ and $\sigma_{\ln IDR|Sa}$ are the mean and standard deviation of $\ln IDR|S_a$.

This assumption of normality also enables the use of a mathematical relationship to address the dependency between structural response and seismic intensity variables. Since the $\ln IDR|S_a$ variable is conditioned on the seismic intensity at a specific building site, it also correlates with the $\ln S_a$ variables at all other sites within a relatively close proximity. In a loss study of lifeline networks, Miller et al. (2011) addresses this complexity with a functional relationship, introducing a new random variable independent of the seismic intensity. Adapting this additional step to building losses, Equation (4.4) can be rewritten as:

$$\ln IDR|S_a = \mu_{\ln IDR|Sa} + \left(\frac{\sigma_{\ln IDR|Sa}}{\sigma_{MAX}}\right)\gamma_{IDR} \quad (4.5)$$

where σ_{MAX} is the maximum $\sigma_{\ln IDR|Sa}$ for all S_a values, and γ_{IDR} is the new random variable characterized by a normal distribution with zero mean and the lognormal standard deviation σ_{MAX}. In this equation, γ_{IDR} is used to model the variability of $\ln IDR|S_a$. By assigning γ_{IDR} as the random variable in this manner, the dependency between seismic demand and structural response is included deterministically rather than between the random variables that model the reliability problem. Note that this functional relationship in Equation (4.5) is only valid if $\ln IDR|S_a$ follows a normal distribution.

In this study, each building-specific γ_{IDR}variable is assumed independent of those for other buildings. A potential source of correlation between buildings would be similarities in design or construction techniques, or physical interactions between building performances, as outlined in Section 2.2. While there are not sufficient inventory data to make this inference for this study, this correlation could be added to the reliability model at a later time.

4.2 Limit State Formulation

In a reliability analysis, limit states define the requirements that must be satisfied to ensure performance of a particular level. The goal of this study is to quantify the distribution of total repair cost to a building portfolio, represented as a percentage of the total building replacement cost. This means that the performance limit state must be formulated as a function of the cost incurred to each building site. In this study, building repair costs are a function of:

- Structural repair and replacement costs (L_S)

- Nonstructural drift-sensitive repair and replacement costs (L_{NSD})
- Nonstructural acceleration-sensitive repair and replacement costs (L_{NSA})

Structural repair and replacement costs are specific to any building components used to resist load. Nonstructural damage is divided into two categories: components that are sensitive to building drifts and those that are sensitive to floor accelerations. Nonstructural drift-sensitive damage includes damage to partitions, exterior walls facades and glass. Nonstructural acceleration-sensitive damage includes damage to ceilings, mechanical and electrical equipment, piping and elevators. Total loss can be written as:

$$TL = L_S + L_{NSD} + L_{NSA} \tag{4.6}$$

This definition is extended in Chapter 6 to include post-disaster time-dependent losses related to community resilience.

The total repair cost for each representative building type and occupancy category is computed using loss calculations proposed in the HAZUS-MH methodology (NIBS 2012), written as the following:

$$L_S = \sum_{oc=1}^{33} BRC_{oc} * \sum_{bt=1}^{28} \sum_{ds=1}^{4} PS_{bt,ds} * RS_{oc,ds} \tag{4.7}$$

$$L_{NSD} = \sum_{oc=1}^{33} BRC_{oc} * \sum_{bt=1}^{28} \sum_{ds=1}^{4} PNSD_{bt,ds} * RNSD_{oc,ds} \tag{4.8}$$

$$L_{NSA} = \sum_{oc=1}^{33} BRC_{oc} * \sum_{bt=1}^{28} \sum_{ds=1}^{4} PNSA_{bt,ds} * RNSA_{oc,ds} \tag{4.9}$$

where BRC is the building replacement cost for occupancy category oc, and $PS_{bt,ds}$, $PNSD_{bt,ds}$ and $PNSA_{bt,ds}$ are the probabilities building type bt is in damage state ds specific to structural, nonstructural drift-sensitive and nonstructural acceleration-sensitive damage, respectively. $RS_{oc,ds}$, $RNSD_{oc,ds}$ and $RNSA_{oc,ds}$ are the structural, nonstructural drift-sensitive and nonstructural acceleration-sensitive damage ratios for occupancy category oc in damage state ds. Building replacement costs and damage repair ratios are provided in NIBS (2012) specific to each of 36 representative building types and 33 occupancy categories.

To calculate $PS_{bt,ds}$, $PNSD_{bt,ds}$ and $PNSA_{bt,ds}$ used in Equation (4.7) - (4.9), an additional calculation is required the compute the probability of exceeding different levels of structural and nonstructural damage. For structural and nonstructural drift-sensitive damage, $PS_{bt,ds}$ and $PNSD_{bt,ds}$ are computed by evaluating the resulting ln$IDR|S_a$ computed in Equation (4.5) relative to the distributions of *IDR* associated with each damage state threshold. This distribution is extrapolated from HAZUS-MH fragility curve information for each categorized building type. For acceleration-sensitive nonstructural damage, the fragility curves are used directly to compute $PNSA_{bt,ds}$ for each building type and damage state, given seismic intensity values computed based on the random variable lnS_a for each building site.

To evaluate the probability that the total loss exceeds a specified threshold, the following limit state equation is specified:

$$P(F) = P(TL_F - TL \leq 0) \tag{4.10}$$

where TL_F is the threshold of total repair cost associated with a specified failure level.

4.3 Limit State Evaluation

A FORM-based analysis is used to evaluate the failure probability in Equation (4.10) for varying portfolio limit state thresholds. The probability distribution of loss is then computed based on these threshold-specific failure probabilities. As mentioned earlier, when evaluating limit state exceedance using FORM, it is useful to transform the random variables (and therefore, limit states) to standardized, normal, uncorrelated space. For illustrative purposes, a transformed bivariate probability distribution for building-specific random variables $\ln S_a$ and γ_{IDR} is shown in Figure 4.3. $\ln S_a$ and γ_{IDR} variables transformed to standardized, normal space are labeled as $[\ln S_a]$ and $[\gamma_{IDR}]$. The limit state surfaces associated with different thresholds of building repair costs, which are a function of the individual building replacement cost (*BRC*), are also shown.

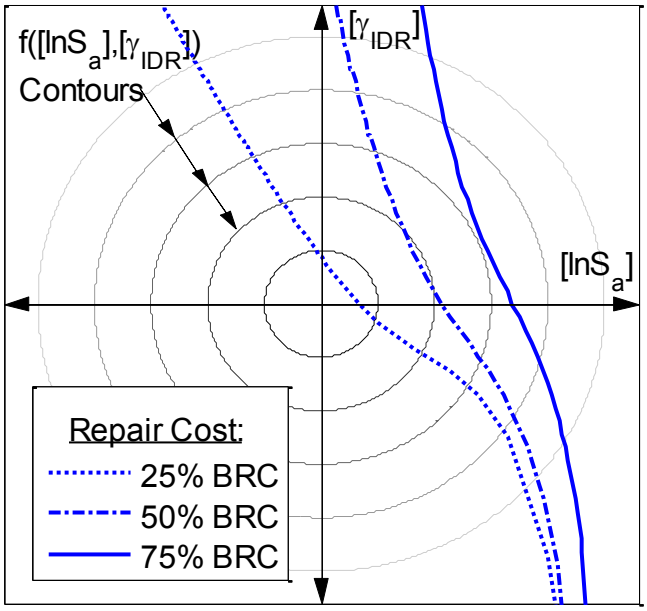

Figure 4.3: Bivariate density function for standardized, normal variables $[\ln S_a]$ and $[\gamma_{IDR}]$ for one representative building. Performance limit states are associated with varying levels of building repair cost.

In Figure 4.4, the blue shaded region represents the failure domain for the limit state characterized by a repair cost equal to 75% *BRC* in Figure 4.3. The safety index, β, is computed

using Equation (3.7), and shown below with the design point y^* (i.e., the closest point on the limit state to the origin in standardized space). A linearized limit state fit tangent to the design point is also shown with the corresponding approximate failure space assumed by FORM.

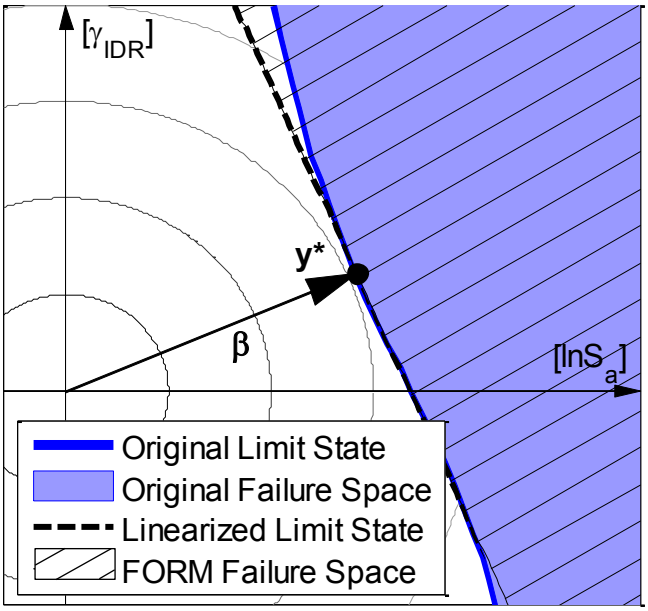

Figure 4.4: Original nonlinear limit state surface and corresponding failure space as a function of standardized, normal variables [lnS_a] and [γ_{IDR}] for one representative building. The linearized limit state and corresponding failure space assumed by FORM is shown for a repair cost threshold of 75% *BRC*.

For this single building case, computing β using Equation (3.7) involves only two variables. As a result, minimizing β is achieved easily through basic iteration. The reliability evaluation becomes more complex, however, for a portfolio of buildings where the optimization problem may consist of thousands of variables. To increase computational efficiency for such large reliability problems, β is computed using the TOMLAB large-scale optimization platform (TOMLAB 2012). The probability of failure is then computed as a function of β using Equation (3.8).

As seen in Figure 4.4, the original limit state is slightly convex relative to the origin. This indicates that the failure probability estimated using FORM will likely be larger than the actual failure probability, because the linearized limit state assumed by FORM encapsulates more failure space. FORM is expected to give reasonably accurate results, however, because there is little nonlinearity in the original limit state surface, specifically around the design point. This may not be the case in the loss evaluation of multiple buildings, when the limit state surface must be evaluated in a high dimension reliability space. It is impossible to visualize the behavior of such a limit state surface, which makes it important to further assess the accuracy in using FORM for large reliability problems of this nature. The following section will examine the accuracy in using FORM to evaluate loss for multiple buildings, as well as identify sources of nonlinearity leading to inaccuracies in in FORM results.

4.4 Sensitivity Analysis Using FORM

The ability to perform a sensitivity analysis efficiently is one of the primary advantages to using FORM for regional loss evaluation. By computing sensitivity measures, information is provided that relates the change in system reliability relative to an incremental change in each random variable parameter. Sensitivity measures computed relative to the γ_{IDR} variable for each building site can be used to provide insight into the reduction in portfolio reliability per dollar spent on retrofit for each vulnerable building type. By using the γ_{IDR} variable in such an analysis, this study prioritizes retrofit relative to a maximized reduction in drift-sensitive damage. This can be expanded, however, to include sensitivity measures for upgrading acceleration-sensitive building components in a similar fashion with the addition of a third random variable at each site.

The proposed sensitivity measure, labeled $\partial\beta/\partial C_R$, provides the change in the reliability index (β) for the portfolio loss evaluation, per dollar of retrofit cost (C_R). This measure can be mathematically written as:

$$\frac{\partial\beta}{\partial C_R} = \frac{\partial\beta}{\partial\gamma_{IDR}} * \frac{\partial\gamma_{IDR}}{\partial C_R} \tag{4.11}$$

where $\partial\beta/\partial\gamma_{IDR}$ is the sensitivity measure directly computed to find the design point in a FORM assessment by differentiating the reliability index relative to the structural response random variable γ_{IDR}. This involves taking the derivative of the limit state in Equation (4.10) for a specified loss threshold.

The term on the right side of Equation (4.11) represents the marginal change in γ_{IDR} for each dollar spent on retrofit. This also corresponds to a change in estimated *IDR* given a specified seismic intensity level as is shown in Equation (4.5). This study uses typical seismic retrofit cost estimates provided in FEMA-156 (1994b) for groups of buildings, which are assumed to provide retrofit measures, that in general, upgrade the seismic design code level for each building type. While common retrofit measures can be specific to upgrading resistance to only drift-sensitive or acceleration-sensitive components, or may not influence either, upgrading structures to a new seismic design code level have been shown to upgrade both (NIBS 2012).

Retrofit alternatives considered in the proposed sensitivity analysis are specific to structural upgrading policies for groups of buildings within a region. Using disaggregated HAZUS-MH building inventory data provided by Porter (2013), buildings are grouped by census tract locations, structural building types, occupancy types and seismic design code level. The set of retrofit alternatives is created by all possible combinations of each category. Consistent with the assumptions made in previous studies, typical retrofit costs listed in FEMA 156 are

considered most representative for pre-code buildings retrofitted to a moderate-code design level (Kircher et al. 2006; NIBS 2002). In addition, retrofit for low-code buildings is considered to cost 25% less than for pre-code structures (Mahsuli and Haukaas 2013). Only low- and pre-code building types are considered for retrofit in this study, because it is assumed that retrofitted structures will generally not satisfy high-code seismic design requirements (Kircher 2013).

Given these assumptions, $\partial\gamma_{IDR}/\partial C_R$ is computed based on typical retrofit costs and change in γ_{IDR} associated with each retrofit alternative. Assuming normality in $\ln IDR|Sa$ in Equation (4.5), an incremental change in γ_{IDR} per dollar of retrofit can be related to a change in $\mu_{\ln IDR|Sa}$ for each retrofitted building type as follows:

$$\frac{\partial\gamma_{IDR_i}}{\partial C_{R_i}} = \frac{\Delta\mu_{\ln IDR|Sa}}{C_{R_i}} = \frac{\mu_{\ln IDR|Sa_i} - \mu_{\ln IDR|Sa_{i*}}}{C_{R_i}} \tag{4.12}$$

where $\mu_{\ln IDR|Sa_i}$ is the mean natural logarithm of *IDR* given S_a for an original building i, and $\mu_{\ln IDR|Sa_{i*}}$ is for the retrofitted building modeled by building type i*. Estimated $\mu_{\ln IDR|Sa}$ values are computed from the capacity curves provided in the HAZUS-MH methodology for the original and retrofitted building.

Since $\partial\beta/\partial\gamma_{IDR}$ in Equation (4.11) is computed relative to exceeding a specified level of loss, the magnitude and order of sensitivity measures depends on the loss threshold of interest. Therefore, when prioritizing retrofit to reduce regional loss, sensitivity measures should be computed relative to the desired level of loss to be minimized. For a region interested primarily in minimizing small, frequent losses, sensitivities should be computed relative to a lower loss threshold for optimal retrofit prioritization. Similarly, a high loss threshold can be used to compute $\partial\beta/\partial\gamma_{IDR}$ when it is of interest to reduce less frequent, high consequence portfolio

losses. The implication a chosen loss threshold has on optimal retrofit prioritization for varying loss levels is explored further in the case study assessment.

Depending on the vulnerable building types in question, the ordering of sensitivity measures computed in Equation (4.11) can be used to provide insight into the most cost-effective retrofit schemes for reducing seismic-induced loss for a building portfolio. It is emphasized that by computing sensitivity measures relative to γ_{IDR}, the marginal change in reliability as shown in Equation (4.11) is only a function of an increase in resistance to drift-sensitive damage. In this study, this includes changes to direct structural damage and drift-sensitive nonstructural damage (e.g., damage to partitions, exterior walls facades and windows). Therefore, the sensitivity measures can be used to suggest retrofit prioritization to reduce the collective drift-sensitive losses for a building portfolio, but additional information is needed provide more complete information for prioritizing cost-effective retrofit schemes to reduce all repair costs. If a random variable is added to the analysis to model structural response to floor accelerations resulting from a given seismic intensity, the same principles can be applied to compute sensitivity measures relative to this type of damage.

While it is useful to prioritize buildings based on the cost-effectiveness of retrofit, developing regional retrofit schemes solely based on budgetary constraints is often unrealistic. This is because most buildings are privately owned, and there is no universal source of funding to mitigate risk present at a regional level. Instead, the financing of retrofit is often the responsibility of the owners of vulnerable buildings, and either voluntary or mandatory depending on regional ordinances and building type.

To incentivize retrofit, both state and local governments have employed a variety of funding mechanisms including interest-free loans, fee waivers and design rebates. In addition,

many local jurisdictions have exercised other requirements to promote retrofit including requiring engineering reports to be made public for vulnerable buildings, zoning requirement exemptions, and in some cases, making retrofit mandatory. When trying to develop efficient ordinances, whether with respect to mandating retrofit or in determining the extent of retrofit incentives, many jurisdictions are interested in prioritizing the retrofit of vulnerable buildings within their region. For example, the City of Sonoma, California requires mandatory retrofit of seismically vulnerable structures within a predefined time period based on a building's retrofit priority (FEMA 1994c). Building prioritization is based on the building type and hours of use, number of stories, proximity to public sidewalks and adjacent buildings, and structural adjustments. Vulnerable buildings with the highest priority must be retrofitted in a shorter time frame than those considered less risky.

The sensitivity analysis proposed in this section provides additional useful information for building prioritization, not only based on building vulnerability, but also on the cost-effectiveness of retrofit. It is assumed that building owners are more incentivized to take retrofit action if they know that the future benefit largely outweighs the initial cost. Therefore, comparing sensitivity measures computed in Equation (4.11) for different building types can offer reasoning to mandate or emphasize mitigating risk activities for buildings with the most cost-effective retrofit schemes. Other factors such as prioritizing based on life safety, building importance to the community, number of vulnerable buildings within a specified class, potential fatalities and injuries, and other social consequences should also be addressed in order to produce a more comprehensive retrofit prioritization based on reducing regional vulnerability.

4.5 FORM Accuracy

Since it is impossible to visualize the extent of nonlinearity in high dimension limit state surfaces, other methods must be used to assess the accuracy in using FORM. In this study, results computed using the proposed FORM method are compared to Monte-Carlo Simulation (MCS) results to test the accuracy in using FORM for the reliability assessment of multiple, non-identical buildings. This assessment is based on the condition that the number of simulation runs produces at least 100 expected failure events. For example, $P(F) = 1/10$ is computed with respect to at least 1,000 simulation runs (Mann et al. 1974; Melchers 1999). The resulting accuracy is considered sufficient for comparison purposes. In this section, conclusions drawn from such a comparative assessment are used to identify sources of limit state nonlinearity and FORM-based errors. The identification of these factors may assist in future studies focused on developing a technique to refine FORM-based loss estimation results.

The reliability results for a system of two buildings are examined prior to analyzing the distribution of losses for a large portfolio. These results, shown in Figure 4.5(a), are illustrated using loss exceedance curves. The two structures used in this study are both wood, multi-family residential buildings, with identical, yet independent, seismic intensity distributions. The assumption of zero correlation in seismic intensity may be representative of two sites located a considerable distance from each other. The x-axis in Figure 4.5(a) is representative of the repair cost expressed as a percentage of the total building replacement cost for both buildings (ΣBRC), and the y-axis is the probability of exceeding each threshold of loss, plotted in log space. The vertical purple lines, representing varying thresholds of loss, will be discussed below.

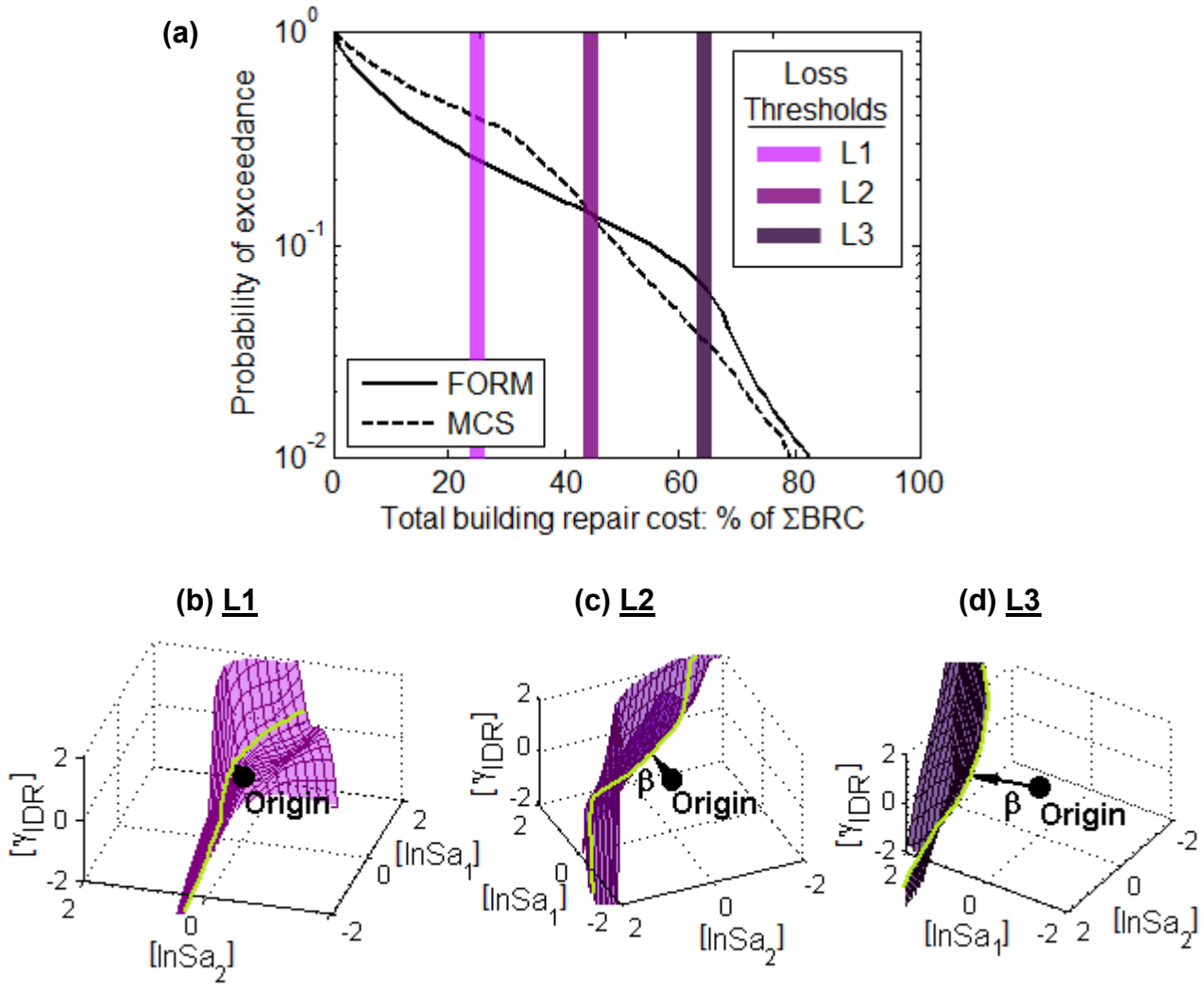

Figure 4.5: (a) Loss exceedance curves for a two building system computed with FORM and MCS. Random variables and corresponding limit state surfaces are shown in standardized, normal space for a repair cost equal to (b) 25% Σ*BRC*, (c) 45% Σ*BRC* and (d) 65% Σ*BRC*.

It can be seen in Figure 4.5(a) that while the FORM results follow a similar trend to those obtained with MCS, there is a deviation between results from the two methods. This is likely due to nonlinearity in the limit state surface, which is not captured by the limit state linearization assumed in FORM calculations. Since it is not easy to visualize the limit state surface in four dimension space required to model the two building case (i.e., two random variables per site), some simplifying approximations can be used to reduce the reliability problem to three

dimensions. In this case, it is assumed that each structural response random variable is fully correlated and can be modeled by a shared γ_{IDR} variable. This means that the structures at each site have identical building characteristics; however, their behavior and corresponding loss is based on the seismic intensity specific to each site (see Section 4.1.2 and 4.2). With this assumption, the reliability space consists of only three dimensions: [lnS_{a1}] (site 1), [lnS_{a2}] (site 2) and [γ_{IDR}] (sites 1 and 2); all transformed to standardized, normal and uncorrelated space. Figure 4.5(b-d) show the limit state surfaces for the 25%, 45% and 65% Σ*BRC* loss thresholds labeled by the purple vertical lines in Figure 4.5(a). To provide a better visualization of the limit state surface curvature, a green contour line is added and each figure is rotated accordingly.

It can be seen that the limit state surface shown in Figure 4.5(b) for a loss threshold of 25% Σ*BRC* appears to be concave relative to the origin. As a result of this nonlinearity, there is less failure space associated with a linearized limit state surface assumed by FORM than with the actual failure surface, which is why FORM underestimates the failure probability for this loss threshold. The limit state surface in Figure 4.5(c), representing a loss threshold of 45% Σ*BRC*, looks to include concave and convex sections relative to the origin. It can be seen that the limit state at the design point, which behaves similarly to an inflection point, is relatively linear. At this threshold, the nonlinearities in the limit state have a tendency to balance out, which explains why FORM provides very similar results to simulation (i.e., more accurate). Finally, the limit state surface appears convex relative to the origin in Figure 4.5(d) for the higher loss threshold of 65% Σ*BRC*, indicative of overestimating the failure space using FORM. The loss thresholds specific to 25%, 45% and 65% Σ*BRC* were chosen for this two-building system as representative in identifying nonlinearities present in each limit state surface.

It was hypothesized initially that the Second-Order Reliability Method (SORM) could account for these noted nonlinearities, and therefore provide more accurate results for this type of problem. SORM is a reliability transformation method that involves a second-order, as opposed to linear, approximation of the limit state surface at the design point. Figure 4.6 shows the results using FORM, SORM and MCS for the same two building problem discussed above. It can be seen that the SORM results provide a slight improvement for larger repair cost thresholds, but do not improve accuracy significantly. Moreover, the deviations in results are the opposite as those seen using FORM.

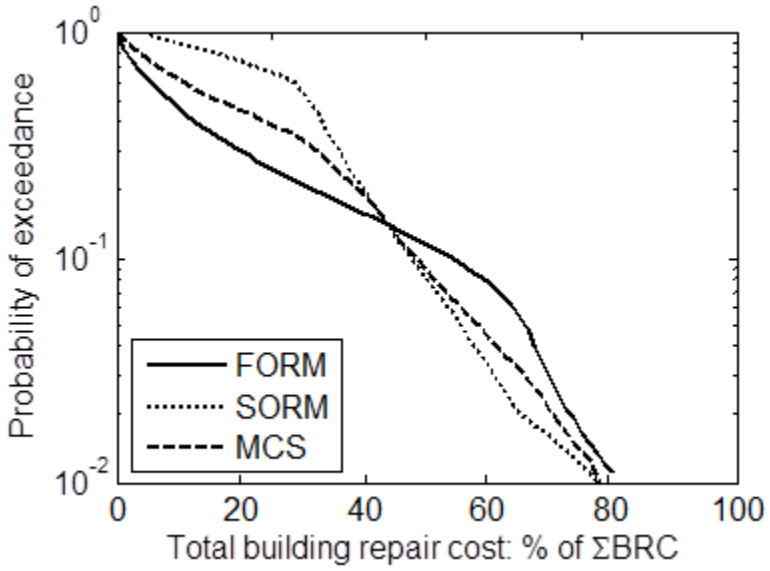

Figure 4.6: Loss exceedance curves for a two building system computed with FORM, SORM and MCS.

This inconsistency in SORM results is because the second-order surface fit to the design point does not adequately capture the limit state nonlinearity. For example, while the limit state surface may have one type of curvature at the design point, the limit state curvatures may change shape in regions that still contain considerable probability density. Therefore, SORM may overestimate the actual failure space when FORM assumes less, and vice versa. Similar

deviations in SORM results were noted for reliability evaluations of more than two buildings. In addition to a lack of improved accuracy, it is also noted that computationally, SORM is much more expensive than FORM. This is because it requires the computation of second-order derivatives of the limit state with respect to each random variable.

The limit state nonlinearities that lead to inaccuracies in FORM and SORM results appear to be a function of the range of random variable values that satisfy a limit state constraint. For example, in Figure 4.6, it can be seen that for very low and high loss thresholds, FORM, SORM and MCS all yield similar results. This is because all or most random variables must be close to an extreme of their distribution in order to achieve such low or high loss levels. For loss thresholds in between these extremes, however, there are many different values random variables can assume to satisfy the limit state constraints. The extent of these possible combinations becomes even greater when the reliability space increases in size, resulting in a possible increase in limit state nonlinearity. In many cases, this nonlinearity may create a limit state surface with local minima, each representative of high probability density. In this scenario, there may be considerable error in using FORM and SORM, since these approximation methods are unable to capture these nonlinearities with a linear or second order approximated surface.

The extent of random variable combinations that satisfy a limit state constraint is dependent on the similarity among variables and their correlation structure. If variable distributions are independent or largely dissimilar, it is assumed that there will be a greater range of random variable values that satisfy a limit state equation. For example, if the two building sites discussed above have fully correlated seismic intensity and structural response variables, there is only one value of each that can satisfy the limit state threshold. On the other hand, when these variables have zero correlation, as is the case for seismic intensities in Figure 4.5(a), they

can assume a larger range of values. This leads to more limit state nonlinearity, and less accuracy in using FORM.

To further investigate this concept, Figure 4.7(a) shows loss exceedance curves for a small sample portfolio of ten buildings using FORM and MCS. Similar to the two building case above, all are wood, multi-family residential buildings, with identical seismic intensity distributions. In this case, however, the spatial correlation (ρ) between seismic intensities at each building site varies from 0 to 1. Figure 4.7(b) shows the ratio of exceedance probability (*Pe*) assumed by FORM with that computed using simulation.

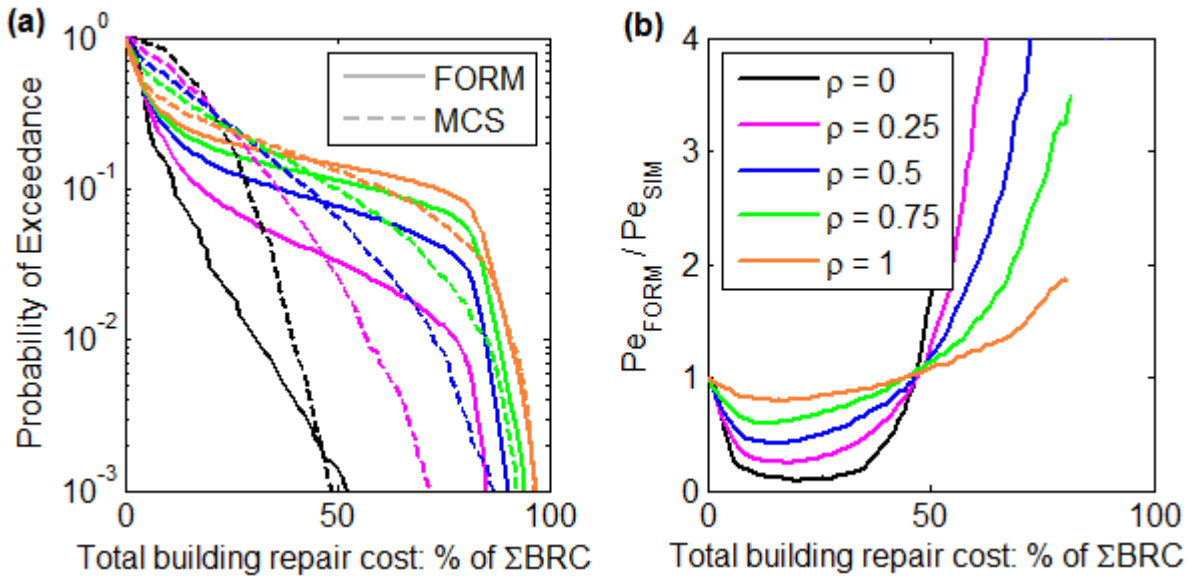

Figure 4.7: (a) Loss exceedance curves using FORM and MCS and (b) ratio of exceedance probabilities using FORM and MCS for a 10 building sample portfolio with varying spatial correlation between seismic intensities (ρ).

Both figures show that the error associated with using FORM increases when the spatial correlation decreases. As the seismic intensities become more correlated, there is less variability in the values each random variable can assume to satisfy a limit constraint. As such, there is less nonlinearity in the limit state surface for each loss threshold, and thus more accuracy in using

FORM. Figure 4.7(a) and Figure 4.7(b) also show that FORM yields comparable results to those computed using MCS at a similar building repair cost threshold for each spatial correlation assignment. For this sample portfolio, this occurs at a loss threshold around 45% Σ*BRC*.

It is further investigated whether this deviation in FORM results is consistent for different size building portfolios. In Figure 4.8(a), probability exceedance curves are shown using FORM and MCS for portfolios comprised of different numbers of buildings, given the portfolio characteristics assumed in the study above. Similar to Figure 4.7(b), Figure 4.8(b) shows the ratio of exceedance probability (*Pe*) assumed by FORM with that computed using simulation. In this sample study, the spatial correlation between all building sites is considered to be 0.5.

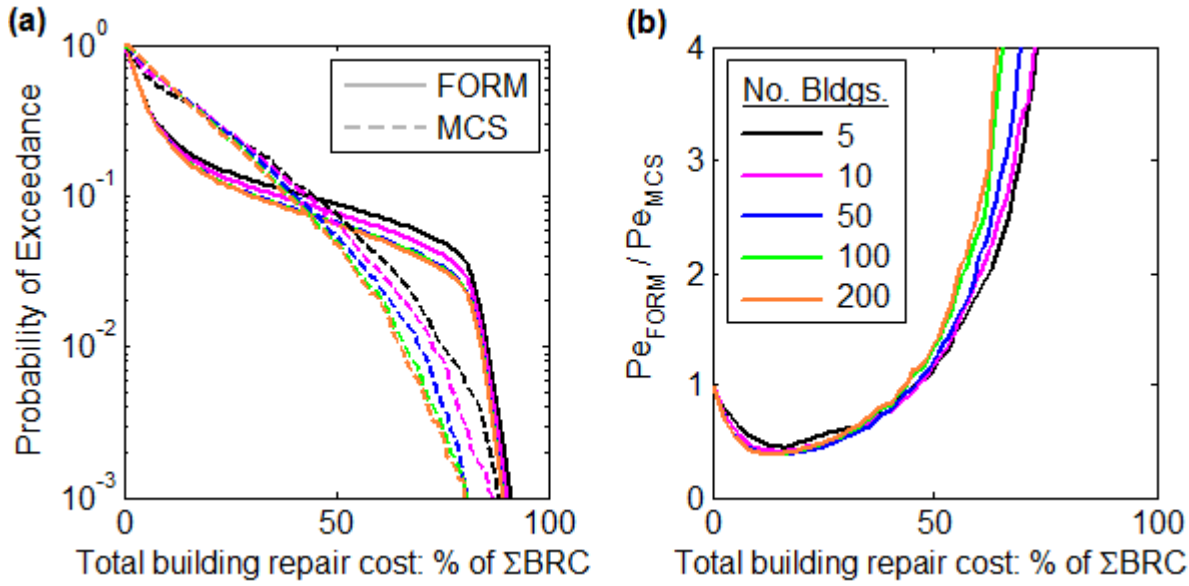

Figure 4.8: (a) Loss exceedance curves using FORM and MCS and (b) ratio of exceedance probabilities using FORM and MCS for portfolios consisting of different numbers of buildings with a fixed spatial correlation of 0.5 between all seismic intensities.

Figure 4.8 shows that the deviation in FORM results is consistent for portfolios of different sizes for this sample study. In Figure 4.8(b), the portfolio with 100 buildings exhibits a very similar ratio of FORM to MCS results as the portfolio with 200 buildings. Therefore, it

appears that the deviation in FORM results will generally stay consistent for larger portfolios of different sizes, assuming the distribution of buildings and seismic intensities do not vary.

FORM accuracy may also be influenced by additional limit state nonlinearity resulting from dissimilarities in building types within a portfolio. For example, urban building portfolios may consist of many different building types characterized by a wide array of building heights, materials, etc. The structural response variable (γ_{IDR}) associated with each of these building types will also vary, potentially leading to more limit state nonlinearity. Building portfolios in residential settings, however, may have many of the same building types and more similar γ_{IDR} variables.

It can also be seen that, independent of the dissimilarity in variables, FORM accuracy may be a function of the probability of system failure. For example, consider a building portfolio consisting primarily of buildings lacking any seismic design. This portfolio is likely to experience failure given most loss thresholds. Even if the sites are completely uncorrelated, all or most random variables may assume a value on the low end of the distribution in order to achieve a high probability of exceeding a loss threshold.

The discussion in this section is intended to identify potential sources of limit state nonlinearity to further understand the deviation in FORM results. Furthermore, the identification of these factors can assist in developing a refinement technique to increase accuracy in using FORM to estimate portfolio loss. The error in using FORM shown in the above studies is hypothesized to be a direct function of the dissimilarity in variables and level of failure probability. With further investigation, an empirical refinement algorithm may be developed and used to limit this error, while preserving the many benefits of using the FORM technique.

Chapter 5. Case Study

This chapter presents a loss assessment evaluation for a selected building inventory in San Francisco, California using the proposed FORM method and MCS. In Section 4.3 and 4.5, the accuracy in FORM results was assessed for basic sample portfolios consisting of identical buildings and seismic intensities. A realistic building portfolio is instead comprised of many building types and a spatially distributed, non-uniform seismic intensity. A much larger reliability space is required to model each variable, and there exists the potential for significant nonlinearity in the resulting limit state for certain loss thresholds. Therefore, comparing FORM results to those computed using MCS is essential to assess the accuracy in using FORM to evaluate the distribution of loss for an actual building portfolio. It is also desired to verify the optimization of reliability results using the TOMLAB optimization solver for such a large reliability space. If there are local minima or discontinuities in the portfolio limit state, it is possible that the optimization function may not converge at the global design point.

This case study also presents a sensitivity analysis, which is used to evaluate the influence retrofit strategies have on loss reduction for the San Francisco portfolio. Vulnerable building types with the highest sensitivity measures are prioritized for retrofit. The resulting

post-retrofit loss exceedance curves are computed with respect to varying retrofit budget constraints.

Finally, pre- and post-retrofit loss exceedance curves are assessed with and without spatial correlation considered. This assessment is intended to provide insight into the importance of considering the spatial correlation in seismic intensity for estimating regional loss and prioritizing retrofit schemes.

5.1 Building Inventory

This study evaluates seismic risk to a portfolio of buildings located in the central business district and surrounding districts of San Francisco. This region, shown in Figure 5.1, has been selected based on available building inventory and scenario earthquake data. The building data are extracted from a database provided by Porter (2013), which disaggregated inventory data provided in NIBS (2012). The buildings are categorized by 36 building types and 33 occupancy categories used in the HAZUS-MH loss estimation methodology. The buildings types are additionally sub-divided by high-, moderate-, and low-seismic design code levels (SDC), and pre-code buildings, which are not seismically designed.

The inventory database lists the total floor area and total building replacement cost for each building combination, characterized by building type, occupancy category and code standard combination by census tract. Default HAZUS-MH building inventory data assumes all model building types are low-rise, meaning one to three stories. This assumption can create numerous errors when estimating loss for a suite of buildings of various height classes. This is particularly the case for urban building portfolios characterized by tall buildings, such as the Financial District of downtown San Francisco.

This study modifies the default HAZUS-MH inventory based on three generic height distributions provided in Kircher et al. (2006) for the San Francisco region. Building height distributions, labeled HG1, HG2 and HG3 in Figure 5.1, are outlined in Table 5.1. The building density for each census tract (i.e., building area per unit area of census tract) is used to assign a height distribution that best characterizes the typical building height classification at each location.

Table 5.1: Three generic building height groups (Kircher et al. 2006).

Height Group	Building Height Distribution			Description of Buildings
	Low-Rise	Mid-Rise	High-Rise	
HG1	0.1	0.1	0.8	City center/tall buildings
HG2	0.4	0.4	0.2	Commercial and dense urban residential buildings
HG3	0.95	0.05	0.0	Suburban, primarily residential buildings

Given computing space constraints and availability of data, the $\ln S_a$ and γ_{IDR} variables for buildings categorized within the same building combination are considered fully correlated within each census tract. It is incorrect, however, to assume these buildings will experience an identical level of loss in a given earthquake. Given this assumption, it is expected that the variance in loss is superficially increased (see Chapter 2). Future extensions of this work should aim to disaggregate the total building area, for each building combination type within each census tract, into individual buildings to better model the variance in predicted loss.

Due to computing space requirements, the loss evaluation only considers building combinations with more than 10,000 square feet of floor area within each census tract. Given the normalization process of building inventory data in HAZUS-MH, there are many building

combinations with much lower floor area (<1,000 square feet). It is assumed that this excluded inventory data will have a minor influence on the expected portfolio repair cost, represented as a percentage of total building replacement cost for all building combinations included in the reliability assessment. Under these constraints, the resultant case study portfolio includes over 1,500 building combinations distributed over 74 census tracts. The reliability problem is therefore modeled by over 3,000 random variables for estimating portfolio loss.

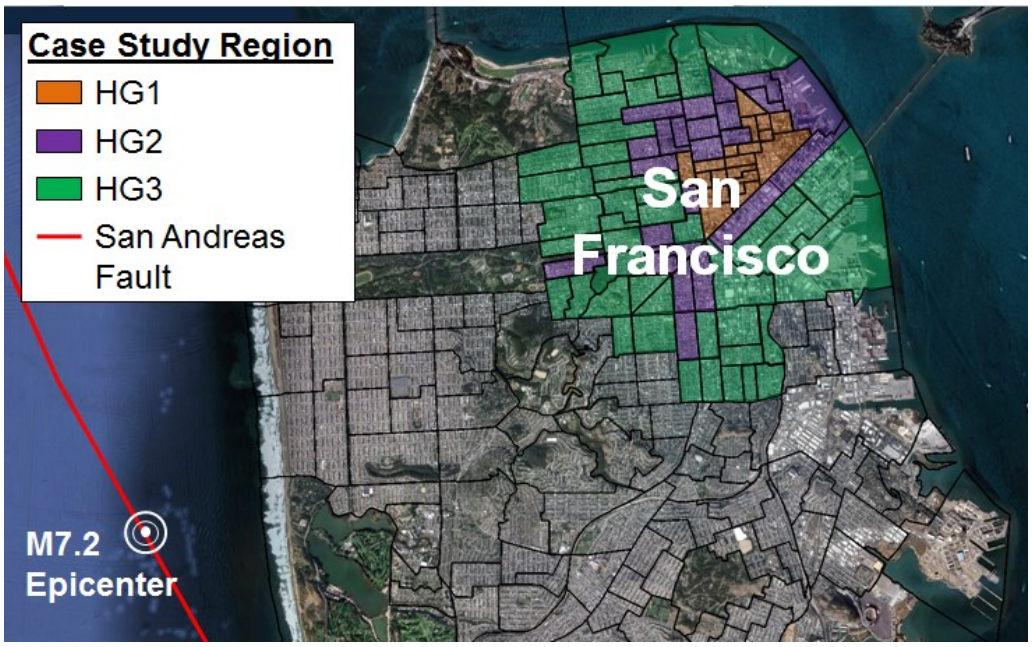

Figure 5.1: Building height distributions defined per census tract in the San Francisco case study portfolio region, shown relative to the scenario M7.2 earthquake epicenter (Google 2012).

Building combinations with a smaller representative floor area are considered in the sensitivity analysis since there may be a large number of different vulnerable building combinations with only a few buildings per census tract. Including such building combinations may have a significant influence on retrofit prioritization, as it is based on a reduction in loss per dollar spent on retrofit, independent of the building combination size.

5.2 Seismic Hazard Analysis

The scenario earthquake used in this study is a magnitude 7.2 earthquake on the peninsula portion of the San Andreas Fault. This is the primary scenario earthquake used by the Applied Technology Council (ATC) in their work on the San Francisco Community Action Plan for Seismic Safety (CAPSS) project (ATC 2010). According to ATC, this type of earthquake could be expected in the area, because enough strain has built up on the San Andreas Fault since 1906 to produce an event of this magnitude.

For a simplistic evaluation, the epicenter of the earthquake is assumed at the midpoint of the peninsula portion of the fault as shown in Figure 5.1. Median V_{S30} values (time-averaged shear-wave velocity averaged over a depth of 30m) are estimated from USGS (2013a) and shown in Figure 5.2 for each census tract. When using ground motion prediction equations, V_{S30} values are used to determine the site amplification in seismic intensity. As discussed in Section 4.1.1, considering a deterministic earthquake magnitude, epicenter location and V_{S30} allows this study to apply the computational efficiency inherent in using FORM. Each of these parameters, however, can be modeled with a distribution rather than a deterministic value. Results are tabulated later in this case study assuming probabilistic V_{S30} values, as well as in the multi-hazard case study presented in Chapter 7 for a probabilistic epicenter location.

The distribution of spatially correlated seismic intensity is calculated at the center of each census tract specific to each representative building combination. Loss is evaluated with and without the consideration of spatial correlation between residual terms, to assess the importance of considering this type of spatial correlation for regional loss estimation and retrofit prioritization. In addition, the probability distribution of loss is tabulated with respect to both deterministic and probabilistic, spatially correlated soil properties. The former utilizes Equation

(4.3) to compute the seismic intensity distribution and is used to assess the computational efficiency potential in using FORM opposed to simulation. The latter requires the simulation procedure outlined in Section 4.1.1 to compute a multivariate distribution for seismic intensity.

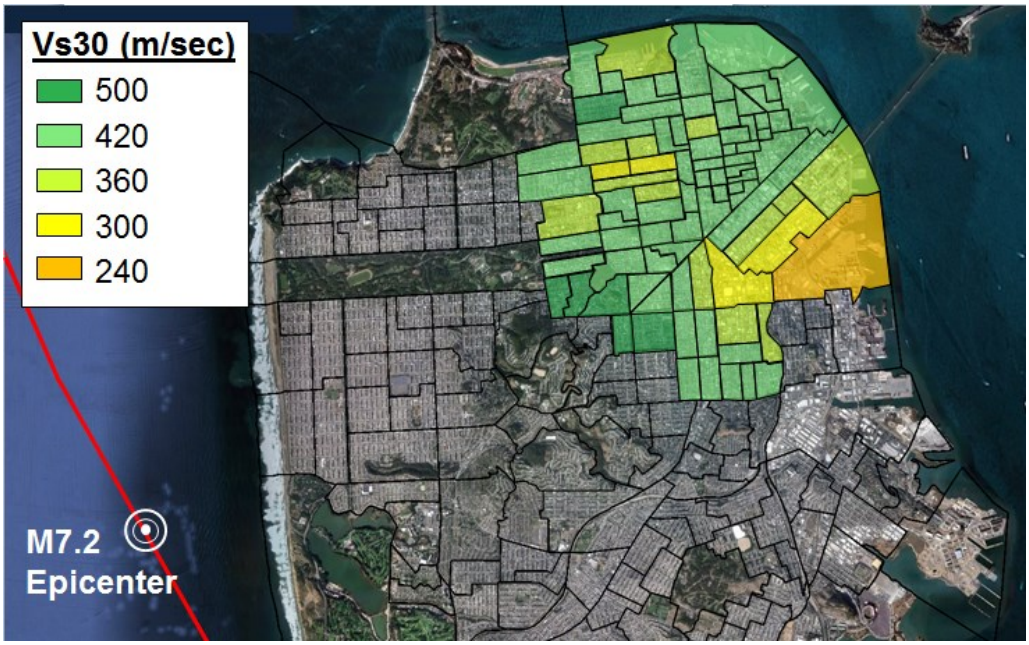

Figure 5.2: Median V_{S30} values per census tract in San Francisco case study portfolio region (USGS 2013a).

The objective of including spatially correlated V_{S30} values in this study is to illustrate the importance of characterizing correlation in soil properties across a building portfolio in regional loss assessments. The distribution of V_{S30} for each census tract reflects median values shown in Figure 5.2 and variances estimated from Holzer et al. (2005). The spatial correlation in V_{S30} is modeled from semivariogram results developed in Thompson et al. (2010) for S_{S30} values (inverse of V_{S30}). Ground motion prediction equations (GMPEs) are limited in use to V_{S30} values greater than 180 m/s (Boore and Atkinson 2008). Therefore, it is assumed that all sites in this study exhibit a shear wave velocity above this threshold. All median values for this case study region are significantly above this threshold for the case study region, however, there may be

soft-soil regions, specifically along the shoreline, that exhibit lower V_{S30} values. It is assumed that these regions will not significantly influence the effect spatial correlation in soil properties has on the distribution of loss. In order to capture more realistic loss estimation, a site-specific nonlinear analysis is required for these soft soil sites.

5.3 Results and Comparison

Figure 5.3 shows the loss exceedance curves for total structural and nonstructural repair costs for the case study portfolio expressed as a percentage of the total building replacement costs (independent of content losses). These results are tabulated using FORM and MCS given the occurrence of the scenario earthquake discussed in the previous section.

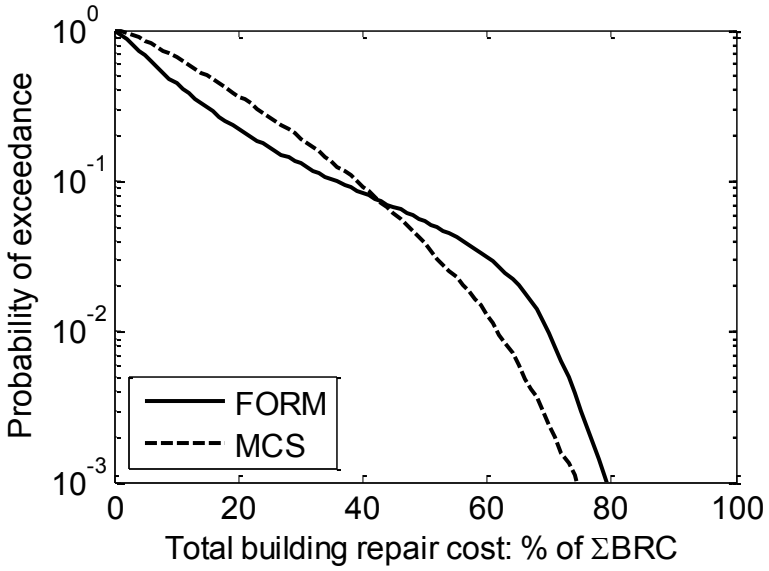

Figure 5.3: Loss exceedance curves using FORM and MCS given a scenario earthquake and median V_{S30}.

It can be seen that the proposed FORM method yields a similar trend in results to those obtained using MCS. There are, however, some deviations between results from the two methods. Similar to the sample study results presented in Section 4.5, FORM results

underestimate the probability of exceeding small losses and overestimate exceedance probabilities for larger, rare losses. As previously noted, this is likely due to the nonlinearities in the limit state surface that are not captured when evaluating a linearized surface assumed by FORM.

The time required to compute the exceedance curves in Figure 5.3 using FORM was considerably less than for MCS. For example, the MCS results for a repair cost threshold of 70% Σ*BRC* for the case study portfolio took approximately 15 minutes to compute. By comparison, optimization required by FORM took approximately 40 seconds on a personal computer with a 2.4 GHz processor and 2GB RAM. To compute the loss exceedance curve, and therefore, the loss distribution, the reliability computations must be ran for multiple loss thresholds. In this respect, FORM is significantly more computationally efficient than MCS. This assessment is based on the condition that the number of simulation runs produces at least 100 expected failure events, and thus considered sufficient for comparison purpose (Mann et al. 1974; Melchers 1999). Therefore, for large consequence thresholds indicative of more rare events, the required computation time using MCS increases, since the sample size must increase.

It is noted that this study uses a crude MCS approach to compute simulation results. More advanced techniques, such as importance sampling, can reduce the simulation computation time. The computation times listed also depend on efficiencies in the code calculations developed to compute loss. Since the computations involving the variables presented in Section 4.1 are consistent between FORM and MCS, a relative comparison of computation time is considered adequate.

Additionally, this study assesses the influence that spatial correlation in seismic intensity has on regional loss assessments (see Section 2.1). In Figure 5.4, loss exceedance curves are

computed using FORM for the same building portfolio and scenario earthquake, specific to three different cases: 1) spatially correlated residual terms and median V_{S30} values, as also shown in Figure 5.3; 2) spatially correlated residual and V_{S30} terms; and (3) without any spatial correlation considered. Note that these results are approximate, as can be seen in the comparison of FORM results with MCS in Figure 5.3. Also, results beyond 60% Σ*BRC* repair costs can be particularly sensitive to assumptions in the loss estimation process.

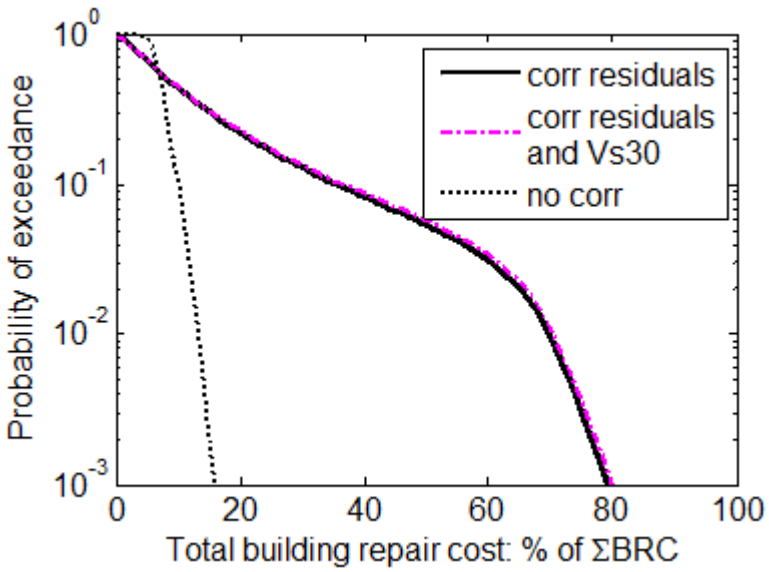

Figure 5.4: Loss exceedance curves using FORM with and without spatial correlation considered between residual and V_{S30} terms.

Figure 5.4 shows that ignoring the spatial correlation between seismic intensities results in an overestimation of the probability of exceeding small losses and a dramatic underestimation of the probability of exceeding large losses. This is consistent with a reduced variability in regional loss, which relates to the mathematical relationship presented in Equation (2.2).

When including correlation between spatially distributed V_{S30}values, it can be seen that there is little change in results compared to when these terms are considered deterministic. This likely occurs because there is not a large variation in V_{S30} values across the region. Therefore, the

variation in expected seismic intensities across the portfolio is not influenced greatly by the dispersion of V_{S30}values. In addition, ground motion amplification factors specific to each site class (based on V_{S30}) are more consistent for lower building periods and higher spectral accelerations (ASCE 2010). Since there many census tracts characterized by mostly low- and mid-rise buildings subjected to high seismic intensities resulting from the scenario earthquake, the ground motion amplification is limited. The high consistency in V_{S30} values and site amplification across the case study region provides a low dispersion in the resulting seismic intensities. This therefore limits the influence that spatial correlation between V_{S30} has on regional loss variability. In order to conclusively evaluate the influence spatial correlation in soil properties has on regional loss assessments, a loss distribution should be evaluated for additional building portfolios that exhibit a larger variation in soil properties and building heights.

5.4 Sensitivity Analysis

Given the constraints listed in Section 4.4 and 5.1, retrofit alternatives are defined by building type, occupancy category, census tract, and either pre- or low-seismic design code levels. Disaggregating the information in this manner may guide the design of policies targeting certain groups of buildings for mitigation. To keep the reliability space manageable, building combinations are limited to those with a total of over 2,000 square feet of floor space per census tract. The sensitivity measure $\partial\beta/\partial C_R$ in Equation (4.11) is evaluated to assess the cost-effectiveness of retrofit for each vulnerable building combination relative to minimizing drift-related losses, and retrofit schemes are prioritized accordingly.

As noted in Section 4.4, the order and magnitude of sensitivity measures depends on the limit state threshold used to compute them. Therefore, retrofit prioritization varies based on the

loss threshold of interest. This threshold is chosen ideally as the desirable level of loss that is to be minimized in a portfolio for a future hazard event. It is emphasized that because the sensitivity measures used to prioritize retrofit are computed relative to changes in γ_{IDR} only, retrofit prioritization is skewed relative to those building combinations that are more sensitive to drift-related damages. As mentioned in Section 4.4, a more comprehensive sensitivity analysis should also include a random variable for modeling resistance to acceleration-sensitive damage. In addition, there are other mitigation measures that do not affect structural response such as ceiling bracing, anchoring equipment, etc. Future inclusion of these parameters will support more effective prioritization of retrofit schemes for all building types.

Figure 5.5 shows the top ten suggested total retrofit expenditures per building type given a budget of $50 million. For illustration purposes, these are arbitrarily based on reducing the probability of exceeding a loss threshold (TL_F) of 50% of the total building replacement cost (ΣBRC). In addition, the respective per-square-foot retrofit expenditures are shown, which provide the suggested retrofit spending normalized by the total vulnerable building area specific to each building type. The figure shows that most of the $50 million retrofit budget should be spent on mid-rise reinforced masonry structures designed to a low-seismic design code, RM1M LC ($12.2 million), and high-rise concrete shear wall buildings also designed to a low-seismic design code, C2H LC ($8.6 million). In addition to the highest total mitigation costs, these building types also assume relatively high per-square-foot suggested retrofit spending. This implies that RM1M LC and C2H LC not only represent a large percentage of floor area relative to the total floor area of vulnerable buildings (9.1 and 6.1%, respectively), but are also characterized by high sensitivities, on average, relative to other building types.

The per-square-foot retrofit expenditures are highest for high-rise, low-code, reinforced masonry buildings with pre-cast concrete diaphragms, RM2H LC ($13.85/sqft), and high-rise, low-code, concrete frame with unreinforced masonry wall buildings, C3H LC ($13.97/sqft). This occurs because the sensitivity analysis suggests mitigating 100% and 91.1% of the total floor area of RM2H LC and C3H LC for the case study portfolio given their high corresponding sensitivity measures. Thus, these building types represent the largest change in β relative to each dollar of retrofit, on average, relative to the other vulnerable building types. Comparing the high per-square-foot retrofit spending to the low suggested total retrofit expenses suggests that RM2H LC and C3H LC have a small percentage of floor area to be retrofitted compared to the total floor area of vulnerable buildings (0.2% and 1.1%, respectively).

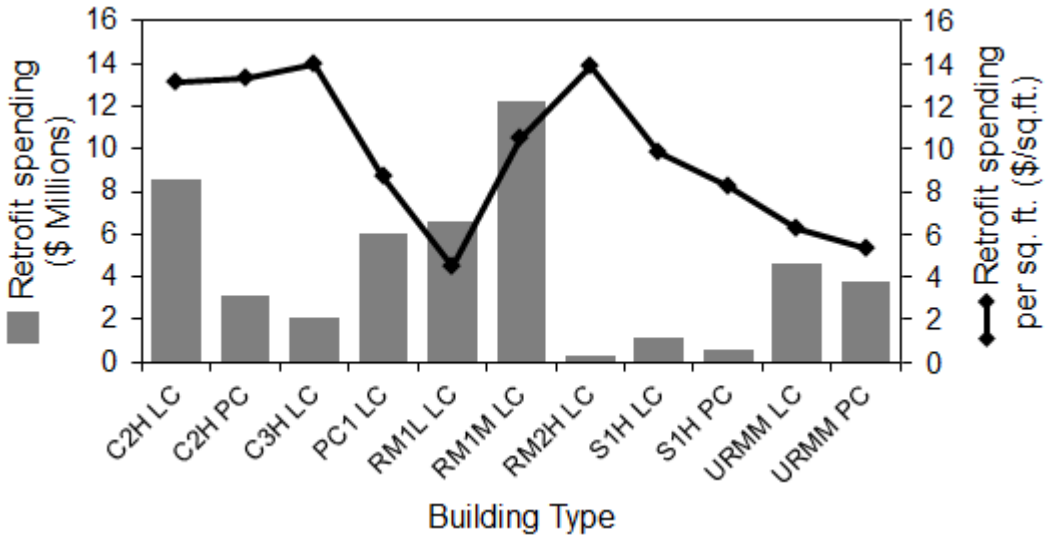

Figure 5.5: Top ten recommended retrofit expenditures by building type given a retrofit budget of $50M and retrofit prioritization based on a sensitivity analysis with TL_F = 50% ΣBRC.

Figure 5.6 shows loss exceedance curves relative to the total repair cost of vulnerable buildings within the case study region, given the scenario earthquake presented in Section 5.2. Given retrofit budgetary constraints of $50 million, $100 million and $150 million, the highest

ranked vulnerable building types are considered for retrofit until each budget limit is met. Results in Figure 5.6(a) are based on retrofit prioritization relative to a loss threshold of 50% Σ*BRC* while Figure 5.6(b) is based on different retrofit prioritization orders corresponding to a TL_F equal to each level of loss listed on the x-axis.

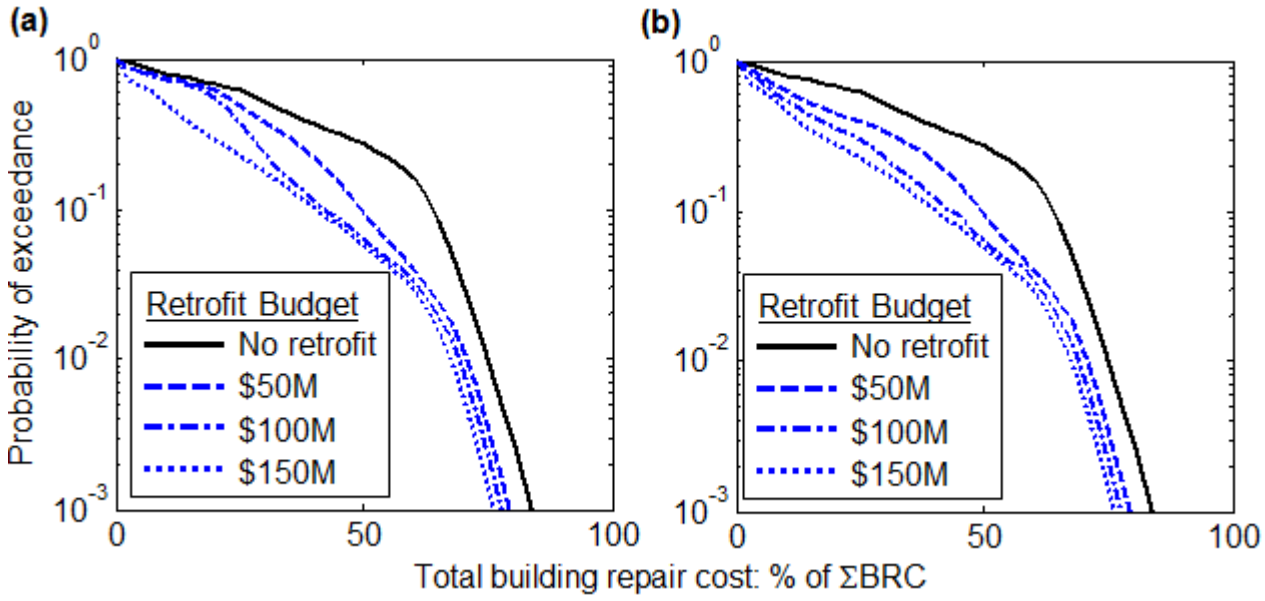

Figure 5.6: Loss exceedance curves for vulnerable buildings with no retrofit and a retrofit budget of $50M, $100M and $150M. Retrofit prioritization is based on a sensitivity analysis with (a) TL_F = 50% Σ*BRC* and (b) TL_F specific to each loss threshold.

It can be seen in Figure 5.6(b) that the effectiveness of retrofit per dollar spent generally decreases as the budget increases for all loss thresholds. This is because a unique retrofit prioritization is considered for each loss threshold and the loss exceedance curve is computed accordingly. For each budget constraint, the most cost-effective building combinations are considered first for retrofit. The cost-effectiveness of retrofit then decreases as the retrofit budget increases and as more building combinations are considered. In contrast, Figure 5.6(a) shows that the chosen retrofit scheme may not necessarily be most effective in reducing overall loss exceedance for all thresholds because it is based only on sensitivity measures computed relative

to a loss threshold (TL_F) of 50% ΣBRC only. Results in Figure 5.6(b) are technically unrealistic given that only one retrofit prioritization scheme would be chosen for a region. This figure, however, shows the importance of choosing the desirable level of loss to be minimized when optimizing retrofit prioritization and portfolio loss reduction.

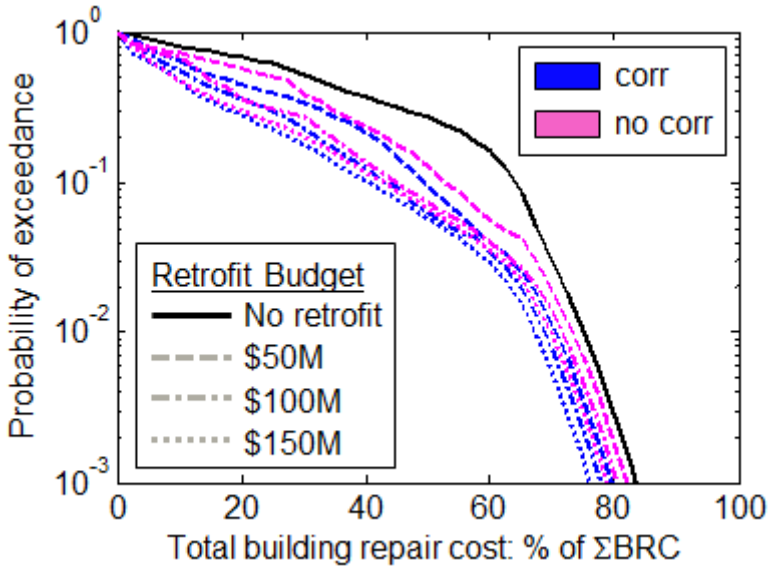

Figure 5.7: Loss exceedance curves for vulnerable buildings with no retrofit and a retrofit budget of $50M, $100M and $150M. Retrofit prioritization is based on a sensitivity analysis with TL_F specific to each loss threshold, and with and without spatial correlation included between seismic intensities.

The final step in this study is performing a sensitivity analysis without spatial correlation included between the seismic intensities across the case study region. This is used to investigate the influence that these correlations, detailed in Section 2.1, have on retrofit prioritization. Loss exceedance curves are shown in Figure 5.7 for retrofitted building combinations prioritized based on sensitivity measures computed with and without correlation. Once building combinations are prioritized for retrofit, the FORM assessment includes spatial correlation to compute the distribution of loss for both cases. These curves are evaluated for the sample

portfolio post-retrofit, assuming a retrofit budget of $50M, $100M and $150M. For illustration purposes, sensitivity measures are calculated for each loss threshold.

When spatial correlation is not included, the reduction in failure probability is generally less than when spatial correlation is considered. Correlation has a large influence on the computed reliability based on Equation (4.10), and consequently, on the corresponding sensitivity measures. This discrepancy in sensitivity calculation thus influences the order of building types for retrofit and therefore, the cost-effectiveness of retrofit given budgetary constraints.

This section demonstrates the use of a sensitivity analysis, computed directly within FORM, for prioritizing retrofit strategies that may be most cost effective for reducing portfolio loss. The results suggest that reinforced masonry buildings and concrete frame with unreinforced masonry wall buildings provide the largest reduction in portfolio loss per dollar spent on retrofit. In addition, it is suggested that to achieve more optimal retrofit prioritization, it is essential to: 1) perform a sensitivity analysis relative to the desirable level of loss to be minimized; and 2) include spatial correlation when computing sensitivity measures. Note that this study prioritizes retrofit only relative to the cost-effectiveness of each mitigation strategy in reducing drift-related losses (see Section 4.4). While post-retrofit portfolio results shown in Figure 5.5 – 5.7 include upgrades to acceleration-sensitive building components as well, future work could include a third variable to compute sensitivities (for prioritizing retrofit) directly related to minimizing acceleration-related damage. In addition, other factors that may influence retrofit decision-making include willingness to pay for retrofit, incurred losses due to retrofit and social importance of vulnerable buildings. It is also noted that the results were computed for a single

scenario earthquake, and a more complete picture would be obtained from selecting a suite of earthquakes, or even incorporating a probabilistic analysis of seismic hazard.

Chapter 6. Community Resilience

6.1 Resilience Introduction and Background

Thus far, the proposed framework presented in this dissertation has quantified seismic risk by estimating the distribution of seismic-induced structural and nonstructural economic loss for a suite of buildings. There are, however additional response and recovery parameters that, when paired with losses that occur immediately following a hazard, define the resilience of a system. Given the additional information provided on the recovery of a system, resilience parameters are considered equally important to loss estimates in hazard management decision making (Cimellaro et al. 2010).

According to the National Academies (2012), resilience is the ability to prepare and plan for, absorb, and recover from adverse events. When focusing on resilience in light of natural hazards, the United Nations (2005) defines resilience as the "capacity of a system, community or society potentially exposed to hazards to adapt, by resisting or changing in order to reach and maintain an acceptable level of functioning and structure." According to Mileti (1999), a disaster resilient community must not only be able to withstand losses to a tolerable level, but also rebuild and recover within an acceptable time frame.

The concept of seismic resilience at a community scale began gaining importance in hazard management in the late 1990's when the Federal Emergency Management Agency (FEMA) initiated a series of community-based pre- and post-disaster (i.e., before and after an earthquake occurrence) mitigation and recovery programs. These programs illustrate how communities can plan for hazard mitigation and disaster recovery through education programs, hazard assessments and mitigation projects (FEMA 2000). FEMA also issued the Disaster Mitigation Act of 2000 and the Disaster-Resistant Universities Program, with the goal of increasing hazard resilience at the state and local level as well as within colleges and universities (FEMA 2003).

Regional hazard resilience also gained international prominence when the United Nations adopted the Hyogo Framework in 2005 (United Nations 2005). This platform launched a series of government programs to improve hazard resilience at both the national and community level. These programs were developed to promote strategic approaches for reducing hazard-induced risks and increase resilience through international and regional collaboration, education programs, and mitigation and management policies.

Despite increasing recognition on the importance of seismic resilience in hazard management, quantifying resilience has been met with many challenges. This likely arises from the complex scope of the definition of resilience. The term "resilience" must account for the numerous sources and characteristics of loss as well as the social, economic and organizational issues within post-disaster recovery. Given these complexities and differing opinions on resilience, a universally agreed-upon method for measuring resilience is still lacking. Many studies within the past decade, however, have proposed various methodologies to measure seismic resilience using quantitative models, empirical algorithms, and professional opinion.

These existing methods, particularly specific to structural system and community resilience, are outlined in the following section. Advantages and limitations to the various approaches are highlighted. A new method to quantify seismic resilience is then proposed, utilizing the FORM-based framework presented earlier. This extended method is applied to assess the resilience of the San Francisco portfolio presented in Chapter 5. Finally, a sensitivity analysis is performed to evaluate the cost-effectiveness of retrofit and restoration mitigation measures in terms of increasing the seismic resilience of a portfolio.

6.2 Quantifying Seismic Resilience

The measurement of resilience is important for understanding, assessing and improving the seismic resilience of infrastructure systems (Bruneau et al. 2003). By identifying and evaluating the inter-related dimensions of resilience, such as the physical, economic and social aspects of a region, quantitative measures can help address why some communities may be more resilient than others. Quantifying resilience is also necessary to identify needs for improved resilience, and how to achieve increased resilience. These applications require quantifying the magnitude and importance of the different components of a system that influence resilience (National Academies U.S. 2012). A consistent metric is also needed to combine each facet into a resilience measurement.

According to Chang and Shinozuka (2004), earthquake loss estimation tools provide a natural starting point for quantifying community resilience. As discussed in Section 3.1, these methods capture the regional impacts of earthquake scenarios based on economic losses, and in many cases, fatalities and injuries. Loss estimation requires information on the seismic hazard,

spatial distribution of an infrastructure system, and the building damage and loss modeling assumptions.

While these parameters relate to community resilience, the notion of resilience suggests a much broader framework, based not only on immediate consequences, but also on time-dependent recovery efforts. The recovery process usually depends on many different criteria, including the availability of technical and human resources, societal preparedness, economic conditions and public policies (Cimellaro et al. 2010; NIBS 2012)

Bruneau et al. (2003) developed one of the first conceptual frameworks for measuring resilience, based on four inter-related dimensions: technical, organizational, social and economic. The technical dimension of resilience describes how well physical systems perform given an earthquake. Organizational resilience refers to emergency response and the ability to carry out critical functions. The social dimension of resilience represents the social impact of losses to critical facilities. Similarly, economic resilience quantifies the direct and indirect economic losses given an earthquake.

In addition, Bruneau et al. (2003) suggested that resilience can be characterized by four main properties: robustness, rapidity, redundancy and resourcefulness. These inter-related parameters are defined by Bruneau et al. (2003) as follows:

- *Robustness*: strength, or the ability of components or systems to withstand a given level of stress or demand without suffering damage or loss of function.
- *Rapidity*: the capacity to meet priorities and achieve goals in a timely manner in order to contain losses and avoid future disruption.
- *Redundancy*: the extent to which components or systems are capable of satisfying functional requirements in the event of disruption, damage, or loss of functionality.

- *Resourcefulness*: the capacity to mobilize resources when conditions exist that threaten to disrupt some component or system of interest.

With reference to resilience, there is a strong correlation between redundancy and resourcefulness, because additional resources can create new redundancies in a system. In addition, changes in redundancy and resourcefulness can greatly influence the robustness and rapidity of a system (Cimellaro and Arcidiacono 2013). For example, additional emergency response resources may increase the efficiency or rapidity of system recovery. Since resourcefulness and redundancies are used to characterize rapidity and robustness, many studies measure resilience primarily in terms of the latter two.

To better understand these inter-related dimensions and properties used to quantify resilience, Table 6.1 shows how each can be applied to the seismic resilience assessment for a suite of buildings.

Table 6.1: Four dimensions of resilience and example applications to a building portfolio

Dimension of Resilience	Performance Measure for a Building Portfolio	Robustness	Rapidity
Technical	Physical condition of buildings	Number of buildings damaged and magnitude of damage	Time required to repair and replace damaged structures
Organizational	The ability of damaged buildings to perform their intended functions	Extent of downtime associated with damaged buildings	Time required to restore usability of buildings
Social	People and businesses displaced due to building damage	How many people and business are displaced	Time required for people and business to return
Economic	Economic losses	Magnitude of economic losses	Time required to repair building functionality and reduce time-dependent loss

While the framework proposed in Bruneau et al. (2003) provided a detailed conceptual approach for measuring seismic resilience of infrastructure systems, it did not offer an explicit procedure to quantify resilience. It did, however, lead to many other studies for measuring resilience, and for extending and modifying the framework that defines it.

Chang and Shinozuka (2004) developed a quantitative measurement of seismic resilience related to the potential losses provided by earthquake loss estimation models. In this framework, resilience is quantified based on the four dimensions of resilience proposed by Bruneau et al. (2003), and categorized with a robustness and rapidity standard. In contrast to previous resilience frameworks, this study reframes the resilience measures in a probabilistic context by measuring the reliability with which a system will meet a minimum acceptable threshold of resilience.

Bruneau and Reinhorn (2007) were the first to quantify resilience based on the relationship between seismic performance, fragility curves, and resilience functions. This approach is applied to measure the resilience of an acute care facility system with respect to the percentage of healthy population and to the treatment capacity of the total hospital infrastructure. Cimellaro et al. (2010) added to the resilience measurement of healthcare facilities with a quantitative method that evaluates seismic resilience based on dimensionless analytical resilience functions. Their model combines loss estimation and recovery models, which are applied to a standard California hospital building.

Renschler et al. (2010) extended resilience quantification to holistically measure the hazard resilience of communities. Quantitative and qualitative models were developed based on seven identified dimensions of community resilience represented by the acronym 'PEOPLES': Population and Demographics, Environmental/Ecosystem, Organized Governmental Services,

Physical Infrastructure, Lifestyle and Community Competence, Economic Development, and Social-Cultural Capital.

The PEOPLES approach provided the basis for quantitative models developed in Cimellaro and Arcidiacono (2013), which are used to continuously measure the functionality and resilience of communities against extreme events. In this approach, resilience measures are suggested to be used as a performance based-metric for structural design and refer to this new design methodology as Resilience-Based Design (RBD). This method is based on optimizing the resilience of structures and their surrounding region, as opposed to focusing solely on the performance of individual structures.

This review of resilience quantification literature, although not exhaustive, brings to light distinct characteristics and potential limitations in the presented methodologies. Many existing approaches only provide a conceptual framework for identifying key properties of resilience to be quantified. While these studies do contribute to the further understanding of quantifying resilience, explicit quantification is the next necessary step to utilize resilience measures in hazard management. Those methods that do quantify resilience analytically often only consider expected value of losses and other resilience metrics, rather than preserving the uncertainties surrounding these. As discussed in Chapter 2, regard for only the expected value of losses suppresses the system effects that significantly influence the variance of regional loss. This includes spatial correlations that may exist between the performances of individual components within a system. Furthermore, most resilience approaches are tailored to quantify the resilience of infrastructure systems, community social structures or healthcare facilities, as opposed to generic building portfolios, which are the focus of this dissertation.

In addition to quantifying resilience, improved hazard management also requires an investigation of increasing future seismic resilience. To accomplish this, pre-disaster conditions and post-disaster recovery must be integrated into a common framework (Chang and Shinozuka 2004). This aggregated assessment is necessary due to the correlated relationship between loss and recovery. As such, a comparative study can be used to evaluate the effectiveness of various pre- and post- disaster loss reduction measures, including structural retrofit and increased efficiency in post-disaster repair and recovery. Many existing studies capture the change in system resilience given structural retrofit. To the author's knowledge, however, there is yet to be a framework that explicitly compares the effectiveness of structural retrofit with changes in post-disaster restoration efficiency.

The method presented in the following section quantifies the resilience of a building portfolio based on its performance over time, following a hazard. The framework utilizes the FORM-based method presented in this dissertation to probabilistically evaluate varying thresholds of seismic resilience. With this approach, an additional random variable is added to the reliability problem to model the variability in recovery time. In addition, a sensitivity analysis is performed to evaluate and compare the cost-effectiveness of increasing portfolio resilience based on pre-disaster retrofit and post-disaster restoration schemes.

6.3 Extension of the Proposed FORM Method

The basis for the resilience quantification used in this study is adapted from the techniques presented in Bruneau et al. (2003) and Cimellaro et al. (2010). Using the FORM-based approach presented earlier in this dissertation, a refined method is then presented, which addresses many of the existing limitations outlined in Section 6.2. This proposed method offers

three important new capabilities over the previous techniques used to quantify resilience: 1) it measures resilience in a probabilistic context; 2) it accounts for spatial correlations between building performances; and 3) it provides sensitivity measures for prioritizing both retrofit and post-disaster restoration measures used to increase the seismic resilience of a building portfolio. While mitigation often refers to risk-reducing measures performed prior to an earthquake, it is used in this chapter to refer to any measure performed pre- or post-earthquake to increase regional resilience.

In this method, each dimension of resilience is combined and tabulated into a common metric for representing the performance of a system (e.g., economic loss given a hazard) over time, $Q(t)$. Resilience (R) is defined graphically in Figure 6.1 as the normalized shaded area under this dimensionless function. This is mathematically defined by the following equation (Bruneau et al. 2003; Cimellaro et al. 2010; Ouyang and Dueñas-Osorio 2012):

$$R(\%) = \int_{T_0}^{T_{RE}} \frac{Q(t)}{T_{RE}} dt \tag{6.1}$$

where T_0 is the time the earthquake occurs and T_{RE} is the total recovery time to restore system performance. Accordingly, the loss of resilience (LoR) is measured as the amount of expected degradation in quality over time. This corresponds to the difference between a normalized resilience of 100% and the reduced resilience given an earthquake event, and can be written as follows:

$$LoR(\%) = 100 - R \tag{6.2}$$

This framework is based on the notion that the system performance, expressed as a percentage, varies in time ranging from 100% (assuming full performance prior to the

earthquake) and 0% (zero performance). The scheme, shown in Figure 6.1, assumes an earthquake occurs at time $T_{0,}$ and that the system performance is reduced immediately to P_0. This initial reduction in performance relates to the robustness of a system (R_o), expressed as a percentage of system performance based on the predicted total losses (TL):

$$R_o(\%) = 100 - \frac{TL}{PTL} \tag{6.3}$$

where PTL is considered the potential total loss associated with a 100% reduction in system performance given an earthquake event and TL corresponds with P_0.

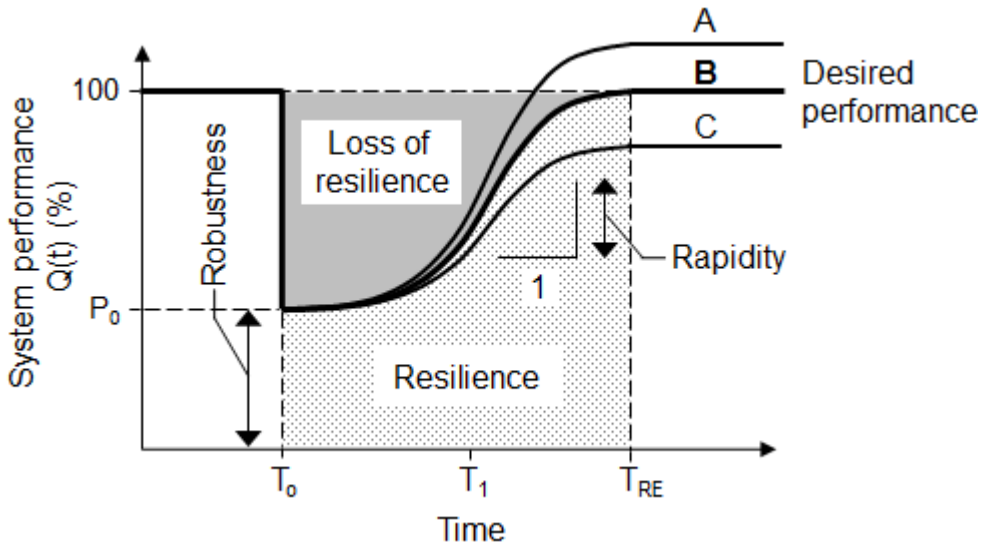

Figure 6.1: Conceptual framework for resilience measurement.

Cimellaro et al. (2010) mathematically define the rapidity of recovery (R_a) as the slope of the performance restoration curve during the post-disaster recovery time. This can be written as:

$$R_a = \frac{\mathrm{d}Q(t)}{\mathrm{d}t} \tag{6.4}$$

Rapidity is shown in Figure 6.1 to vary between T_0 and T_{RE}, based on the rate of restoring

system performance over time.

The shape of the performance restoration curve is a function of changes in system performance due to repair and recovery efforts. The time T_1 represents an intermittent time between an earthquake occurrence and full restoration time, such as time associated with loss of building function. The estimation of time associated with loss of building function and full recovery, and the uncertainty surrounded each, will be discussed in Section 6.3.2. Figure 6.1 assumes that system performance is restored to the pre-earthquake level of baseline performance (curve B). It may be desirable, however, to exceed this level of performance in the repair and recovery process, subsequently decreasing the vulnerability of structures to a similar future hazard (curve A). Conversely, the system may also suffer permanent losses, preventing it from reaching pre-earthquake baseline performance (curve C).

The next section provides a brief overview of the sources and estimation of immediate and time-dependent losses used to quantify the robustness of a system. Many of these additional losses are a function of the total building recovery time and loss of function time. These post-disaster periods are modeled probabilistically by a random variable, as discussed in Section 6.3.2. Using this added variable and the random variables presented in Section 4.1, Section 6.3.3 describes the proposed preliminary evaluation of regional seismic resilience. The sensitivity analysis used to prioritize cost-effective mitigation measures to increase portfolio resilience is also presented.

6.3.1 Loss Function

The total losses computed in this study are divided into two types: Direct losses that occur during or immediately after a hazard event and indirect losses that are considered to be dependent on the period of recovery following an event. Direct losses include:

- Structural repair and replacement costs (L_S)
- Nonstructural acceleration- and drift-sensitive repair and replacement costs (L_{NSA} and L_{NSD}, respectively)
- Building contents losses (L_C)
- Building inventory losses (L_{BINV})

Time-dependent indirect losses include:

- Relocation expenses (L_{RE})
- Loss of business income (L_{BI})
- Loss of rental income (L_{RI})

The computation for each type of loss is adapted from the HAZUS-MH methodology given its availability and applicability to a disaggregated building data set (NIBS 2012). The use of other, more detailed loss functions, however, is encouraged as they become available. Similar to the repair costs computed in Section 4.2, each is computed based on four damage states (slight, moderate, extensive and complete). The losses are then summed over a set of 36 representative building types (bt), 33 occupancy categories (oc) and high-, moderate-, low- and pre-seismic design code levels. A description and computation of structural and nonstructural losses (L_S, L_{NSA} and L_{NSD}) are given in Section 4.2. A brief overview of the additional losses considered in this section and how they are computed, is provided below.

Each additional loss function includes the probability that a specified building type is within each structural or acceleration-sensitive nonstructural damage state ($PS_{bt,ds}$ and $PNSA_{bt,ds}$). Details on computing these terms using the random variables lnS_a and γ_{IDR} are provided in Section 4.2. In addition, each loss function includes a damage ratio used to scale the

value of contents, inventory or potential revenue. These parameters are also taken from the HAZUS-MH methodology, based on building occupancy category and inventory data. Damage ratios are considered a function of the total replacement cost associated with each type of loss. For additional details on the parameters involved in each loss computation, see NIBS (2012).

Content Losses

It is assumed that the majority of damage to building contents, such as furniture, electronics, etc., takes place because of overturned cabinets or tables. According to the HAZUS-MH methodology, this is largely a function of seismic-induced accelerations (NIBS 2012). As such, damage to nonstructural acceleration-sensitive components is considered a good indicator for building content damage. The following equation is used to estimate content losses:

$$L_C = \sum_{oc=1}^{33} \sum_{bt=1}^{28} \sum_{ds=1}^{4} CRV_{oc,bt} * PNSA_{bt,ds} * RCD_{oc,ds} \tag{6.5}$$

where CRV_{oc} is the contents replacement value for occupancy oc and building type bt, $PNSA_{bt,ds}$ is the probability that each building type bt is in nonstructural acceleration damage state ds, and $RCD_{oc,ds}$ is the contents damage ratio for each occupancy category oc in nonstructural acceleration damage state ds.

Business Inventory Losses

In addition to basic contents, many businesses have additional inventory that may yield future revenue. The value of this inventory, corresponding to the potential loss, depends on the type of business and size of building. HAZUS-MH estimates this loss from annual sales associated with each occupancy category. Similar to content damage, building inventory damage

is associated with the likelihood of damage to nonstructural acceleration-sensitive components. Therefore, building inventory loss is given by:

$$L_{BINV} = \sum_{oc=1}^{33} AGS_{oc} * BI_{oc} * FA_{oc} * \sum_{bt=1}^{28} \sum_{ds=1}^{4} PNSA_{bt,ds} * RINV_{oc,ds} \quad (6.6)$$

where FA_{oc}, AGS_{oc} and BI_{oc} are the floor area, annual gross sales per unit area and business inventory as a percentage of annual gross sales, respectively, for occupancy oc. $RINV_{oc,ds}$ is the ratio of inventory damage for each oc in nonstructural acceleration damage state ds. AGS_{oc} and BI_{oc} are provided in NIBS (2012) relative to each occupancy category.

Relocation Expenses

After an earthquake, many buildings may be unfit for occupancy or to be used for their intended purposes. In this case, there are expenses that relate to disruption costs and additional rental costs specific to each occupancy category and building size. For example, a high-tech industrial building will likely experience much higher disruption expenses than a multi-family residential building. These relocation expenses are computed as:

$$L_{RE} = \sum_{oc=1}^{33} FA_{oc} * \begin{bmatrix} \left(1 - \frac{\%OO_{oc}}{100}\right) * \sum_{bt=1}^{28} \sum_{ds=1}^{4} PS_{bt,ds} * DC_{oc} + \\ \frac{\%OO_{oc}}{100} * \sum_{bt=1}^{28} \sum_{ds=1}^{4} PS_{bt,ds} * (DC_{oc} + RENT_{oc} * T_{RE_{oc,ds}}) \end{bmatrix} \quad (6.7)$$

where $\%OO_{oc}$ is the percentage of buildings that are owner occupied, DC_{oc} is the disruption cost and $RENT_{oc}$ is the additional rental cost for occupancy oc, and T_{RE} is the recovery time for occupancy oc in damage state ds.

Loss of Business Income

The downtime associated with building damage also hinders the generation of potential income for businesses. This income includes business-related profits, supplier and royalty payments, labor compensation, bank loan and interest payments, etc. HAZUS-MH computes income losses as a function of expected business income, the likelihood of structural damage and expected downtime. Income loss is calculated as follows:

$$L_{BI} = \sum_{oc=1}^{33} (1 - RF_{oc}) * FA_{oc} * INC_{oc} \sum_{bt=1}^{28} \sum_{ds=1}^{4} PNSA_{bt,ds} * T_{LOF_{oc,ds}} \quad (6.8)$$

where RF_{oc} is the recapture factor related to a reduction in business-related losses for working overtime, INC_{oc} is the income per day and per square foot, and $T_{LOF_{oc,ds}}$ is the loss of function time for occupancy oc in damage state ds.

Loss of Rental Income

In addition to business-related income losses, additional post-disaster losses are associated with disruptions in rental income for residential, commercial and industrial buildings. Loss of rental income is computed as follows:

$$L_{RI} = \sum_{oc=1}^{33} \left(1 - \frac{\%OO_{oc}}{100}\right) * FA_{oc} * RENT_{oc} \sum_{bt=1}^{28} \sum_{ds=2}^{4} PNSA_{bt,ds} * T_{RE_{oc,ds}} \quad (6.9)$$

The total loss, used to compute system performance is therefore computed as the summation of direct losses and time-dependent indirect losses:

$$TL = L_D + L_I \tag{6.10}$$

where:

$$L_D = L_S + L_{NSA} + L_{NSD} + L_C + L_{BINV} \tag{6.11}$$

$$L_I = L_{RE} + L_{BI} + L_{RI} \tag{6.12}$$

6.3.2 Repair and Recovery Time

The loss functions outlined above are based on two types of post-disaster restoration times: T_{RE} for total building recovery time and T_{LOF} for the time that a facility is unable to conduct business. Total building recovery times are a function of post-disaster cleanup and repair, along with any delays in decision-making, financing, inspection, etc. that may accompany the recovery process. These are often accompanied by a large amount of uncertainty as some businesses may accelerate repair and reopen quickly after an earthquake. Others, meanwhile, may close for an extended period of time due to disruptions in the recovery process. T_{LOF} is considered to be shorter than T_{RE}, because businesses are often able to relocate temporarily to alternative locations during cleanup and repair.

The HAZUS-MH loss estimation methodology provides median times for total building recovery specific to each representative occupancy category (NIBS 2012). It also provides factors for computing the occupancy-specific T_{LOF} as a function of T_{RE}. While these data do provide a starting point for incorporating the time trajectory of recovery into regional resilience models, HAZUS-MH rehabilitation times have been criticized as being too rudimentary in modeling building recovery time (Miles and Chang 2006). One reason for this is because

provided median times assume that all buildings, on average, are recovered within two years. This is not always realistic, however, as in the case of the Loma Prieta Earthquake where 50% of the damaged housing units remained unrepaired or un-replaced four years after the earthquake (Comerio et al. 1994).

Inclusion of the uncertainty associated with each post-disaster recovery period helps to build a more realistic model of restoration into this study's proposed resilience assessment. This idea has been seen previously in ATC-13 (1985), which adds results from a questionnaire eliciting expert evaluations on post-disaster recovery times. These results were used as a starting point for the median recovery times used in HAZUS-MH. In the ATC-13 study, experts in various earthquake engineering disciplines were asked to provide estimates of the time required to restore function for each occupancy category to 30%, 60% and 100% of the normal facility function for various levels of damage. Weighted mean and standard deviations were computed based on responses and levels of participant expertise.

The results from ATC-13 are used to model the uncertainty in T_{RE} for this study. The recovery time variable is then used to compute the probability distribution of time-dependent losses in Equations (6.7) – (6.9). It is assumed that the uncertainty associated with total recovery time is represented best by the standard deviations listed in ATC-13 for restoring building function to 100%. While median values and standard deviations associated with T_{RE} are provided for each damage state used in this study, introducing a random variable to model each of these would increase the size and complexity of the reliability problem significantly. Therefore, to minimize the added complexity, a single random variable is used to model the distribution of recovery time associated with the complete damage state for each occupancy category. Deterministic factors are introduced to compute the corresponding recovery times for each

additional damage level. Post-disaster loss of function time (T_{LOF}) is also computed directly from the T_{RE} random variable using factors provided in NIBS (2012).

Modeling the recovery path assumed by *Q(t)* in Figure 6.1 is even more complex given the uncertainties and interdependencies within a system's recovery process. Limited literature exists on comprehensive and analytical recovery models, likely due to this complexity and uncertainty. Three typical recovery functions that are often assumed in resilience studies are based on linear (Bruneau and Reinhorn 2007; CRSI 2011; Zobel and Khansa 2011), trigonometric (Chang and Shinozuka 2004) and exponential (Cimellaro et al. 2010; Gilbert 2010; Kafali and Grigoriu 2004) functions as shown in Figure 6.2.

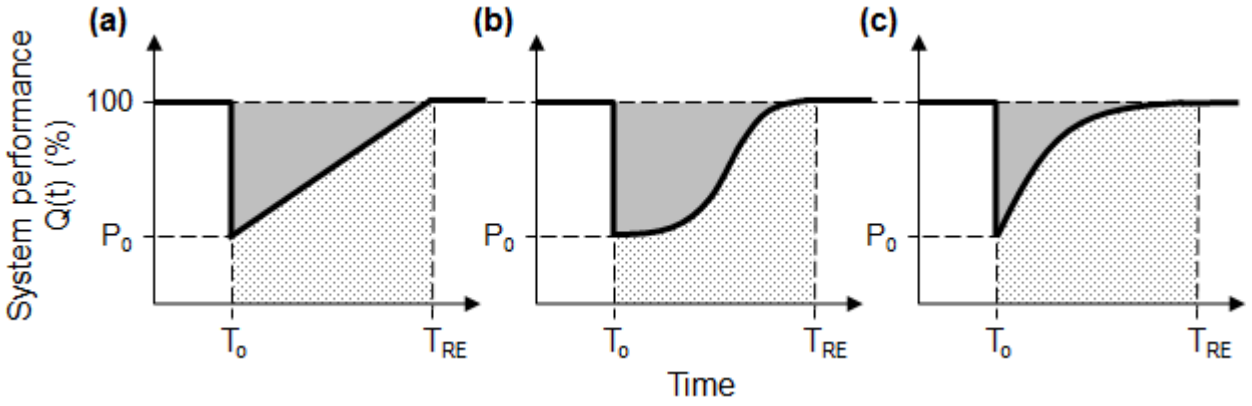

Figure 6.2: Recovery function curves: (a) linear, (b) trigonometric and (c) exponential.

Each recovery function relates to a system's response and recovery over time, and therefore relate to pre-disaster parameters such as preparedness and economic activity. For example, the exponential recovery function may be used when there is a high initial rate of recovery given a large influx of labor, material, and economic resources. In this case, the rapidity of recovery then decreases over time as there is a decreased availability in resources. The trigonometric function may be used when there is slow recovery following a hazard because there is a lack of preparedness or available resources. Rapidity increases, however, as the system

becomes organized and resources become available. The linear function typically is applied when there is limited information for preparedness, response or available resources following a hazard. The resilience assessment proposed in this dissertation will assume the linear recovery function for two reasons: 1) due to lack of data on regional preparedness and response; and 2) to satisfy the objective of generalizing the proposed method for different portfolios and regions.

The recovery time variable (T_{RE}) and linear recovery function used in this study are considered a preliminary model for capturing the time trajectory of recovery. These may, however, be associated with significant assumptions and potential error, thus requiring more investigation on community-specific recovery processes to provide a more accurate resilience assessment. Additional assumptions are also made by considering a deterministic relationship between a single random variable used to model recovery time at the complete damage state and recovery times for other damage levels. Given that the primary contribution of this study is the application of the FORM-based method to predict portfolio resilience, rather than developing a comprehensive model for recovery time, the use of a single recovery time variable specific to each occupancy category is considered sufficient.

6.3.3 Resilience Evaluation

The loss of resilience, computed in Equation (6.2), is used in the following equation to evaluate the probability of exceeding a resilience loss threshold (LoR_F):

$$P(F) = P(LoR_F - LoR \leq 0) \tag{6.13}$$

Similar to Equation (4.10), FORM is used to compute the probability of exceeding varying *LOR* thresholds, and the resulting failure probabilities are used to compute a distribution of resilience loss.

Figure 6.1 suggests that an increase in seismic resilience can relate directly to an increase in the robustness or rapidity of a system. Changes to these parameters and the resulting reduction in system resilience loss are depicted in Figure 6.3. For illustrative purposes, an increase in system rapidity (ΔR_a) is based on a constant drop in system performance (P_0) given an earthquake event.

A sensitivity analysis using FORM is performed to evaluate and prioritize the effectiveness of changes to the robustness and rapidity of building performance relative to an increase in community seismic resilience. As defined previously, a change in robustness relates to a change in component or system strength. In this study, structural retrofit is considered to provide an increase in robustness for when the structure is subjected to earthquake loading. Using the approach presented in Section 4.4, sensitivity measures are used to prioritize the retrofit of vulnerable buildings based on the change in seismic resilience per dollar of retrofit. The sensitivities are computed using Equation (4.11), but $\partial\beta/\partial\gamma_{IDR}$ is computed relative to the limit state in Equation (6.13).

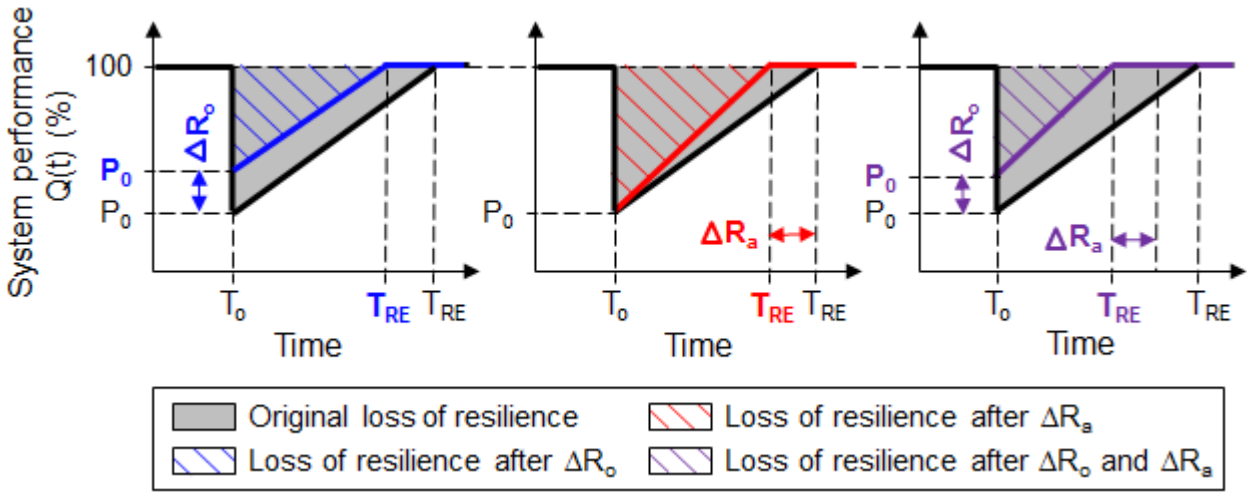

Figure 6.3: Conceptual illustration of changes in measured resilience as a function of increased robustness (ΔR_o), increased rapidity (ΔR_a) and increased robustness and rapidity. The model

used in this study assumes a linear recovery function.

As seen in Figure 6.3, increasing seismic resilience is also a function of an increase in post-disaster system rapidity. This increase may be associated with changes in the restoration period following an earthquake including, but not limited to: 1) increased preparedness in the emergency response, cleanup and building repair process; 2) decreased time to obtain financing, permits or design; and 3) more efficient decision-making. In this study, a more efficient response and recovery following an earthquake is considered represented directly by a decrease in recovery time. This decrease is modeled by a change in the random variable T_{RE} for each building combination. Using this additional variable, sensitivity measures are computed based on the increase in seismic resilience per marginal change in recovery time.

It is often desired to achieve an increase in seismic resilience in the most efficient and cost-effective manner. Therefore, a comparative assessment in terms of increasing resilience through changes in robustness, rapidity or a combination of the two is required. Using the sensitivity measures computed relative to pre-disaster retrofit and changes in post-disaster recovery time, a change in the reliability index specific to a resilience threshold may be compared directly to the corresponding retrofit cost or change in recovery time. Nevertheless, this comparison would be more useful if the loss reduction measures were represented by a common unit of cost. Assigning a monetary value to changes in recovery time is a complex task, however, because there are many components that influence the recovery process, each surrounded by large uncertainties.

In order to perform such a comparative assessment, this study assumes that money invested in increasing the rapidity of system recovery relates directly to a change in recovery time following an earthquake occurrence. For example, more money may incentivize faster

procurement of required materials and labor for repair, or in more efficient repair design, construction, decision-making, etc. Sensitivity measures associated with a change in reliability for a resilience threshold, relative to the cost allocated to decreasing post-disaster recovery time ($C_{\Delta T_{RE}}$) are computed as:

$$\frac{\partial \beta}{\partial C_{\Delta T_{RE_i}}} = \frac{\partial \beta}{\partial T_{RE_i}} * \frac{\partial T_{RE_i}}{\partial C_{\Delta T_{RE_i}}} \tag{6.14}$$

where $\partial \beta / \partial T_{RE_i}$ is the sensitivity measure computed to find the design point in a FORM assessment by differentiating the reliability index relative to T_{RE} for building *i*. The term $\partial T_{RE} / \partial C_{\Delta T_{RE}}$ represents the marginal change in T_{RE} for each dollar spent to decrease the full restoration time following an earthquake.

For a preliminary assessment, it is assumed that doubling the repair cost for a building will reduce recovery time by 50%. This relationship is assumed to be linear, and considered consistent for each building combination, based on building type, seismic design code era and occupancy category. With this assumption, the incremental change in T_{RE} per dollar spent on reducing recovery time can be approximated as:

$$\frac{\partial T_{\mathrm{RE}}}{\partial C_{\Delta T_{RE}}} \approx \frac{0.5 * T_{RE}}{RC} \tag{6.15}$$

where RC is the total repair cost associated with structural, nonstructural drift-sensitive and nonstructural acceleration-sensitive damage. These total repair costs are considered TL in Equation (4.6) prior to the introduction of additional immediate and time-dependent losses in this chapter. It is stressed that this is only a preliminary measurement of the cost associated with a change in post-disaster repair time. This cost may vary depending on building material, location,

occupancy, etc. and also based on post-disaster recovery factors such as demand surge (Olsen and Porter 2011). Further investigation is required to more accurately assign a monetary value to this change in recover time.

Using the proposed sensitivity measures, $\partial\beta/\partial C_R$ computed using Equation (4.11) and $\partial\beta/\partial C_{\Delta T_{RE}}$ computed using Equation (6.14), pre- and post-earthquake loss reduction measures can be prioritized based on the increase in portfolio seismic resilience per dollar spent. This can provide valuable information for decision makers for finding the optimal balance of allocating money to structural retrofit and/or to post-disaster recovery measures.

The method presented in this section offers a preliminary tool for quantifying seismic resilience for a building portfolio and identifying measures to increase resilience. A more comprehensive assessment will need to consider the influence the relationship between building assets over time has on time dependent losses. This is outside the scope of this dissertation, because it depends on the complex, interdependent system of building resource supply and production availability and alternatives within a portfolio. Details on the parameters involved in this type of computation are included in NIBS (2012). Such information is not included in the building inventory data used in this study.

A more complete resilience framework should consider fatalities and injuries resulting from a hazard. While it is possible to include the estimation of fatalities into this method, the scope of this study is restricted to only monetary losses. Future research could focus on including hazard-induced fatalities and injuries into the results, however, the controversy surrounding the concept of assigning a monetary value to each fatality must be considered.

In addition to building-related measures, evaluating the consequences to other infrastructure units can provide a more extensive framework to quantify regional resilience. This

may include roadway networks, utility systems or emergency response lifelines, as well as the correlation between these systems. These can be evaluated in a similar manner to the building portfolio resilience assessment, but with different variable inputs specific to the infrastructure system, and consideration correlation between system performances.

6.4 Case Study

The resilience quantification procedure described above is now applied to the San Francisco building portfolio introduced in Section 5.1. The portfolio is subjected to the scenario earthquake presented in Section 5.2, assuming median V_{S30} values and spatially correlated residual terms at each census tract. Given the building inventory constraints listed in Section 5.1 and the additional T_{RE} random variable, the resilience evaluation consists of over 4,500 random variables.

Results in the form of loss exceedance curves are shown in Figure 6.4. These are computed using FORM and MCS with respect to a range of loss of resilience (*LoR*) thresholds listed on the x-axis. Results are also shown without spatial correlation in order to evaluate the influence that correlation between sites may have on regional seismic resilience studies.

Although the FORM approach yields a similar trend in results to those obtained using MCS, there are notable deviations. When compared to the loss exceedance curves shown in Figure 5.3 for structural and nonstructural losses, it is observed that a larger error is associated with the FORM computation for the resilience-based results, particularly for the larger *LoR* thresholds. As discussed in Section 4.5, these errors are likely due to nonlinearities in the limit state surface not captured using FORM. When there is a large range of values random variables can assume to satisfy a given limit state constraint, this will often be associated with considerable

limit state nonlinearity. The resilience-based assessment has 50% more random variables compared to the loss assessment in Chapter 4 and Chapter 5, which are used to capture the variability in recovery time. Since each of these additional variables are considered independent from others, more nonlinearity will likely occur in the resulting limit state surface, which leads to more error in the FORM results. Figure 6.4 and Figure 5.3 do show, however, that the proposed FORM method does provide a reasonable approximation to the much more computationally intensive simulation approach. Sources of limit state nonlinearity that can potentially be limited for improvement to FORM results are identified in Section 4.5.

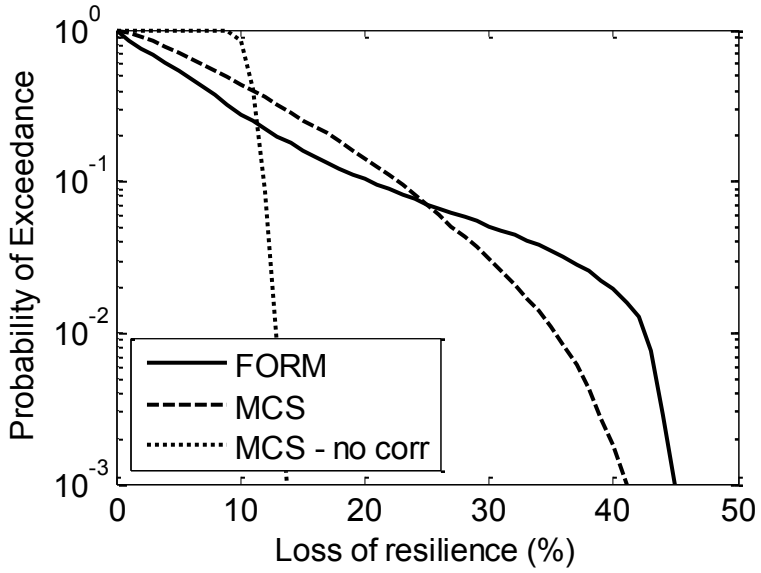

Figure 6.4: Loss exceedance curves capturing loss of portfolio resilience using FORM and MCS given the scenario earthquake outlined in Section 5.2.

Additionally, it is observed that neglecting the spatial correlation that exists between seismic intensities results in an overestimation of the probability of exceeding small resilience losses and a dramatic underestimation of the probability of exceeding large resilience losses. This emphasizes the importance of considering spatial correlation when quantifying portfolio resilience as a probability distribution.

The time required to compute the exceedance curves in Figure 6.4 using FORM took considerably less time than with MCS. For example, the MCS results for a *LoR* threshold of 40% took about 20 minutes to compute. By comparison, optimization required by FORM took approximately 60 seconds on a personal computer with a 2.4 GHz processor and 2GB RAM. To compute the loss exceedance curve, and therefore, the distribution of *LoR*, the reliability computations must be ran for multiple *LoR* thresholds. The required computation time for MCS also increases for larger consequence thresholds indicative of more rare events, because the sample size must also increase. In these respects, FORM is significantly more computationally efficient than MCS.

In the second part of this case study, sensitivity measures relative to retrofit and restoration are computed in order to prioritize mitigation measures for increasing the seismic resilience of the portfolio. These measures are evaluated for all vulnerable building combinations designed to a pre- or low-seismic design code level and a total floor area greater than 2,000 square feet per census tract. As noted in Section 4.4 and 5.4, the order and magnitude of sensitivity measures depends on the limit state threshold used to compute them. As such, mitigation prioritization and the resulting post-mitigation *LoR* exceedance probability vary based on the resilience threshold of interest. This threshold is ideally chosen as the desirable level of *LoR* to be minimized for a portfolio.

Figure 6.5 shows the probability (referred to as *Pe* in the figure) of exceeding various loss of resilience thresholds for multiple cases where money is spent on mitigation measures specific to ΔR_o, ΔR_a or a combination of both. The highest ranked vulnerable building types are considered for retrofit or heightened restoration efficiency up to each specific budget constraint. For illustration purposes, mitigation prioritization and the corresponding exceedance probability

is computed relative to each LoR_F threshold on the x-axis. When applied to an actual building portfolio, however, optimal mitigation prioritization should be based on a specified level of *LoR* to be mitigated.

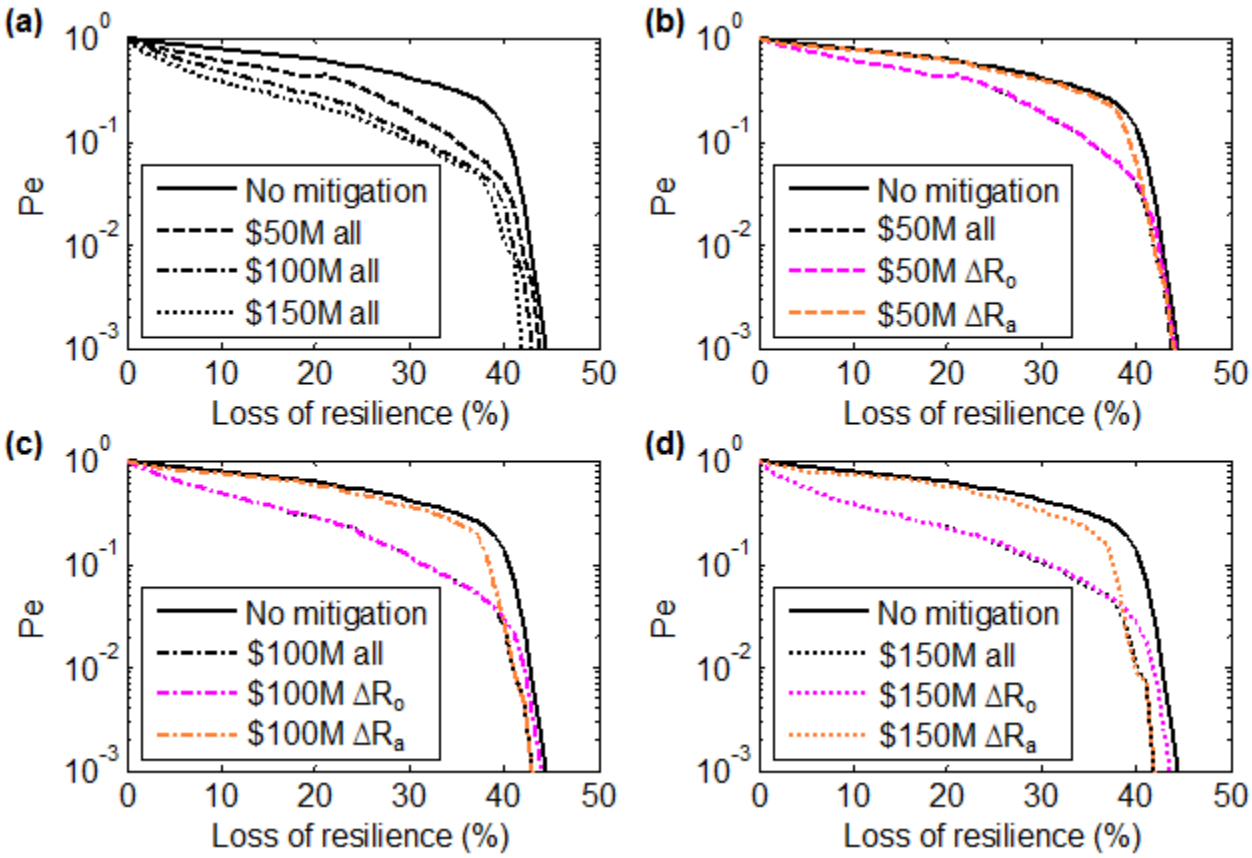

Figure 6.5: (a) Loss exceedance curves for vulnerable buildings within the case study portfolio without mitigation, and with mitigation measures specific to ΔR_o and ΔR_a (all) given budgetary constraints of \$50M, \$100M and \$150M. Loss exceedance curves for ΔR_o and ΔR_a (all), only ΔR_o and only ΔR_a are shown given a mitigation budget of (b) \$50M, (c) 100M, and (d) \$150M. Mitigation prioritization is based on a sensitivity analysis with LoR_F specific to each loss of resilience threshold.

Figure 6.5(a) shows loss exceedance curves relative to the total loss of resilience before and after mitigation relative to changes in ΔR_o and ΔR_a (referred to as "all" in the figure). In general, the effectiveness of mitigation per dollar spent decreases as the budget increases for all resilience loss thresholds. This is because a unique mitigation prioritization scheme is considered

for each threshold, and the loss exceedance curve is computed accordingly. For each budget constraint, the most cost-effective building combinations are considered first for mitigation based on ΔR_o and ΔR_a sensitivity measures. The cost-effectiveness of mitigation then decreases as the budget increases and as more building combinations are considered.

Figure 6.5(b-d) disaggregate the loss exceedance curves in order to compare changes in resilience loss relative to only ΔR_o or ΔR_a mitigation, and a combination of the two, for each budget constraint. For most resilience thresholds and budget constraints, a change in building robustness (through retrofit) is a more cost-effective mitigation measure, compared with money allocated for reducing recovery time following an earthquake. For example, given a budgetary constraint of $100 million, the probability of exceeding a 30% loss in resilience is reduced from 0.41 to 0.12 with retrofit. In contrast, the exceedance probability is reduced from 0.41 to 0.35 with mitigation specific only to post-disaster restoration.

At higher resilience loss thresholds associated with lower probability of exceedance, restoration mitigation measures become most cost-effective for increasing portfolio resilience. For the case study region, this transition occurs at a resilience loss threshold of around 40%, depending on the mitigation budget. The disparity in cost-effectiveness between ΔR_o and ΔR_a mitigation measures increases as the budget increases. This phenomenon is consistent with the expectation that primarily time-dependent losses are associated with changes in resilience loss at high thresholds. Since resilience losses specific to robustness are no longer prevalent at these thresholds, retrofit spending has little impact on reducing the corresponding loss of resilience.

It is emphasized that the comparison between ΔR_o or ΔR_a sensitivities depends completely on the cost assignment for recovery time change shown in Equation (6.15). A smaller or larger change in T_{RE} per dollar of retrofit would influence the cost-effectiveness of ΔR_a

mitigation relative to that for changes in ΔR_o significantly. This may influence the prioritization shown above greatly. In addition, as discussed in Section 4.4 and 5.4, retrofit prioritization in this study may be skewed relative to building combinations more sensitive to drift-related damages.

For an additional comparison of retrofit and restoration mitigation measures, Figure 6.6 presents the top ten total mitigation expenditures per building type given a budget of $50 million. In addition, the respective per-square-foot mitigation expenditures are shown, which provide the suggested spending normalized by the total vulnerable building area specific to each building type. These are shown for mitigation specific to ΔR_o, ΔR_a or for a combination of the two, per building type. The suggested mitigation expenditures are based on reducing the probability of exceeding a loss of resilience of 40%. At this threshold, both ΔR_o and ΔR_a measures contribute to optimal mitigation spending, as illustrated in Figure 6.5.

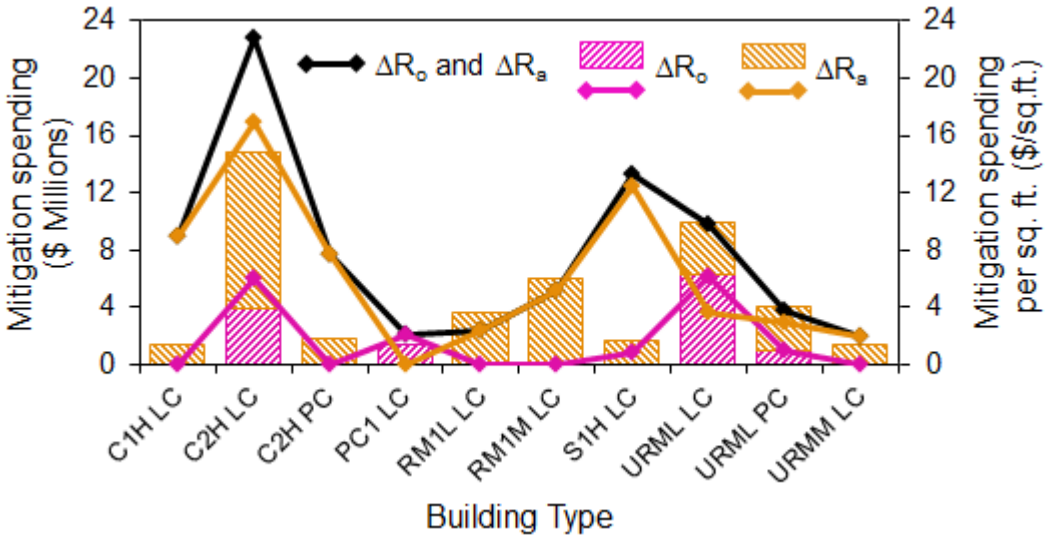

Figure 6.6: Top ten recommended mitigation expenditures by building type for a mitigation budget of $50M and mitigation prioritization based on a sensitivity analysis with *LoR* = 40%.

This figure shows that, when considering both ΔR_o and ΔR_a mitigation measures, a large portion of the $50 million mitigation budget is suggested to be spent on high-rise, low-seismic

code concrete shear wall structures, C2H LC ($14.9 million), and low-rise, low-code unreinforced masonry structures, URML LC ($9.9 million). In addition to acquiring the highest total mitigation spending, these building types are also associated with a relatively high suggested spending normalized by the vulnerable building area. This implies that C2H LC and URML LC represent not only a large percentage of floor area relative to the total floor area of vulnerable buildings (5.1 and 8.0%, respectively), but are also characterized on average by high sensitivities, relative to other building types.

The per-square-foot suggested mitigation spending is largest for high-rise, low-code concrete shear wall structures, C2H LC ($22.78/sqft) and high-rise, low-code steel moment frame buildings, S1H LC ($13.24/sqft). This is because, given their high corresponding sensitivity measures, the sensitivity analysis recommends mitigating 32% and 20% of the total floor area of C2H LC and S1H LC, respectively, for the case study portfolio, which is higher than the other building types listed. This is because these building types represent the largest change in β relative to each dollar of mitigation, on average, relative to the other vulnerable building types shown in Figure 6.6. In addition, a large percentage of the mitigation for each of these building types is specific to ΔR_a mitigation measures, which cost more per square foot. Comparing the high per-square-foot mitigation spending to the low total cost for S1H LC suggests that, relative to the total floor area of vulnerable buildings, this building type has a small percentage of floor area needing retrofits (0.2%).

Finally, for the building types listed, the majority of the mitigation expenditures shown are assigned to reducing post-earthquake recovery times (ΔR_a, $33.6 million), as opposed to retrofit (ΔR_o, $12.7 million). This is consistent with the spending that is suggested for the entire $50 million budget, and is supported by the fact that there is a larger reduction in exceedance

probability for ΔR_a mitigation versus ΔR_o measures at this *LoR* threshold. As noted above, this varies depending threshold used to compute the sensitivity measures, and ΔR_o measure will be more cost-effective for lower thresholds. It also depends on the unit mitigation cost assigned to ΔR_a, as shown in Equation (6.15).

While preliminary, the results in this sensitivity analysis offer valuable information for increasing seismic resilience through pre-disaster retrofit and increased efficiency in post-disaster restoration. By prioritizing these measures based on their cost-effectiveness, limited resources can be allocated to the most optimal scheme for the increase of portfolio's seismic resilience.

Chapter 7. Multi-hazard Loss Assessment

Risk-assessment frameworks for structures subjected to different natural hazards share many similarities including the quantification of the hazard intensity and the associated probable loss and damage. This study desires to extend the proposed FORM-based approach for seismic loss assessment to other types of hazards. Specifically, this extension focuses on estimating the probability distribution of loss for a portfolio under mutually exclusive multi-hazard conditions. Regions subjected to both earthquake and hurricane wind hazards are the primary emphasis in this study. Techniques applied in extending the proposed approach to multi-hazard conditions, however, are applicable to other types of hazards as well.

The first section of this chapter introduces the implications and importance of multi-hazard loss assessments. The hazard and risk-assessment methods presented earlier are extended to hurricane wind hazards in Section 7.2, along with a method for probabilistically modeling structural response to wind. Finally, the proposed approach is applied to quantify multi-hazard risk for a building portfolio in Charleston County, South Carolina.

7.1 Introduction

Many areas of the world are subjected to multiple hazards such as earthquakes, tsunamis,

hurricanes, snow storms, etc. While a specific hazard may dominate the design of structures for a region, there are many regions where more than one hazard may pose a significant threat to buildings. In the United States, many coastal areas are exposed to both hurricane and earthquake hazards, such as Boston, MA and Charleston, SC. The nature of the hazards varies greatly in terms of frequency, return period in design, warning time, and mitigation strategies. The physical, economic and social impacts of these hazards may, however, be quite similar (Scawthorn et al. 2006).

For example, Charleston, South Carolina has experienced a large amount of losses from both earthquake and hurricane occurrences. The Charleston Earthquake of 1886 is considered the most damaging earthquake in the southeastern United States. The M7.3 earthquake damaged over 2,000 buildings, resulting in $6 million worth of damage (approximately 25% of the whole city worth at the time) and killing at least 60 people (USGS 2013b). This level of devastation was reiterated in 1989 when Hurricane Hugo made landfall just north of Charleston resulting in over $7 billion in damage, 27 fatalities and leaving 100,000 homeless (National Research Council 2003). These statistics demonstrate that despite the unique characteristics of earthquake and wind hazards, their impacts on society may be remarkably similar.

In such multi-hazard regions, the risk of exceeding a performance-based limit state may be larger than for those regions subjected to only one hazard. In fact, the level of risk that a structure is exposed to in a multi-hazard situation may be twice as high as anticipated for a single hazard (Crosti et al. 2011). In current practice, however, the final design of structures exposed to multiple hazards is governed by the more demanding of the existing hazard loading conditions. Structures are first analyzed as if they are subjected to one hazard, and then as if they are subjected to others. The controlling design corresponds to the highest demand for each member.

Such an approach ignores the increased risk of exceeding a performance limit state for the additional less demanding hazard(s).

In order to account for the additional risk of the less dominant hazard(s) and achieve a desired building performance over time, design and construction practices should address the risk due to multiple hazards in an integrated manner (Crosti et al. 2011; Duthinh and Simiu 2010; Li and Ellingwood 2009; Li and van de Lindt 2012). Assuming negligible probability that two hazards will occur simultaneously, the probability of exceeding a performance limit state criterion for at least one can be expressed as:

$$P(s_1 \cup s_2) = P(s_1) + P(s_2) \tag{7.1}$$

where $P(s_1)$ is the probability of exceeding a performance limit state criterion s_1 associated with one hazard event and $P(s_2)$ is the probability of exceeding a performance limit state criterion s_2 associated with a different hazard. $P(s_1 \cup s_2)$ is the probability of exceeding either s_1 or s_2. For example, $P(s_1 \cup s_2)$ may represent the probability of exceeding an economic loss threshold associated with earthquake and hurricane wind hazards over the lifetime of a structure. Equation (7.1) shows that $P(s_1 \cup s_2) > P(s_1)$ and $P(s_1 \cup s_2) > P(s_2)$. Therefore, the risk associated with multiple hazards is greater than that associated with one dominant hazard. It is emphasized that while there is a small probability of s_1 and s_2 occurring simultaneously, this is considered negligible in this study. Each event, however, has a unique probability of occurring over a specified period of time.

Many researchers have examined the performance of individual structures under such an integrated multi-hazard approach. For example, Wen (2001) showed that the optimal design of structures subjected to more than one hazard is not governed exclusively by the dominant hazard

but is also influenced by a less dominant hazard. Similarly, Li et al. (2012) introduced a conceptual performance-based design approach for optimal structural design and risk mitigation for buildings subjected to multiple hazards. The level of significance that an integrated multi-hazard approach holds for potential risk varies for different hazards and regions. The contribution of less dominant hazards to hazard-induced risk over time, however, is recognized.

A comparative assessment of the impact individual hazards have on a structural system also provides valuable information for public policy, insurance underwriting and disaster planning purposes (Li and van de Lindt 2012). Performance-based engineering requires structural performance objectives for various hazard levels. These are characterized by the return periods associated with design-level hurricanes and earthquakes, and on the level of disparity and impact resulting from each hazard. For example, lack of advanced warnings for earthquakes makes life safety more of a threat in seismic design, compared with advanced warning systems associated with hurricanes. While the different nature of hazards lends to a non-uniform assumed risk in the design for various hazards, competing hazards must be addressed consistently to achieve overall building performance goals (Li and van de Lindt 2012; Wen 2001).

A comparative assessment of hurricane and earthquake risks may also provide a tool for rank-ordering strategies for managing risks due to multiple hazards. Mitigating one risk may reduce building vulnerability for another, or in some cases, may increase potential risk. For instance, a lighter structure may reduce seismic forces, while simultaneously increasing the potential for wind damage. To address this tradeoff, Li and Ellingwood (2009) performed a comparative assessment of potential risk for wood-frame residential construction given earthquake and hurricane wind hazards. The effectiveness of multi-hazard mitigation strategies is evaluated through comparison of the reduction in risk for each competing hazard.

In this extended study, the proposed FORM method is used to perform an integrated and comparative risk assessment for earthquake and hurricane wind hazards. For each assessment, consequences are modeled as the probability of exceeding a specified level of monetary loss as discussed in Section 4.2 and computed using FORM. Since the intensity of each is expressed in incompatible units (spectral acceleration and wind speed), the return period for each hazard is used as a common variable. Examining retrofit options relative to multi-hazard loss is beyond the scope of this study. This study does discuss, however, how future application of the sensitivity analysis presented in Section 4.4 can be used to prioritize mitigation strategies for competing hazards.

7.2 Extension of Proposed FORM Method: Wind

The techniques developed in this dissertation for seismic risk assessments are modified to estimate risk due to hurricane wind hazards. A multivariate distribution for modeling spatially distributed hurricane winds is characterized similar to that used to model correlated seismic intensities in Section 4.1.1. Section 2.1 illustrates the importance of considering spatial correlation in seismic intensities for obtaining accurate risk estimates. This study also investigates the potential for comparable inaccuracies caused by ignoring the spatial correlation in wind fields during hurricane risk assessments.

Structural response specific to wind-induced building damage is often modeled quite differently from the seismic building response model presented in Section 4.1.2. This is a result of the distinct failure mechanisms unique to wind loading, as opposed to a representative structural response parameter indicative of most structural damage. The following example uses

several component-specific fragility models to assess probabilistic wind-related building damage levels. These damage probabilities are then used to compute structural and nonstructural losses.

7.2.1 Wind Intensity

In this study, the wind intensity at each site is characterized by the 3-s peak wind gust at 10m elevation. This intensity measuring is used in wind contour maps of ASCE Standard 7-10 (2010) for computing design loading conditions. Spatially distributed hurricane wind speeds are computed based on the following model proposed by Jayaram and Baker (2010b):

$$\ln(V_i) = \ln(\bar{V}_i) + \varepsilon_i \tag{7.2}$$

where V_i is the peak wind speed at site i, $\bar{V}_i$ is the median peak wind speed at site i computed using wind field prediction models and ε_i denotes the residual or error term at site i. Significant correlation exists between the wind intensity at two closely spaced sites, due to similarities in the wind source, site effects and site location (Jayaram and Baker 2010b; Legg et al. 2010; Pang et al. 2012). In general, this correlation is partially accounted for in the wind speed models used to predict median peak wind speeds. There is additional correlation, however, between residual terms used to model the uncertainty in wind speed at each site.

Proposed wind speed models such as Batts et al. (1980), Vickery et al. (2000) and Vickery et al. (2009) are used to predict wind speeds by propagating key parameters characterizing potential hurricane occurrences. These are a function of the expected value and uncertainties surrounding the central pressure, translational speed, radius to maximum winds, occurrence rates and wind speed decay. Residual terms are modeled by a multivariate distribution, characterized by the associated uncertainty at each site and by a correlation matrix

computed based on empirical distributed wind field correlation models (Jayaram and Baker 2010b; Legg et al. 2010; Pang et al. 2012)

When the predicted wind speed at each site is considered random, median wind speeds as well as spatially correlated residuals at each site are sampled randomly following the simulation approach proposed in Section 4.1.1. The predicted wind speeds and simulated residuals are then combined using Equation (7.2) to obtain realizations of the wind speeds at all sites of interest. A multivariate distribution is fit to the simulated wind speeds at each site and linear regression is used to compute the total spatial correlation in wind intensity between sites. If median wind speeds are considered deterministic (assuming an expected central pressure, translation speed, occurrence rate, etc.), the multivariate distribution can then be characterized directly from the predicted wind speeds, associated uncertainty, and computed correlation matrix, without using simulation (see Section 4.1.1).

This study assumes deterministic median wind speeds at each site, modified based on distance inland, as a representation of wind decay after landfall. Predicted wind speeds are taken from Li and Ellingwood (2009). The reduction in wind speed is computed based on wind field decay models proposed by Kaplan and DeMaria (1995) with translational hurricane speeds predicted based on historical hurricane occurrences (Purvis and McNab 1985).

For a simplistic evaluation, the wind field distribution used in this example is considered to be Gaussian, based on findings in Jayaram and Baker (2010b). Following an empirical study of wind fields from Hurricane Jeanne (2004) the residual terms in Equation (7.2) are assumed to follow a multivariate normal distribution with a mean of zero and standard deviation of 0.15. The residual distribution is characterized by a correlation matrix computed using the empirical model fit to Hurricane Jeanne wind field data (Jayaram and Baker 2010b).

It is noted that many studies suggest that wind fields are best modeled by a Weibull distribution rather than a Gaussian distribution (Batts et al. 1980; Li and Ellingwood 2009). Additional information on the uncertainty and spatial correlation of distributed wind fields may be used to refine the wind field distribution used in this study for future applications.

7.2.2 Structural Response: Wind

Unlike seismic induced damage, which can be largely related to excessive lateral drift for most building systems, wind-related damage is characterized by a variety of building parameters. The most vulnerable part of a building to hurricane winds is its envelope (i.e., building enclosure). This can be breached as a result of roof-to-wall connection failure due to wind uplift, roof panel uplift, breakage of windows and doors due to excessive wind-induced pressure or projectile impact (Li and Ellingwood 2006). The type of engineering demand parameter used to model wind-related structural response is highly dependent on the building type and damage mode of interest (Petrini et al. 2009).

Many quantitative wind damage prediction models rely heavily on expert opinion and insurance claims as there is a lack of test data on building behavior in extreme wind loading. Extrapolating building wind vulnerability relationships on insurance losses, however, is still filled with uncertainty as there lacks an abundance of insurance losses to develop and calibrate the damage prediction models (Khanduri and Morrow 2003). When insurance losses are available, they are generally amassed over a suite of buildings, making it difficult to disaggregate damage data specific to building type classes.

In this study, wind-related damage is modeled based on damage bound probability density functions proposed in Unanwa et al. (2000). These are specific to representative building types and are primarily developed and calibrated based on expert opinion. The model considers

each building type to consist of the following components: roof covering, roof structure, exterior doors and windows, exterior walls, interior (including contents), structural system and foundation. Upper and lower bound damage thresholds are determined with respect to each building component, and are associated with the highest and lowest probabilities of failure in a wind hazard.

Each building component may experience damage through direct wind impact or due to propogational effects resulting in damage to other components. Figure 7.1 shows a schematic of the damage process assumed in this model.

For each building component *i*, the probability of full component failure resulting from direct wind impacts (P_{fi}^{D}) is computed based on probability density functions provided in Unanwa et al. (2000). Conditional probability data due to damage propagation (P_{fi}^{P}) are also provided. The final probability of failure for each component (P_{fi}) is computed as:

$$P_{fi} = P_{fi}^{D} + P_{fi}^{P} - P_{fi}^{D}P_{fi}^{P} \tag{7.3}$$

where $P_{fi}^{D}P_{fi}^{P}$ is the joint probability of damage due to both direct and propogational damage. The total degree of damage (DD) for building and occupancy category *j* at wind hazard level l is then computed as:

$$DD(l)_j = \sum_{i=1}^{n} P_{fi} * CCF_{ij} * \alpha_i \tag{7.4}$$

where CCF_{ij} is the component cost factor for component *i* and building and occupancy category *j* relative to the total building cost, and α_i is a component location factor.

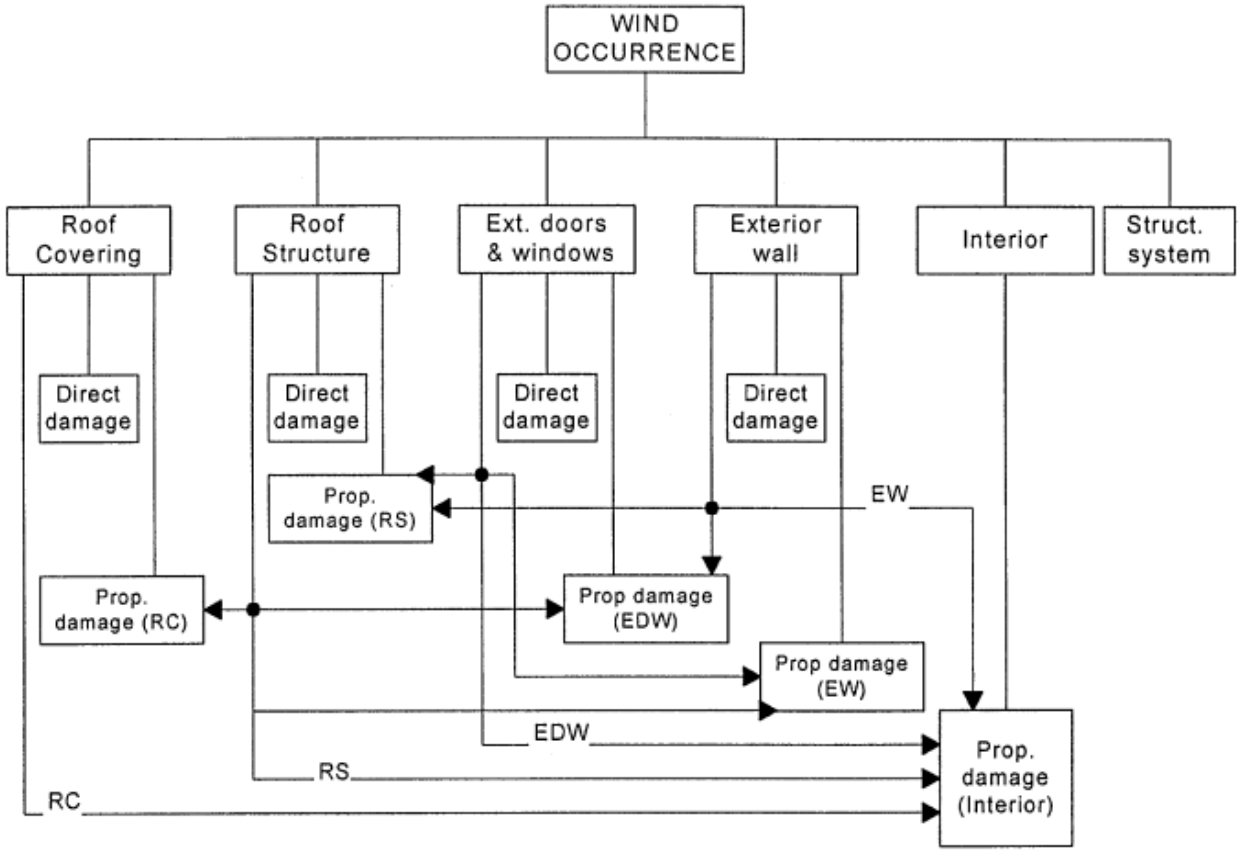

Figure 7.1: Wind direct and propagated damage process (Unanwa et al. 2000).

For determining loss to a portfolio of buildings, Unanwa (2000) provides the following algorithm for computing total portfolio loss (TL) as a function of upper and lower damage bands:

$$TL(l) = \sum_{j=1}^{4} RRI_j^{av} * \left(DD(l)_j^U + DD(l)_j^L\right) * BRC_j \tag{7.5}$$

where RRI_j^{av} is the average relative resistivity index for building/occupancy category j, $DD(l)_j^U$ and $DD(l)_j^L$ are the upper and lower bound damage degrees computed in Equation (7.4) given hazard level l, and BRC_j is the total building replacement cost for building/occupancy category j. This method assumes building/occupancy types can be classified into four primary categories: 1-3 story residential, 1-3 story commercial/industrial, 1-3 story government/institutional and 4-10

story buildings and further disaggregated based on occupancy for the component cost factor listed in Equation (7.4).

Using the wind hazard model described in Section 7.2.1, FORM is used to evaluate the probability of exceeding various loss thresholds based on Equations (4.10), (4.6) and (7.5). For an integrated multi-hazard assessment, earthquake and hurricane wind losses are combined using Equation (7.1). These are then used to compute the probability of exceeding a specified level of portfolio loss given either earthquake or hurricane wind hazards characterized by a common return period.

7.3 Case Study: Multi-hazard Loss Assessment

The building portfolio in Charleston County, South Carolina is chosen for this case study since the region is at risk to both earthquake and hurricane-wind hazards. For comparison purposes, a 500-year return period is used as the control variable to perform an integrated and comparative assessment of losses for each hazard.

Charleston County's building inventory is disaggregated in a similar manner to the San Francisco portfolio presented in Section 5.1. The case study region includes 78 census tracts with over 2,000 building combination types, yielding a reliability space of over 4,000 random variables.

Figure 7.2 shows the case study region relative to the Charleston seismic zone consisting of three fault segments: North Woodstock Fault, South Woodstock Fault and the Sawmill Branch Fault. As a result of its high earthquake occurrence rate density, Charleston is most strongly influenced by potential earthquakes within this fault zone (Student 1997). Therefore, it is assumed that the seismic activity from these faults best represent the potential earthquake hazard

for this study. From paleoseismicity studies, a magnitude 7.0 earthquake is considered the characteristic magnitude with a 500-year recurrence interval from this zone (Talwani and Schaeffer 2001). According to Student (1997), it is assumed that there is equal probability of such a characteristic earthquake occurring at any point along this fault zone. Given these assumptions, the simulation procedure outlined in Section 4.1.1 is used to compute realizations of seismic intensity at the center of the 78 Charleston County census tracts.

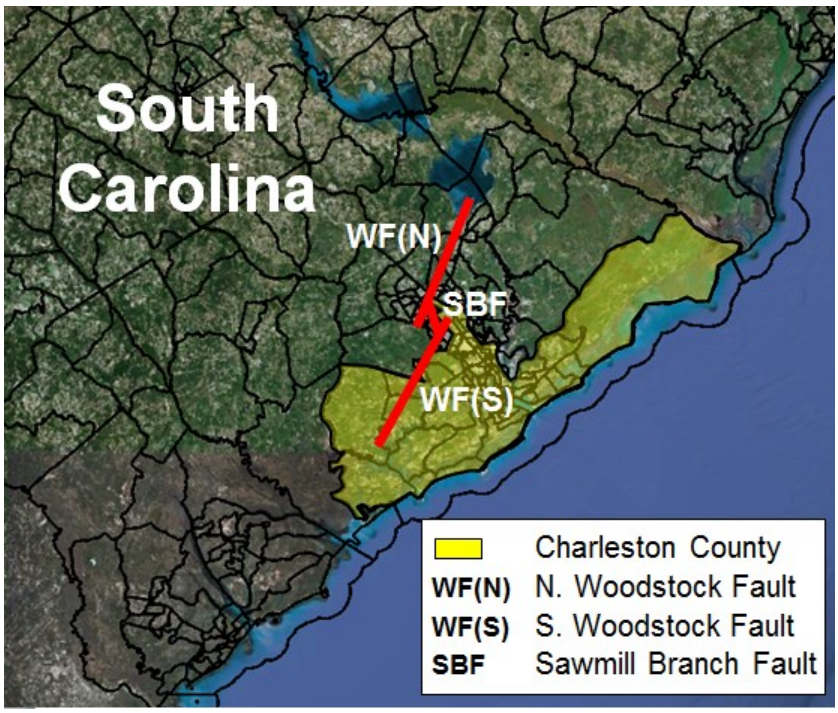

Figure 7.2: Charleston County case study portfolio region and potential earthquake fault zone (Google 2012).

The hurricane intensity distribution characterized by a 500-year return period is computed based on a median wind speed taken from Li and Ellingwood (2009), spatially correlated residuals computed from the method proposed in Jayaram and Baker (2010b) and using the wind decay model by Kaplan and DeMaria (1995).

The exceedance probabilities computed for the portfolio using FORM and MCS are shown in Figure 7.3 for earthquake and hurricane wind hazards characterized by a 500-year return period. The exceedance probabilities obtained by ignoring the spatial correlation between the hazard intensity at each site are also shown.

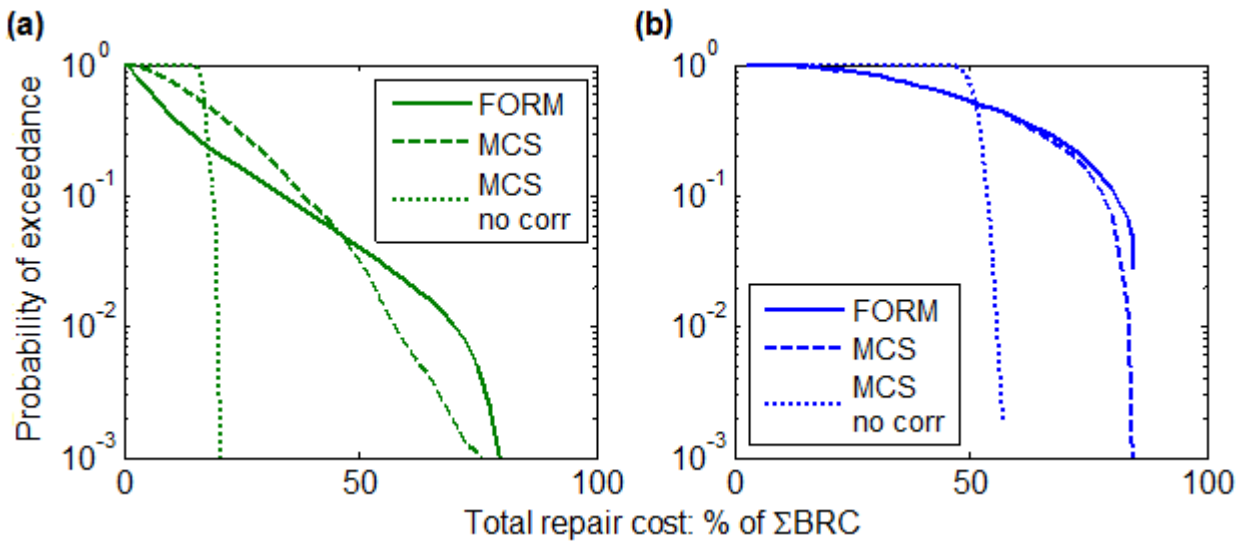

Figure 7.3: Loss exceedance curves using FORM and MCS for (a) earthquake and (b) hurricane wind hazards characterized by a 500-year return period. MCS results are shown with and without including spatial correlation between hazard intensities.

Figure 7.3 shows that ignoring the spatial correlation between hazard intensities results in an overestimation of the probability of exceeding small losses and an underestimation of the probability of exceeding large, rare losses. It is also observed that FORM results follow closely with exceedance probabilities computed using MCS for hurricane wind hazards. There are, however, notable deviations in results for earthquake loss, which are similar to the deviations shown in Figure 5.3 for the San Francisco case study. The extent of the overestimation and the underestimation in using FORM is likely to be smaller for hurricane wind hazards because the wind intensities are more highly spatially correlated across the region. As discussed in Section 4.5, the deviations in FORM results are a function of the dissimilarity between variables at each

site. Since the seismic intensities at each site are less correlated than hurricane wind speeds, there is a larger range of values each variable can assume to satisfy a limit state threshold. This is shown to increase the extent of limit state nonlinearities, and therefore decrease the corresponding accuracy in using FORM.

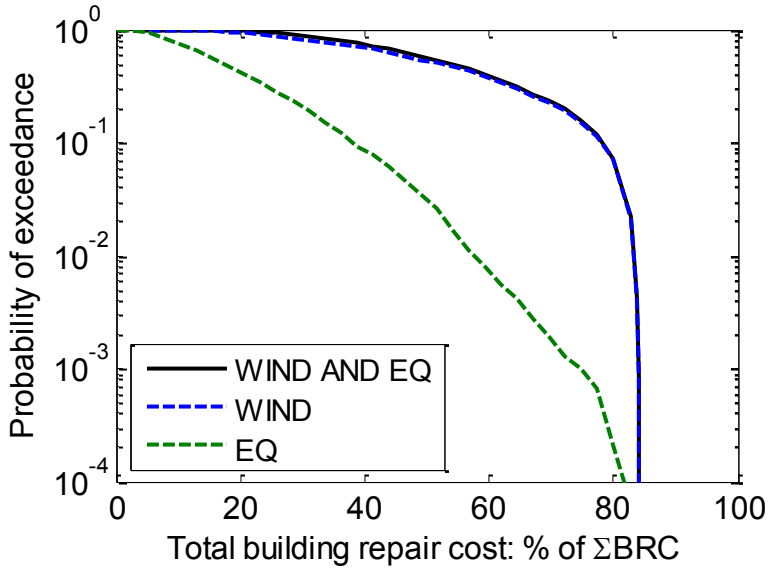

Figure 7.4: Loss exceedance curves using MCS for combined earthquake and hurricane wind hazards characterized by a 500-year return period.

The exceedance probabilities for each hazard are combined using Equation (7.1) to compute the integrated multi-hazard exceedance curves shown in Figure 7.4 for MCS results. In this case study, the majority of regional loss is attributed to hurricane winds as opposed to earthquakes for most loss thresholds. For high loss thresholds associated with low probabilities, however, exceedance probabilities associated with earthquake losses become more comparable to wind loss exceedance. If the trend continues, earthquake loss exceedance probabilities would likely exceed those for wind losses. Generally speaking, the influence of each hazard on regional risk varies based on the region and hazard return period in question.

The results of each assessment, paired with the fundamental characteristics of each hazard and its effects on society, can be used for hazard management in regions exposed to multiple hazards. This may be particularly useful for decision makers in public policy, emergency response planning and insurance underwriting.

The information can also be used to assess the effectiveness of hazard mitigation options in reducing regional risk. A sensitivity analysis following the method proposed in Section 4.4 can be used to prioritize retrofit options specific to either earthquake or wind hazards, or a combination of both, over time. While the less dominant hazard(s) may be less influential in terms of regional loss exceedance over time, retrofit options specific to such hazard type(s) may be cost-effective in reducing total regional loss. To perform this type of sensitivity analysis, future research should assign one or more random variables to model the wind-related structural response. In addition, marginal retrofit costs should be assigned to changes in each structural response variable for each building retrofit scheme. Sensitivity measures would then be computed relative to changes in loss per each dollar of retrofit specific to each hazard of interest.

Chapter 8. Summary and Conclusions

In this dissertation, a new reliability-based approach is developed for the comprehensive and efficient assessment of earthquake risks to a portfolio of buildings. The framework aims to represent the complex problem of quantifying regional earthquake risk by characterizing a building portfolio as a system of interconnected components. The proposed method explicitly models the uncertainties surrounding the hazard demand, building response and losses, as well as additional system effects related to the correlation that exists between building performances in a seismic hazard.

Existing earthquake loss estimation methodologies were reviewed and five main characteristics were identified to be addressed in the proposed approach: 1) provide an analytical approach; 2) probabilistic evaluation of risk; 3) explicit modeling of spatial correlations between building performances; 4) computational efficiency; and 5) easy computation of sensitivity measures. To address these desired properties of regional loss estimation, this dissertation proposes using the First-Order Reliability Method (FORM) for probabilistic portfolio loss evaluation. FORM is an approximate, analytical method used to compute failure probability based on linearizing a performance limit state surface in a transformed reliability space.

In the proposed FORM-based analysis, two random variables are used to model the performance of each building: $\ln S_a$ and γ_{IDR}. The first random variable is modeled by a multivariate distribution representing the distribution of potential seismic intensities at each site, and by the spatial correlation between sites based on residual terms and soil properties. The second random variable models the variability in structural response specific to each building type. Regional loss limit state criterion is defined based on the varying levels of total regional repair costs. This includes losses due to structural and nonstructural damage and is represented as a percentage of the total building replacement cost for the portfolio. FORM is used to compute the regional loss exceedance probabilities. This is based on an optimization process for finding the most probable set of random variable values that may cause failure.

A useful by-product of the optimization process is a set of sensitivity measures that provide information about the change in system reliability relative to a change in each random variable. The sensitivity measures for the structural response random variables are paired with retrofit costs to compute the change in portfolio loss per dollar of retrofit. These measures are used to prioritize the most cost-effective retrofit schemes for a region, which offers valuable information when allocating limited resources to mitigate regional risk.

The proposed framework is applied to compute the probability distribution of loss for a selected San Francisco building portfolio subjected to a scenario earthquake. Results using FORM and Monte Carlo Simulation (MCS) are compared to check the accuracy of the proposed FORM method. The results suggest that failure probabilities computed using FORM follow a similar trend as the MCS results and require much less computing time. There are, however, some notable deviations in FORM results for some loss thresholds, due to the approximations in

using FORM for a limit state characterized by significant nonlinearity. The sources and extent of limit state nonlinearity are identified for future refinement of FORM-based results.

Unlike simulation, FORM also enables easy computation of sensitivity measures, which are used to prioritize the most cost-effective retrofit schemes per building and occupancy type for reducing regional risk for the San Francisco portfolio. In this case study, loss is also evaluated with and without consideration of spatial correlation, thus showing that neglecting correlation can greatly skew computed loss distributions and retrofit prioritization. In addition, results shown that it is essential to perform a sensitivity analysis (used to prioritize retrofit) relative to the desirable level of loss to be minimized in order to achieve optimal retrofit prioritization.

The proposed framework is then extended to evaluate the resilience of a building portfolio by introducing a third random variable to model the recovery time following an earthquake event. Resilience is quantified based on the robustness and rapidity of a portfolio system, which are related to hazard-induced losses and building recovery, respectively. FORM is used to compute the probability of exceeding varying thresholds of portfolio resilience. In addition, a sensitivity analysis is conducted to prioritize the most cost-effective mitigation measures for increasing seismic resilience. Sensitivity measures are computed to capture changes in portfolio resilience relative to a mitigation expenditures allocated to pre-disaster retrofit, increased efficiency in post-disaster restoration or a combination of the two. For most resilience thresholds, retrofit is shown to be most cost-effective in increasing portfolio resilience. Mitigation for increased post-disaster restoration efficiency, however, is considered more cost-effective for reducing the probability of exceeding more severe resilience thresholds.

Finally, the proposed approach is used to assess the potential risk for regions subjected to multiple, mutually exclusive hazards; specifically earthquake and hurricane wind hazards. A

multivariate random variable is used in the study to model the spatially correlated wind intensity for a region and a set of probability density functions are used to model wind-related structural response. FORM is implemented to compute the distribution of loss specific to each hazard for the building portfolio Charleston County, South Carolina. It is also used to perform an integrated assessment for potential risk over time due to both hazards. This case study demonstrates that FORM provides more accurate results for hurricane wind hazards losses compared with computing portfolio risks due to earthquake hazards. It is noted that the significance of evaluating multi-hazard risk as opposed to the risk related to a single dominant hazard is specific to the region and time period of interest.

Originality

This dissertation has two primary objectives: 1) the development of a new approach to quantify potential seismic losses for a building portfolio; and 2) the use of the proposed approach to evaluate the cost-effectiveness of mitigation schemes at a regional level.

The first objective is met by implementing FORM to evaluate loss to the portfolio. The new developments in the proposed approach relative to existing methods include:

- **Analytical:** FORM provides an approximate, yet analytical means of quantifying the distribution of regional loss. This dissertation develops a methodology to express each random variable in closed form. The analytical ability to characterize and quantify portfolio loss is considered advantageous to the simulation techniques often used in existing loss estimation methods.
- **Probabilistic:** The output of the proposed FORM approach is a probability distribution of seismic losses to a building portfolio for a specified earthquake scenario or time

period. This framework addresses the uncertainty surrounding the hazard intensity, structural response, losses and correlation between building performances. In contrast, many existing loss estimation tools limit loss results to the expected value of regional loss. By disregarding the uncertainty surrounding regional losses, influential system effects within a portfolio of buildings are neglected.

- **Modeling of spatial correlation:** The inclusion of correlations between random variables is one of the strengths of FORM. The spatial correlation between hazard intensities at each site is modeled explicitly within the proposed framework. These correlations are shown to be very influential in computing the variance of total portfolio loss, as well as when prioritizing retrofit options.

- **Computationally efficient:** A notable advantage to using FORM is its computational efficiency. Unlike MCS, the required computation time is independent of the likelihood of failure. FORM proffers an efficient tool for evaluating the likelihood of rare events often characterized by large consequences. A robust tool for large-scale optimization computing is used to perform FORM computations to increase efficiency for problems consisting of a large number of random variables, as is the case for many building portfolios (*TOMLAB* 2012).

- **Identification of FORM inaccuracies:** Further investigation is provided giving insight into approximation and corresponding inaccuracy in using FORM to compute portfolio loss. General trends in the deviation in FORM results are identified and related to dissimilarities between random variables and the level of failure probability associated with each limit state threshold. The identification of these factors can assist in developing

a refinement technique to increase accuracy in FORM-based portfolio loss estimates, while preserving the inherent benefits in using FORM.

The second objective of prioritizing retrofit options is also addressed using sensitivity measures inherently computed in FORM computations. In this respect, FORM offers the following advantages:

- **Easy computation of sensitivity measures:** Sensitivity measures are calculated directly and simultaneously using the gradient-based optimization required to minimize β and compute the failure probability assumed by FORM. These measures provide information regarding the order of sensitivity each variable parameter has on the overall system reliability.
- **Prioritize retrofit options:** Mitigation costs are paired with sensitivity measures to compute the marginal change in terms of regional loss per dollar of retrofit. These measures are used to prioritize cost-effective retrofit options based on building location, building type and occupancy category. In addition, the most cost-effective retrofit scheme is identified when allocation it is desired to allocate a limited budget in an optimal manner to reduce risk to a suite of buildings.

Two additional studies were performed that extend the capabilities of the proposed FORM method including a resilience and multi-hazard assessment. New developments in the proposed portfolio resilience evaluation include:

- **Probabilistic evaluation of resilience:** The proposed FORM method is used to compute a probabilistic measure of portfolio resilience given an earthquake scenario. In doing so,

an additional random variable is added to the reliability problem to model the variability in repair and recovery time. Unlike most resilience assessment tools that evaluate resilience qualitatively or using expected values, this resilience measure is computed as a probability distribution, preserving influential system effects.

- **Prioritize measures to increase regional resilience:** A sensitivity analysis is used to evaluate the cost-effectiveness of loss reduction measures in relation to an increase in regional resilience. Sensitivity measures are computed to capture the change in the reliability associated with a specified resilience threshold, relative to a dollar allocated to pre-disaster retrofit or post-disaster restoration efficiency. With these measures, a comparative analysis is performed to evaluate which mitigation measure provides the largest increase in portfolio resilience for each resilience threshold level.

While preliminary in its development, potential advantages in the proposed multi-hazard assessment include:

- **Multi-hazard loss estimation:** The techniques developed in this dissertation for seismic risk assessment are modified to estimate risk due to hurricane wind hazards. The proposed FORM method is used to compute the probability distribution of multi-hazard loss for a specified return period.
- **Prioritize retrofit options:** Following a similar method to the sensitivity analysis for seismic-based losses, sensitivity measures can be computed relative to mitigating risk for multiple hazards. These measures can aid in the prioritization of retrofit options specific to earthquake or wind-related structural resistance for optimizing regional risk-mitigation decision making.

Limitations and Future Research

Four main issues have been identified as potential shortcomings in using the proposed framework for earthquake risk assessments. These are outlined below, accompanied by suggested future research steps to address these limitations. Some additional extensions of this work that can potentially be addressed in future research are also discussed.

- **Accuracy in modeling parameters:** The identification and propagation of uncertainty is the fundamental pillar for probabilistically quantifying building performance. There are many sources of uncertainty involved in modeling the parameters that make up a regional risk assessment. These include epistemic uncertainties resulting from lack of historical data, aleatory uncertainty related to the inherent randomness in the hazard, structural response or recovery, modeling errors, etc. Since FORM requires variables to be modeled by closed form distributions, there is a potential for inaccurate modeling of the parameters within the reliability problem. Whether attributed to lack of data or inaccuracies in modeling the data with the closest matching distribution, inaccurate modeling may skew the computed reliability of a system.

  Future research can aim to limit this epistemic uncertainty by gathering additional information to more accurately model the prevailing parameters. For example, the recovery time distribution used in the resilience study is primarily based on expert opinion. Modeling this variable based on gathered data from historical events or on quantitative recovery models may provide a more accurate representation for recovery times following an earthquake event. The limited inventory of historical events from which to extrapolate risk-assessment models may, however, create challenges for limiting epistemic uncertainty.

- **FORM accuracy:** FORM provides approximate reliability results when the limit state surface is not linear in standard normal reliability space. The level of accuracy in using FORM relates to the extent of nonlinearities in the limit state surface. Potential sources of limit state nonlinearity are shown to be a function of the range of values random variables can assume to satisfy a limit state constraint. These identified sources likely contribute to the inaccuracies in using FORM, and can facilitate in developing a technique to refine the FORM-based results for future research. While it is impossible to improve the accuracy provided by direct use of FORM, additional research can focus on methods to reduce potential errors, while preserving the benefits of using FORM. To develop such a technique, it would be advantages to evaluate a larger set of portfolios of different sizes and locations, to further identify general or portfolio-specific trends in deviations in FORM results.

- **Additional considerations when prioritizing retrofit options:** The sensitivity analysis used to prioritize retrofit options is a function of resistance to drift-sensitive damage only. Many building types are affected greatly, however, by acceleration-sensitive nonstructural damage, which is not accounted for in computing sensitivity measures. Future research can introduce a new random variable to model this additional structural resistance parameter, and then run sensitivity analyses relative to changes in both drift- and acceleration-related structural response. In addition, other factors that may influence retrofit decision-making may be introduced either quantitatively or qualitatively, such as willingness to pay for retrofit, incurred losses due to retrofit and social importance of vulnerable buildings.

- **Modeling a building portfolio:** Given computing space constraints and availability of data, all buildings categorized within the same building type, occupancy category and seismic design level are considered fully correlated within each census tract. It is incorrect, however, to assume these buildings will experience an identical level of loss given an earthquake. Given this assumption, it is expected that the variance in loss is superficially increased. Future extensions of this work should aim to disaggregate the total building area for each building combination type within each census tract into individual buildings. This would help to more accurately model the predicted variance in loss for the portfolio system. Since the number of buildings (i.e., random variables) may become unmanageable from a computational standpoint, further investigation would be required to develop more realistic modeling assumptions to limit the size of the reliability problem and maintain computational efficiency.

- **Additional future extensions:** Additional limitations in the proposed method include the inability to account for soft soil sites in the existing methodology. In future extensions of this approach, soft soil sites can be incorporating by using a site-specific nonlinear analysis to assess the seismic intensity and resulting building response and damage at such sites. In addition, the fundamental building period can be adjusted to modify the seismic intensity experienced by a structure in soft soil conditions. Future research can also aim to extend the proposed FORM method from a strictly building portfolio analysis to other infrastructure units. For other critical infrastructure, system limit states for "failure" can be expressed in terms of similar variables to those proposed in this approach (e.g., seismic intensity and a physical performance variable). By considering other types

of critical infrastructure systems in a FORM-based approach, correlations between the losses experienced by multiple systems could be incorporated.

Bibliography

Abrahamson, N., and Silva, W. (2008). "Summary of the Abrahamson & Silva NGA Ground-Motion Relations." *Earthquake Spectra*, 24(1), 67–97.

Algermissen, S., Rinehart, W., Dewey, J., Steinbrugge, k, Degenkolb, H., Cluff, L., and Gordon, R. (1972). *A Study of Earthquake Losses in the San Francisco Bay Area: Data and Analysis*. Environmental Research Laboratories of National Oceanic & Atmospheric Administration, Office of Emergency Preparedness: U.S. Department of Commerce, Rockville, MD.

Allen, T. I., and Wald, D. J. (2009). "On the Use of High-Resolution Topographic Data as a Proxy for Seismic Site Conditions (VS30)." *Bulletin of the Seismological Society of America*, 99(2A), 935–943.

American Society of Civil Engineers (ASCE). (2010). *Minimum Design Loads for Buildings and other Structures*. ASCE 7-10. Reston, VA.

Applied Technology Council (ATC). (1985). *Earthquake Damage Evaluation Data for California*. ATC-13. Applied Technology Council, Redwood City, CA.

Applied Technology Council (ATC). (2010). *Potential Earthquake Impacts*. Here Today—Here Tomorrow: The Road to Earthquake Resilience in San Francisco. ATC-52-1. Applied Technology Council, Redwood City, CA.

Baise, L. G., Higgins, R. B., and Brankman, C. M. (2006). "Liquefaction Hazard Mapping - Statistical and Spatial Characterization of Susceptible Units." *Journal of Geotechnical and Geoenvironmental Engineering*, 132(6), 705–715.

Baker, J. W., Bozorgnia, Y., Di Alessandro, C., Chiou, D., Erdik, M., Somerville, P., and Silva, W. (2012). "GEM-PEER Global GMPEs Project Guidance for Including Near-Fault Effects in Ground Motion Prediction Models." 15 WCEE, Lisbon, Portugal.

Baker, J. W., and Cornell, C. A. (2006). "Correlation of Response Spectral Values for Multicomponent Ground Motions." *Bulletin of the Seismological Society of America*, 96(1), 215–227.

Batts, M. E., Cordes, M. R., Russell, L. R., Shaver, J. R., and Simiu, E. (1980). *Hurricane Wind Speeds in the United States*. U.S. Department of Commerce, National Bureau of Standards.

Bayraktarli, Y., and Faber, M. (2007). "Bayesian Probabilistic Network Approach for Managing Earthquake Risks of Cities." International Forum on Engineering Decision Making (IFED), Shoal Bay, Australia, 1–29.

Bazzurro, P., and Luco, N. (2005). "Accounting for Uncertainty and Correlation in Earthquake Loss Estimation." International Conference on Structural Safety & Reliability (ICOSSAR), Rome, Italy.

Bensi, M. T., Der Kiureghian, A., and Straub, D. (2009). "A Bayesian Network Framework for Post-earthquake Infrastructure System Performance Assessment." TCLEE 2009: Lifeline Earthquake Engineering in a Multihazard Environment, Oakland, CA.

Boore, D. M., and Atkinson, G. M. (2008). "Ground-Motion Prediction Equations for the Average Horizontal Component of PGA, PGV, and 5%-Damped PSA at Spectral Periods between 0.01s and 10.0s." *Earthquake Spectra*, 24(1), 99–138.

Boore, D. M., Thompson, E. M., and Cadet, H. (2011). "Regional Correlations of Vs30 and Velocities Averaged Over Depths Less Than and Greater Than 30 Meters." *Bulletin of the Seismological Society of America*, 101(6), 3046–3059.

Brand, D. (1988). "Soviet Union Vision of Horror." *TIME Magazine*.

Bruneau, M., Chang, S. E., Eguchi, R. T., Lee, G. C., O'Rourke, T. D., Reinhorn, A. M., Shinozuka, M., Tierney, K., Wallace, W. A., and von Winterfeldt, D. (2003). "A Framework to Quantitatively Assess and Enhance the Seismic Resilience of Communities." *Earthquake Spectra*, 19(4), 733–752.

Bruneau, M., and Reinhorn, A. (2007). "Exploring the Concept of Seismic Resilience for Acute Care Facilities." *Earthquake Spectra*, 23(1), 41–62.

Campbell, K. W., and Bozorgnia, Y. (2008). *Campbell-Bozorgnia NGA Ground Motion Relations for the Geometric Mean Horizontal Component of Peak and Spectral Ground*. Technical Report PEER 2007/02. Pacific Earthquake Engineering Research Center (PEER), Berkeley, CA.

Chang, S. E., and Shinozuka, M. (2004). "Measuring Improvements in the Disaster Resilience of Communities." *Earthquake Spectra*, 20(3), 739–755.

Chiou, B.-J., and Youngs, R. R. (2008). "An NGA Model for the Average Horizontal Component of Peak Ground Motion and Response Spectra." *Earthquake Spectra*, 24(1), 173–215.

Cimellaro, G. P., and Arcidiacono, V. (2013). "Resilience-Based Design for Urban Cities." *Resilience and Urban Risk Management*, Taylor & Francis Group, London, 127–141.

Cimellaro, G. P., Reinhorn, A. M., and Bruneau, M. (2010). "Framework for analytical quantification of disaster resilience." *Engineering Structures*, 32(11), 3639–3649.

Comerio, M., Landis, J., and Rofe, Y. (1994). *Post Disaster Residential Rebuilding*. Institute of Urban and Regional Development, University of California, Berkeley, CA.

Community Resilience System Initiative (CRSI). (2011). *Community Resilience System Initiative (CSRI) Steering Committee Final Report: A Roadmap to Increased Community Resilience.* Community & Regional Resilience Initiative, Washington, D.C.

Cornell, C. (1969). "A Probability Based Structural Code." *ACI Journal*, 66(12), 974–985.

Crosti, C., Duthinh, D., and Simiu, E. (2011). "Risk Consistency and Synergy in Multihazard Design." *Journal of Structural Engineering*, 137(8), 844–849.

Crowley, H., and Bommer, J. J. (2006). "Modelling Seismic Hazard in Earthquake Loss Models with Spatially Distributed Exposure." *Bulletin of Earthquake Engineering*, 4(3), 249–273.

DeBock, D. J., Garrison, J. W., Kim, K. Y., and Liel, A. B. (2013). "Incorporation of Spatial Correlation between Building Response Parameters in Regional Seismic Loss Analysis." *Bulletin Seismological Society America*, In Press.

DeGroot, D. J., and Baecher, G. B. (1993). "Estimating Autocovariance of In-Situ Soil Properties." *Journal of Geotechnical Engineering*, 119(1), 147–166.

Duthinh, D., and Simiu, E. (2010). "Safety of Structures in Strong Winds and Earthquakes: Multihazard Considerations." *Journal of Structural Engineering*, 136(3), 330–333.

Ellingwood, B., Galambos, T., MacGregor, J., and Cornell, C. A. (1980). *Development of a Probability-Based Load Criterion for American National Standard A58*. National Bureau of Standards, Washington, D.C.

Federal Emergency Management Agency (FEMA). (1988a). *Rapid Visual Screening of Buildings for Potential Seismic Hazards: A Handbook*. FEMA-154. Washington, D.C.

Federal Emergency Management Agency (FEMA). (1989). *Estimating Losses from Future Earthquakes: Panel Report and Technical Background*. FEMA-177. Washington, D.C.

Federal Emergency Management Agency (FEMA). (1994a). *Assessment of the State-of-the-art Earthquake Loss Estimation Methodologies*. FEMA-249. National Institute of Building

Sciences (NIBS) and Risk Management Software, Inc. (RMS), California Universities for Research in Earthquake Engineering (CUREe), Washington, D.C.

Federal Emergency Management Agency (FEMA). (1994b). *Typical Costs for Seismic Rehabilitation of Existing Buildings*. FEMA-156. Washington, D.C.

Federal Emergency Management Agency (FEMA). (1994c). *Seismic Retrofit Incentive Programs: A Handbook for Local Governments*. FEMA-254. Washington, D.C.

Federal Emergency Management Agency (FEMA). (2000). *Prestandard and Commentary for the Seismic Rehabilitation of Buildings*. FEMA-356. Applied Technology Council, Federal Emergency Management Agency, Washington, D.C.

Federal Emergency Management Agency (FEMA). (2002). *State and Local Plan Interim Criteria under the Disaster Mitigation Act of 2000*. Washington, D.C.

Federal Emergency Management Agency (FEMA). (2003). *Building a Disaster-Resistant University*. Washington, D.C.

Federal Emergency Management Agency (FEMA). (2009). *Quantification of Building Seismic Performance Factors*. FEMA P-695. Applied Technology Council, Federal Emergency Management Agency, Washington, D.C.

Federal Emergency Management Agency (FEMA). (2012). *Seismic Performance Assessment of Buildings*. FEMA P-58. Applied Technology Council, Federal Emergency Management Agency, Washington, D.C.

Freeman, J. (1932). *Earthquake Damage and Earthquake Insurance: Studies of a Rational Basis for Earthquake Insurance, also Studies of Engineering Data for Earthquake-Resisting Construction*. McGraw-Hill, New York, NY.

Gilbert, S., W. (2010). *Disaster Resilience: A Guide to the Literature*. National Institute of Standards and Technology, Building and Fire Research Laboratory, Gaithersburg, MD.

Goda, K., and Hong, H. P. (2008). "Estimation of Seismic Loss for Spatially Distributed Buildings." *Earthquake Spectra*, 24(4), 889–910.

Google. (2012). *Google Earth*.

Grant, D. N., Bommer, J. J., Pinho, R., Calvi, G. M., Goretti, A., and Meroni, F. (2007). "A Prioritization Scheme for Seismic Intervention in School Buildings in Italy." *Earthquake Spectra*, 23(2), 291–314.

Holzer, T. L., Bennett, M. J., Noce, T. E., and Tinsley, J. C. (2005). "Shear-Wave Velocity of Surficial Geologic Sediments in Northern California: Statistical Distributions and Depth Dependence." *Earthquake Spectra*, 21(1), 161–177.

Huyck, C., Chung, H.-C., Cho, S., Mio, M., Ghosh, S., Eguchi, R., and Mehrotra, S. (2006). "Loss Estimation Online Using INLET (Inter-based Loss Estimation Tool)." San Francisco, CA.

Idriss, I. M. (2008). "An NGA Empirical Model for Estimating the Horizontal Spectral Values Generated By Shallow Crustal Earthquakes." *Earthquake Spectra*, 24(1), 217–242.

Jayaram, N., and Baker, J. W. (2008). "Statistical Tests of the Joint Distribution of Spectral Acceleration Values." *Bulletin of the Seismological Society of America*, 98(5), 2231–2243.

Jayaram, N., and Baker, J. W. (2010a). "Efficient sampling and data reduction techniques for probabilistic seismic lifeline risk assessment." *Earthquake Engineering & Structural Dynamics*, 39, 1109–1131.

Jayaram, N., and Baker, J. W. (2010b). *Probablistic Seismic Lifeline Risk Assessment Using Efficient Sampling and Data Reduction Techniques*. The John A. Blume Earthquake Engineering Center, Stanford University, Stanford, CA.

Kafali, C., and Grigoriu, M. (2004). *Fragility Based Rehabilitation Decision Analysis*. Student Research Accomplishments, Multidisciplinary Center for Earthquake Engineering Research (MCEER), University at Buffalo, Buffalo, NY.

Kaplan, J., and DeMaria, M. (1995). "A Simple Empirical Model for Predicting the Decay of Cyclone Winds after Landfall." *Journal of Applied Meteorology*, 34, 2499–2512.

Karamchandani, A., and Cornell, C. A. (1992). "Sensitivity Estimation within First and Second Order Reliability Methods." *Structural Safety*, 11(2), 95–107.

Khanduri, A. C., and Morrow, G. C. (2003). "Vulnerability of buildings to windstorms and insurance loss estimation." *Journal of Wind Engineering and Industrial Aerodynamics*, 91(4), 455–467.

Kircher, C. A. (2013). "Personal Communication."

Kircher, C. A., Seligson, H. A., Bouabid, J., and Morrow, G. C. (2006). "When the Big One Strikes Again—Estimated Losses due to a Repeat of the 1906 San Francisco Earthquake." *Earthquake Spectra*, 22(S2), 297–339.

Lee, R. G., Fan, Y. Y., and Kiremidjian, A. S. (2009). "Transportation System Direct Loss Exceedence Analysis and Subsystem Reliability under Retrofit Action." American Society of Civil Engineers, Oakland, CA, 1–11.

Lee, R., and Kiremidjian, A. S. (2006). "Probabilistic Seismic Hazard Assessment of Spatially Distributed Systems." Fifth National Seismic Conference on Bridge and Highways, San Francisco, CA.

Lee, R., and Kiremidjian, A. S. (2007). "Uncertainty and Correlation for Loss Assessment of Spatially Distributed Systems." *Earthquake Spectra*, 23(4), 753–770.

Legg, M. R., Nozick, L. K., and Davidson, R. A. (2010). "Optimizing the selection of hazard-consistent probabilistic scenarios for long-term regional hurricane loss estimation." *Structural Safety*, 32(1), 90–100.

Li, Y., Ahuja, A., and Padgett, J. E. (2012). "Review of Methods to Assess, Design for, and Mitigate Multiple Hazards." *Journal of Performance of Constructed Facilities*, 26(1), 104–117.

Li, Y., and Ellingwood, B. R. (2006). "Hurricane damage to residential construction in the US: Importance of uncertainty modeling in risk assessment." *Engineering Structures*, 28(7), 1009–1018.

Li, Y., and Ellingwood, B. R. (2009). "Framework for Multihazard Risk Assessment and Mitigation for Wood-Frame Residential Construction." *Journal of Structural Engineering*, 135(2), 159–168.

Li, Y., and van de Lindt, J. W. (2012). "Loss-based formulation for multiple hazards with application to residential buildings." *Engineering Structures*, 38, 123–133.

Liel, A. B., and Deierlein, G. G. (2013). "Cost-Benefit Evaluation of Seismic Risk Mitigation Alternatives for Older Concrete Frame Buildings." *Earthquake Spectra*, In Press.

Lindell, M. K., and Prater, C. S. (2003). "Assessing Community Impacts of Natural Disasters." *Natural Hazards Review*, 4(4), 176–185.

Loth, C., and Baker, J. W. (2012). "A Spatial Cross-Correlation Model of Spectral Accelerations at Multiple Periods." *Earthquake Engineering & Structural Dynamics*, 42(3), 1–22.

Lou, M., Wang, H., Chen, X., and Zhai, Y. (2011). "Structure–soil–structure interaction: Literature review." *Soil Dynamics and Earthquake Engineering*, 31(12), 1724–1731.

Mahsuli, M., and Haukaas, T. (2011). "Regional Risk by Reliability Analysis." *Applications of Statistics and Probability in Civil Engineering*, K. Nishijima, ed., CRC Press, 1991–1999.

Mahsuli, M., and Haukaas, T. (2013). "Sensitivity Measures for Optimal Mitigation of Risk and Reduction of Model Uncertainty." *Reliability Engineering & System Safety*, 117, 9–20.

Mann, N. R., Schafer, R. E., and Singpurwalla, N. D. (1974). *Methods for Statistical Analysis of Reliability and Life Data*. John Wiley, New York, NY.

Melchers, R. E. (1999). *Structural Reliability Analysis and Prediction*. John Wiley, Chichester, New York.

Miles, S. B., and Chang, S. E. (2006). "Modeling Community Recovery from Earthquakes." *Earthquake Spectra*, 22(2), 439–458.

Mileti, D. S. (1999). *Disasters by Design: A Reassessment of Natural Hazards in the United States*. Natural hazards and disasters, Joseph Henry Press, Washington, D.C.

Miller, M., Baker, J. W., Lim, H. W., Song, J., and Jayaram, N. (2011). "A FORM-Based Analysis of Lifeline Networks Using a Multivariate Seismic Intensity Model." 11th International Conference on Applications of Statistics and Probability in Civil Engineering (ICASP), Zurich, Switzerland.

Morio, J. (2011). "Global and Local Sensitivity Analysis Methods for a Physical System." *European Journal of Physics*, 32(6), 1577–1583.

National Academies (U.S.). (2012). *Disaster Resilience: A National Imperative*. National Academies Press, Washington, D.C.

National Institute of Building Sciences (NIBS). (1997). *Earthquake Loss Estimation Methodology, HAZUS 97: Technical Manual*. Federal Emergency Management Agency, Washington, D.C.

National Institute of Building Sciences (NIBS). (2002). *A Guide to Using HAZUS For Mitigation*. Federal Emergency Management Agency, Washington, D.C.

National Institute of Building Sciences (NIBS). (2012). *Multi-hazard Loss Estimation Methodology, Earthquake Model, HAZUS-MH 2.1 Technical Manual*. Federal Emergency Management Agency, Washington, D.C.

National Research Council. (2003). *Hurricane Hugo, Puerto Rico, the Virgin Islands, and Charleston, South Carolina, September 17-22, 1989*. National Academies Press, Washington, D.C.

Oh, E. H., Deshmukh, A., and Hastak, M. (2010). "Vulnerability Assessment of Critical Infrastructure, Associated Industries, and Communities during Extreme Events." Construction Research Congress, Banff, Alberta.

Olsen, A. H., and Porter, K. A. (2011). "What We Know about Demand Surge: Brief Summary." *Natural Hazards Review*, 12(2), 62–71.

Ouyang, M., and Dueñas-Osorio, L. (2012). "Time-dependent resilience assessment and improvement of urban infrastructure systems." *Chaos: An Interdisciplinary Journal of Nonlinear Science*, 22(3), 033122.

Padgett, J. E., Dennemann, K., and Ghosh, J. (2010). "Risk-Based Seismic Life-Cycle Cost–Benefit (LCC-B) Analysis for Bridge Retrofit Assessment." *Structural Safety*, 32(3), 165–173.

Pang, W., Liu, F., and Li, Y. (2012). "Spatial Correlation and Wind Speed Uncertainties of Hurricane Wind Field Model." EMI/PMC 2012, Notre Dame, IN.

Park, J., Bazzurro, P., and Baker, J. W. (2007). "Modeling Spatial Correlation of Ground Motion Intensity Measures for Regional Seismic Hazard and Portfolio Loss Estimation." Tenth International Conference on Application of Statistic and Probability in Civil Engineering (ICASP10), Tokyo, Japan.

Petrini, F., Ciampoli, M., and Augusti, G. (2009). "A Probabilistic Framework for Performance-Based Wind Engineering." EACWE 5, Florence, Italy.

Porter, K. (2013). "Personal Communication."

Porter, K. A., Scawthorn, C. R., and Beck, J. L. (2006). "Cost-Effectiveness of Stronger Woodframe Buildings." *Earthquake Spectra*, 22(1), 239–266.

Purvis, J. C., and McNab, A. (1985). *Hurricane Vulnerability For Charleston County*. State of South Carolina Water Resources Commission, Columbia, SC.

Reitherman, R. (1985). "A Review of Earthquake Damage Estimation Methods." *Earthquake Spectra*, 1(4), 805–847.

Renschler, C. S., Frazier, A. E., Arendt, L. A., Cimellaro, G. P., Reinhorn, A. M., and Bruneau, M. (2010). "Developing the 'PEOPLES' Resilience Framework for Defining and Measuring Disaster Resilience at the Community Scale." Toronto, Ontario, Canada.

Riederer, K. A., and Haukaas, T. (2007). "Cost-Benefit Importance Vectors for Performance-Based Structural Engineering." *Journal of Structural Engineering*, 133(7), 907–915.

Rinaldi, S. M., Peerenboom, J. P., and Kelly, T. K. (2001). "Identifying, Understanding, and Analyzing Critical Infrastructure Interdependencies." *IEEE Control Systems Magazine*, 11–25.

Robert, B., Morabito, L., and Debernard, C. (2013). "Simulation and Anticipation of Domino Effects among Critical Infrastructures." *International Journal of Critical Infrastructures*, In Press.

Rose, A., Porter, K. A., Dash, N., Bouabid, J., Huyck, C., Whitehead, J., Shaw, D., Eguchi, R., Taylor, C., McLane, T., Tobin, T., Ganderton, P., Godschalk, D., Kiremidjian, A. S., Tierney, K., and Taylor West, C. (2007). "Benefit-Cost Analysis of FEMA Hazard Mitigation Grants." *Natural Hazards Review*, (November), 97–111.

Rosenblatt, M. (1952). "Remarks on a Multivariate Transformation." *The Annals of Mathematical Statistics*, 23(3), 470–472.

Saltelli, A., Ratto, M., Tarantola, S., and Campolongo, F. (2006). "Sensitivity Analysis Practices: Strategies for Model-Based Inference." *Reliability Engineering & System Safety*, 91(10-11), 1109–1125.

Scawthorn, C. R., Schneider, P. J., and Schauer, B. A. (2006). "Natural Hazards - The Multi-hazard Approach." *Natural Hazards Review*, 7(2), 39.

Schubert, M., and Faber, M. H. (2012). "Common Cause Effects in Portfolio Loss Estimation." *Structure and Infrastructure Engineering*, 8(5), 497–506.

Smyth, A. W., Altay, G., Deodatis, G., Erdik, M., Franco, G., Gulkan, P., Kunreuther, H., Lus¸, H., Mete, E., Seeber, N., and Yuzugullu, O. (2004). "Probabilistic Benefit-Cost Analysis for Earthquake Damage Mitigation: Evaluating Measures for Apartment Houses in Turkey." *Earthquake Spectra*, 20(1), 171–203.

Sokolov, V., and Wenzel, F. (2011). "Influence of Spatial Correlation of Strong Ground Motion on Uncertainty in Earthquake Loss Estimation." *Earthquake Engineering & Structural Dynamics*, 40(9), 993–1009.

Steinbrugge, K., McClure, F., and Snow, A. (1969). *Studies in Seismicity and Earthquake Damage Statistics*. Department of Housing and Urban Development, Washington, D.C.

Student, H. H. (1997). "Assessing the Seismic Hazard in Charleston, South Carolina: Comparisons Among Statistical Models." Master of Science, Virginia Polytechnic Institute and State University, Blacksburg, VA.

Takahashi, Y., Kiureghian, A. D., and Ang, A. H.-S. (2004). "Life-cycle Cost Analysis Based on a Renewal Model of Earthquake Occurrences." *Earthquake Engineering & Structural Dynamics*, 33(7), 859–880.

Talwani, P., and Schaeffer, W. T. (2001). "Recurrence Rates of Large Earthquakes in the South Carolina Coastal Plain Based on Paleoliquefaction Data." *Journal of Geophysical Research*, 106(B4), 6621–6642.

Tesfamariam, S., and Saatcioglu, M. (2008). "Risk-Based Seismic Evaluation of Reinforced Concrete Buildings." *Earthquake Spectra*, 24(3), 795–821.

Thompson, E. M., Baise, L. G., and Kayen, R. E. (2006). "Spatial Correlation of Shear-Wave Velocity within San Francisco Bay Sediments." *Soil Dynamics and Earthquake Engineering*, (27), 144–152.

Thompson, E. M., Baise, L. G., Kayen, R. E., Tanaka, Y., and Tanaka, H. (2010). "A Geostatistical Approach to Mapping Site Response Spectral Amplifications." *Engineering Geology*, 114(3-4), 330–342.

TOMLAB. (2012). TOMLAB Optimization.

Unanwa, C. O. (2000). "A Model for Probable Maximum Loss in Hurricanes." PhD Dissertation, Texas Tech University, Broadway Lubbock, TX.

Unanwa, C. O., McDonald, J. R., Mehta, K. C., and Smith, D. A. (2000). "The development of Wind Damage Bands for Buildings." 84(1), 119–149.

United Nations. (2005). *Report of the World Conference on Disaster Reduction*. Kobe, Hyogo, Japan.

United States Geological Survey (USGS). (2012). *The Uniform California Earthquake Rupture Forecast, Version 3 (UCERF3)*. Working Group on California Earthquake Probabilities (WGCEP), California Geological Survey, U.S. Geological Survey.

United States Geological Survey (USGS). (2013a). *Global Vs30 Map Server*. U.S. Geological Survey.

United States Geological Survey (USGS). (2013b). "Historic Earthquakes." <http://earthquake.usgs.gov> (Aug. 12, 2013).

Vickery, P. J., Skerlj, P. F., and Twisdale, L. A. (2000). "Simulation of Hurricane Risk in the U.S. Using an Empirical Track Model." *Journal of Structural Engineering*, 126(10), 1222–1237.

Vickery, P. J., Wadhera, D., Twisdale, L. A., and Lavelle, F. M. (2009). "U.S. Hurricane Wind Speed Risk and Uncertainty." *Journal of Structural Engineering*, 135(3), 301–320.

Wen, Y. K. (2001). "Minimum Lifecycle Cost Design Under Multiple Hazards." *Reliability Engineering & System Safety*, 73, 223–231.

Whitman, R. V., Reed, J. W., and Hong, S.-T. (1973). "Earthquake Damage Probability Matrices." Fifth World Conference on Earthquake Engineering, Rome, Italy.

Zhang, J., and Du, X. (2010). "A Second-Order Reliability Method with First-Order Efficiency." *Journal of Mechanical Design*, 132(10), 101006.

Zobel, C. W., and Khansa, L. (2011). "Characterizing Multi-Event Disaster Resilience." *Computers & Operations Research*, 42, 83–94.